Ana Luísa Queirós Carvalho

Exploitation of new chromene-based compounds as promising agents for cancer treatment

Exploitation of new chromene-based compounds as promising agents for cancer treatment

Ana Luísa Queirós Carvalho

UMinho | 2021

march of 2021

Ana Luísa Queirós Carvalho

Exploitation of new chromene-based compounds as promising agents for cancer treatment

Master's Dissertation
Master in Applied Biochemistry
Specialization in Biomedicine

march of 2021

COPYRIGHT AND CONDITIONS OF USE OF THE WORK BY THIRD PARTIES

This is an academic work that can be used by third parties as long as the internationally accepted rules and good practices regarding copyright and related rights are respected.

Accordingly, this work may be used as provided in the license below.

If the user needs permission to use the work under conditions not foreseen in the license indicated, he should contact the author, through RepositóriUM of University of Minho.

Acknowledgements

Along this journey, many were the people that supported me and collaborated to the development of the dissertation and I want to thank each and everyone!

First of all, I cannot start this dedicatory if not by the very person that made all of this possible, my supervisor Marta Costa! I am so grateful for finding an excellent professional, very dedicate, a true mentor that passed down so many values, provided me countless learning opportunities and helped me mature as a professional. More than all of this, she is an extraordinary person, extremely gentle, caring and concerned, that never let me give up and always believed in me and in my capabilities. There are no words to describe this feeling of gratitude towards you! Two years filled with strong emotions has gone by and I will always carry your words of motivation written in that pink post-it, "I Want, I Can, I Got It"... Without a doubt, you are one of the most exceptional people I have ever met in my life.

To Professor Fernanda Proença, co-supervisor of this thesis, I would like to demonstrate my gratitude for all the time invested, for all the assistance and confidence placed in me.

To Professor Fátima Baltazar I must show my appreciation for all the support offered during this journey.

To the girls, Sofia and Olívia, who always brightened my day and made me always see the positive side of things. Undoubtedly, two beautiful human beings! Thank you for every learning, for the companionship, the laughs, the conversations, the motivation...

To my dearest friends, for all the emotional support, for putting up with all my daydreams, for giving me all the strength in the world to move on and for believing that I would achieve this and so much more. You nurture my dreams! Thank you so much!

Lastly, but not least, my greater appreciation to my family! They provided the opportunity to get here and pushed me forward in life. They always struggle to give me the best and encouraged me to fight for nothing less than the very best. Thank you for all the life lessons and for making this journey so more much easy!

STATEMENT OF INTEGRITY

I hereby declare having conducted this academic work with integrity. I confirm that I have not used plagiarism or any form of undue use of information or falsification of results along the process leading to its elaboration.

I further declare that I have fully acknowledged the Code of Ethical Conduct of the University of Minho.

Abstract

Cancer is a devastating disease, responsible for 9.9 million deaths worldwide in 2020. Female breast cancer is the most diagnosed cancer and with the highest mortality rate. The statistics show that this tendency will continue to rise in the next years, becoming urgent the development of new and more effective drugs capable to overcome resistance and toxicity problems, associated to the current available therapies.

The chromene moiety has been recognized in several natural and synthetic compounds, exhibiting very interesting biological activities, namely anticancer activity.

The present work aimed to assess the anticancer potential of two synthesized chromene-based family – FD and DL-chromene-based compounds, in the breast cancer cell model.

The anticancer potential of the FD-chromene-based compounds was evaluated through a first screening of the compounds in different BC cell lines. Chromenes displaying the best activity profile proceeded to IC_{50} determination and *in vitro* and *in vivo* toxicity assays, using a non-neoplastic cell line (MCF-10A) and the *Caenorhabditis elegans* model, proving their non-toxic profile. To study their mechanism of action, more specific *in vitro* assays were conducted and the results showed the ability of the compounds to induce cell death through apoptosis, cell cycle arrest, to inhibit cell migration, proliferation and to interfere with key enzymes in the glycolytic process. Lastly, two lead compounds were identified and the Chick Chorioallantoic Membrane (CAM) model was used for *in vivo* efficacy studies. The analyzed chromenes were able to inhibit tumor proliferation and angiogenesis, evidencing their potential as anticancer drug candidates.

The anticancer potential regarding DL-chromene-based compounds was initiated in a previous project. In the present work, three of the most promising molecules were selected to investigate their influence in the expression levels of proteins related to cell death and metabolism, to characterize their mechanism of action. The results showed that the chromenes were able to induce cell death through apoptosis as well as to reduce the expression levels of multiple key enzymes involved in the glycolytic process.

Keywords: Cancer | Breast cancer | Chromenes | Lead compound

Resumo

O cancro é uma doença devastadora responsável globalmente por 9.9 milhões de mortes em 2020. O cancro da mama é o mais diagnosticado e mortal nas mulheres. Esta tendência vai continuar a aumentar nos próximos anos, tornando-se urgente o desenvolvimento de novas moléculas mais eficazes, capazes de ultrapassar os problemas de resistência e toxicidade associados às terapias atualmente usadas.

O núcleo de cromeno foi reconhecido em múltiplos compostos naturais e sintéticos que exibem atividades biológicas interessantes, nomeadamente atividade anticancerígena.

Este trabalho teve como objetivo avaliar o potencial anticancerígeno no modelo de células do cancro da mama de duas famílias de compostos sintetizadas no grupo de investigação, com base na unidade de cromeno (compostos FD e DL).

O potencial anticancerígeno da família de compostos FD foi avaliada através de um primeiro *screening* dos compostos em diferentes linhas celulares do cancro da mama. Os cromenos que mostraram um perfil de atividade mais promissor, prosseguiram para ensaios de determinação de IC_{50} e toxicidade *in vitro* e *in vivo*, usando uma linha celular não neoplásica (MCF-10A) e o modelo *Caenorhabditis elegans,* provando ter um perfil seguro. De seguida, para estudar o seu mecanismo de ação, ensaios *in vitro* mais específicos foram realizados, mostrando a capacidade para induzir morte celular por apoptose, paragem do ciclo celular, inibição da migração, proliferação celular e interferência com enzimas-chave envolvidas no processo glicolítico. Por último, foram identificados dois compostos *lead* e o modelo da membrana corioalantóica de embrião de galinha (CAM) foi usada para estudar o perfil de eficácia *in vivo*. Estes cromenos demonstraram a capacidade de inibir a proliferação tumoral e angiogénese, evidenciando o seu potencial como agentes anticancerígenos.

O perfil anticancerígeno dos cromenos DL já tinham sido iniciado num projeto anterior. Neste trabalho, as três moléculas mais promissoras foram selecionadas para investigar o nível de expressão de proteínas associadas à morte e metabolismo celular. Os resultados obtidos mostraram que os cromenos foram capazes de induzir morte celular por apoptose, assim como reduzir a expressão de várias enzimas-chave envolvidas no processo glicolítico.

Palavras-chave: Cancro | Cancro da mama| Cromenos | Compostos *lead*

Index

Abbreviations

BC – Breast Cancer

HDI – Human Development Index

BRAC 1/2 – Breast cancer type 1/2 gene

DNA – Deoxyribonucleic Acid

RNA – Ribonucleic Acid

mRNA – Messenger Ribonucleic Acid

MRI – Magnetic Resonance Imaging

ACS – American Cancer Society

BCSCs – Breast Cancer Stem Cells

ISH – *In Situ* Hybridization

RT-PCR – Reverse Transcriptional Polymerase Chain Reaction

NGS – Next Generation Sequencing

HER2 – Human Epidermal Growth Factor Receptor 2

IHC – Immunohistochemistry

TNBC – Triple Negative Breast Cancer

ER – Estrogen Receptor

PR – Progesterone Receptor

BL – Basal-like

CDKs – Cyclin-dependent kinases

FDA – Food and Drug Administration

Fab – Fragment antigen-binding

PDB – Protein Data Base

PARP – Poly (ADP-ribose) polymerase

PD-L1 – Programmed Cell Death ligand 1

PD-1 – Programmed Cell Death 1

IUPAC – International Union of Pure and Applied Chemistry

C3 – Caspase 3

C8 – Caspase 8

C9 – Caspase 9

HK2 – Hexokinase 2

PKM2 – Pyruvate Kinase Isoenzymes M2

Glut1 – Glucose transporter 1

Hif-1α/2α – Hypoxia-inducible factor 1α/2α

GAPDH – Glyceraldehyde-3-phosphate Dehydrogenase

LDHA – Lactate Dehydrogenase A

CAIX – Carbonic Anhydrase IX

G3P – Glyceraldehyde-3-phosphate

1,3 BPG – 1,3 Bisphosphoglyceric acid

NADH – Nicotinamide Adenine Dinucleotide

ER-α36 – Estrogen Receptor α36

EGFR – Epidermal Growth Factor Receptor

IC$_{50}$ – half maximal inhibitory concentration

GI$_{50}$ – half maximal growth inhibition concentration

LD$_{50}$ – median lethal dose

qRT-PCR – quantitative RT-PCR

TrxR – Thioredoxin Reductase

PI – Propidium Iodide

ROS – Reactive Oxygen Species

ATCC – American Type Culture Collection

DMEM – Dulbecco's Modified Eagle Medium

FBS – Fetal Bovine Serum

PBS – Phosphate Bovine Saline

Trypsin – TrypLE™ Express Enzyme

DMSO – Dimethyl sulfoxide

TCA – Trichloroacetic acid

SRB – Sulforhodamine B

TBS – Tris-buffered saline

BrdU – 5-bromo-2'-deoxyuridine

BSA – Bovine Serum Albumin

DAPI – 4',6 – Diamidino-2-Phenylindole, Dihydrochloride

CAM – Chick Chorioallantoic Membrane

SD – Standard Deviation

SI – Selectivety Index

OD – Optical Density

TNF – Tumor Necrosis Factor

TNFR – Tumor Necrosis Factor Receptor

MOMP – Mitochondrial Outer Membrane Permeabilization

TRAF – TNF Receptor Associated Factor

ICE – Interleukin-1β-converting Enzyme

ATP- Adenosine Triphosphate

MSAs – Microtubule-Stabilizing Agents

MDAs – Microtubule-Destabilizing Agents

ROCK – Rho-associated Protein Kinase

List of Figures

List of Tables

Chapter I - Introduction

1. Cancer

Cancer is a disease resultant from molecular modifications and involves dynamic changes in the genome, leading to the transformation of normal cells into highly malignant derivatives [1, 2]. Cancer cells have faults in regulatory circuits, responsible for normal cell proliferation and homeostasis [1]. It has become the major cause of death worldwide and, although the main reasons are complex, they seem to be related with the growth and aging of the population, especially in less economically developed countries. The adoption of some lifestyle habits like smoking, poor diet, physical inactivity, and reproductive adjustments, which include lower parity and later age at first birth, represent major risk factors for the development of cancer[3, 4].

In 2020, 19.2 million new cancer cases and 9.9 million cancer deaths were registered [5]. Breast cancer (BC) was the most diagnosed cancer worldwide and lung cancer emerges in second place, followed by prostate and colorectal cancer. Regarding to mortality, lung cancer leads the ranking followed by colorectal, stomach, and liver cancer, closely followed by breast cancer, the 5th cancer-related death cause worldwide. Unfortunately, the perspectives for the future are not favorable, since it is expected that this malignance will reach 30.2 million cases by the year of 2040, of which 1 million are new breast cancer cases [6]. Considering this devastating reality, the development of more effective and safer treatment options is an urgent unmet need.

The most frequently diagnosed cancer and the leading cause of cancer death varies across countries and is dependent on the degree of economic development and lifestyle habits, as mentioned before [3]. Cancer prevention could help decrease a substantial proportion of this burden through the widespread application of existing cancer control knowledge, including tobacco control and vaccination for liver and cervical cancers, early detection and the promotion of healthy lifestyle patterns, such as physical activity and an equilibrated diet [4].

For researchers and clinicians, the primary events of genesis and progression of cancer remains a challenge. Though, many evidences indicate that tumorigenesis in humans is a multistep event. In 2000, Hanahan *et al.* presented an overall of six essential capabilities acquired by malignant cells, which are shared by all types of human tumors, including self-sufficiency in growth signals, insensitivity to growth-inhibitory signals, evasion of programmed cell death, limitless replicative potential, sustained angiogenesis, tissue invasion and metastasis [1]. In 2011, they identified four additional characteristics that were recognized as 'emerging' cancer hallmarks, illustrated in **Figure 1** as the deregulation of cellular energetics, the avoidance of immune destruction, tumor promoting

inflammation and genomic instability and mutation [7, 8]. These abilities acquired during tumor development represent the breaching of an anticancer defense mechanism.
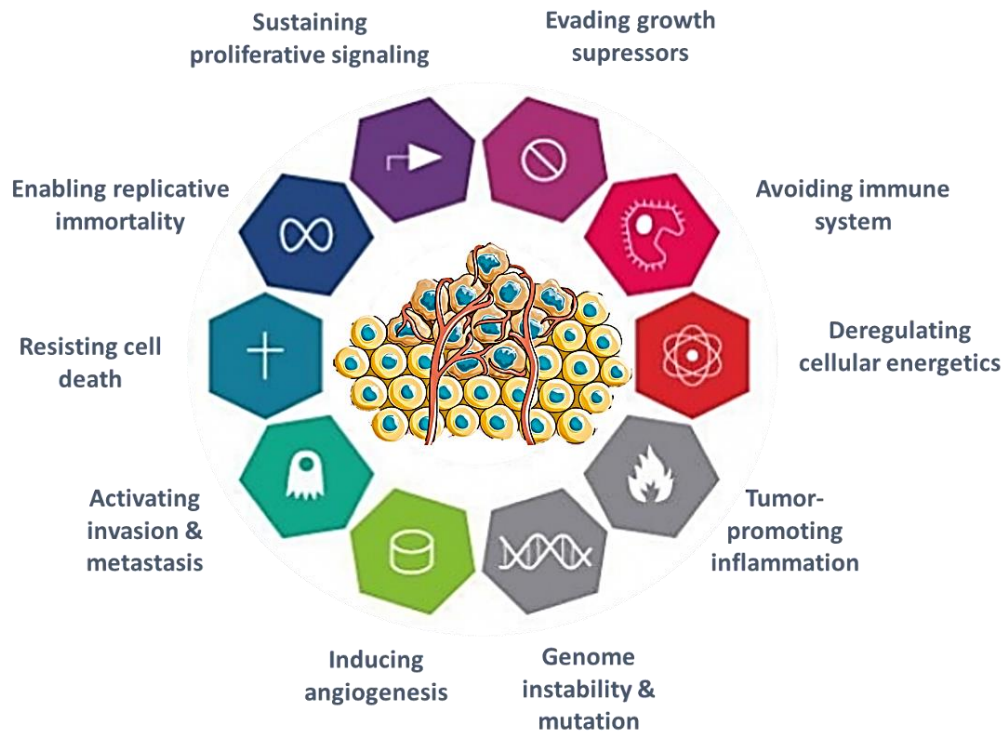
Figure 1 - Hallmarks of cancer. Illustration of the abilities acquired by cancer cells during tumorigenesis and tumor progression. Adapted from [7].

1.2. Breast cancer

In 2012, BC was the second most common cancer in the world with an estimated 1.67 million female cases diagnosed, representing 25% of all cancers in the world. In 2018, 2.1 million new female breast cancer cases were diagnosed, and for the year of 2040, 3 million new cases are estimated, pointing out the rising of breast cancer cases and therefore rushing the urgent development of more effective and safe treatments [3].

This disease is the most frequently diagnosed cancer in most countries, and contrary to popular belief, the highest breast cancer incidence resides in countries with high Human Development Index (HDI), such as Australia and New Zealand, Western and Northern Europe countries and Northern America (**Figure 2**) [3]. Regarding the mortality, the scenario changes, since it is higher in countries with low HDI, namely on Melanesia and Polynesia.
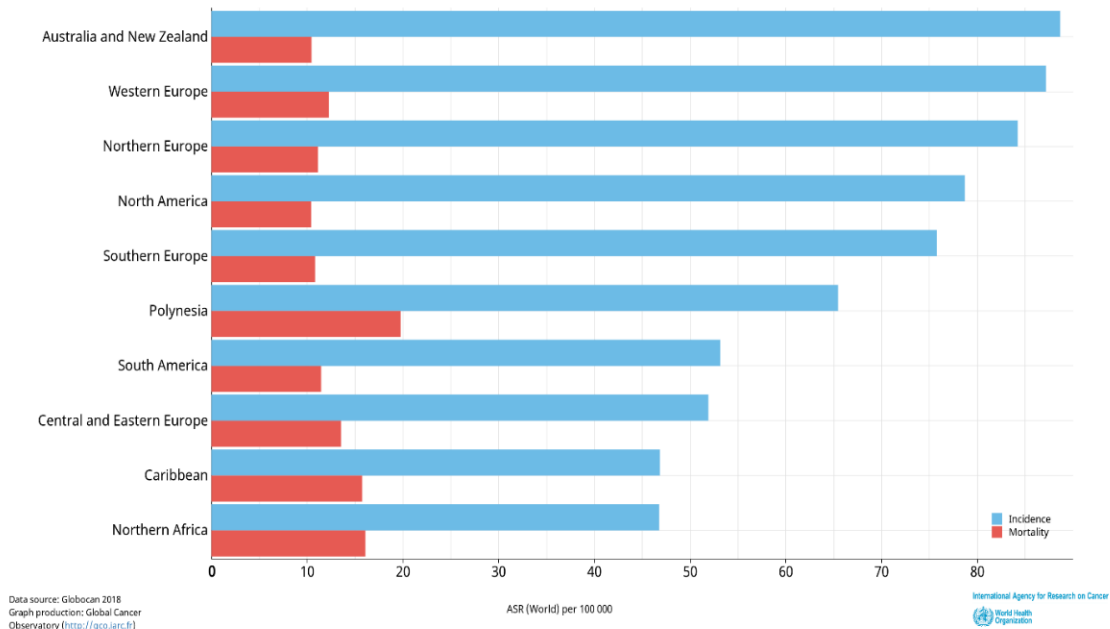
Figure 2 - Bar chart of incidence and mortality worldwide, age-standardized rates for female breast cancer in 2018, sorted by incidence [3].

In Portugal, female breast cancer is the most frequent and the second main cause of mortality, with 7041 new cases and 1864 deaths in the year of 2020, contributing to 26.4% of all cancer cases and 15.5 % of all cancer-related deaths [9].

Recent studies show that approximately 10% of breast cancers are associated to family medical history and to inherited mutations in key genes, like *BRAC1* and *BRAC2*, although this varies frequently by ethnicity and across countries [3, 10]. *BRAC1* and *BRAC2* are two high-penetrance tumor suppressor genes, whose proteins are involved in DNA repair, and their mutation show an autosomal-dominant inheritance pattern associated with an average cumulative risk of developing breast cancer [10]. The remaining 90% of cases reside within the nonhereditary factors that are responsible for the observed global and interethnic differences in incidence. For example, the high incidence of breast cancer in countries with an elevated HDI is related with the continued exposure to known risks factors. Although, in countries with a lower HDI, the incidence is associated to other

known risk factors, such as the early and later ages of the first menarche and of the menopause, respectively. The null birth, the later age of the first child, the fewer children, the use of oral contraceptives, the diet and the anthropometry are also prevalent factors associated to this high incidence. On the opposite, breastfeeding and physical activity are known as protective factors [3].

More recently, the decline in incidence rates observed in some of the western countries has not passed unnoticed. It is possible that this decline is associated to the reduction in the use of postmenopausal hormone replacement therapy and to an increased adhesion to mammography screening [11]. However, there is still a high worldwide incidence of breast cancer and many of these cases end in death.

Mammography and breast magnetic resonance imaging (MRI) should be implemented as a preventive health intervention to all women, together with the encouragement to recognize their own family health history [12, 13]. An early diagnose can dictate a more favorable outcome, since there are higher probabilities of a better response to the treatments in early stages of the disease. The *American Cancer Society* (ACS) highlighted the importance to perform mammography in women around the age of 40 at risk of developing breast cancer [14].

Nowadays the triple-modality approach is in vogue and includes mammography, ultrasound and MRI [13]. This approach provides the highest detection rates, although it also produces higher rates of false positives, with higher costs associated. However, Riedl *et al.* carried out a study in which they confirm that for women with a high family incidence and risk for breast cancer, the MRI technique has a higher sensitivity for pre-invasive and invasive cancer, comparatively to the other two mentioned techniques, regardless of age, mutation status or breast density [13].

Studies on human carcinogenesis moved forward suggesting that a small portion of tumor stem cells influences and modifies neoplastic cell behavior and aggressiveness, as well as the therapeutic response. Also, this subpopulation of cells, similar to stem cells, known as breast cancer stem cells (BCSCs), enhances the ability of breast cancer to proliferate, progress and spread [15].

BC tumors are a very heterogeneous group, which differs in morphology, gene profiling, prognosis, and therapeutic response and are originated from the epithelial cells lining the milk ducts [12]. The first classification system was based on histological appearances but revealed to be inconsistent since the diagnostic criteria became subjective. Over the past years, different

techniques have been developed in the molecular biology laboratory, including *in situ* hybridization (ISH), reverse transcriptional polymerase chain reaction (RT-PCR), next generation sequencing (NGS) and expression microarrays. These techniques provided important gene expression information that allowed the development of a new classification system, introduced by Perou *et al.,* that identified four major intrinsic subtypes of breast cancer, basal-like (including triple-negative), human epidermal growth factor receptor (HER2)-enriched, luminal A and B, each one disposing a specific gene expression pattern [16-18]. Currently, clinical practice uses a surrogate classification of five subtypes based on histological and molecular characteristics, as described in **Table 1** [10, 19]**.**

Table 1 - Molecular subtypes of breast cancer.

Surrogate intrinsic subtypes	IHC classification [a]	Prognosis	Incidence
Luminal A-like	ER and/or PR+ HER2- Low Ki67	Good	60-70%
Luminal B-like HER2 -	ER and/or PR+ HER2- High Ki67	Intermediate	10-20%
Luminal B-like HER2+	HER2+ PR and ER+ High Ki67	Intermediate	13-15%
HER2-enriched	HER2 overexpressed or amplified ER and PR- High Ki67	Intermediate	
Triple negative	PR and ER- HER2- High Ki67	Poor	10-15%

a)   IHC, immunohistochemistry; ER, estrogen receptor; PR, progesterone receptor; HER2, human epidermal growth factor receptor 2. Adapted from [10, 19]

Triple-negative breast cancer (TNBC) subtype represent 10-15% of the cases, presenting a phenotype characterized by negative expression of estrogen receptor (ER), progesterone receptor

(PR) and HER2 [20]. Both luminal A and B breast cancer are characterized by the expression of ER-associated genes. The sub-stratification into two groups occurs based on the expression levels of proliferation-related genes in breast cancer, like Ki67 [16, 20, 21].

In 2011, a study conducted by Lehmann *et al.* allowed the distinction of six TNBC subtypes through the analysis of the gene expression of 386 tumors, each exhibiting unique features [22]. The subtypes included two basal-like (BL1 and BL2), an immunomodulatory, a mesenchymal, a mesenchymal stem-like, and a luminal androgen receptor subtype [23-25]. This classification by molecular subtype enables the future success of clinical trials in patients with TNBC [23].

Breast cancer molecular classification revealed itself as a crucial technique to design target therapies for each subtype of tumors. This improvement led to significant positive outcomes in disease-specific survival. Each intrinsic subtype has specific risk factors for incidence, response to the available treatments, risk of progression and preference for organs to metastasize [12].

In terms of therapy, most luminal tumors are responsive to hormonal interventions, while HER2+ tumors can be effectively controlled through anti-HER2 therapies. Molecular-based targeted treatment for TNBC has not yet been developed, mostly due to the lack of known molecular markers that can be used as target to address the therapy. At current days, the first line of treatment for TNBC is chemotherapy that uses cytotoxic compounds to inhibit the fast proliferation of malignant cells. However, these drugs also negatively affect normal cells with a proliferation rate above average, such as hair follicles, bone marrow and gastrointestinal tract cells leading to undesirable effects [26]. This subtype of cancer has a very aggressive behavior and a very low percentage of positive outcomes in patients, around 20%. Chemotherapy, although showing unsatisfactory therapeutic results, remains the first option to treat TNBC [12]. The development of new and effective treatments for TNBC is one of the highest priorities of current breast cancer research [12].

1.3.   Breast Cancer treatment

The treatment for breast cancer patients depends on the stage and grade of the tumor [27]. There are several conventional therapies, such as surgical intervention, radiotherapy and chemotherapy, including cytotoxic drugs and targeted therapy. Depending on tumor specific subtype and heterogeneity, these treatments can be utilized solely or in combination [28, 29].

For the treatment of the luminal subtype of breast cancer, several effective drugs were developed. Fulvestrant is an ER antagonist that downregulates the receptor and has no agonist effect (**Figure 3**). Tamoxifen is another example of a competitive ER inhibitor and Palbociclib is used as an inhibitor of cyclin-dependent kinases (CDKs) 4 and 6 that prevents DNA synthesis, resulting in cell cycle arrest in G1 or S phase (**Figure 3**) [30-33].
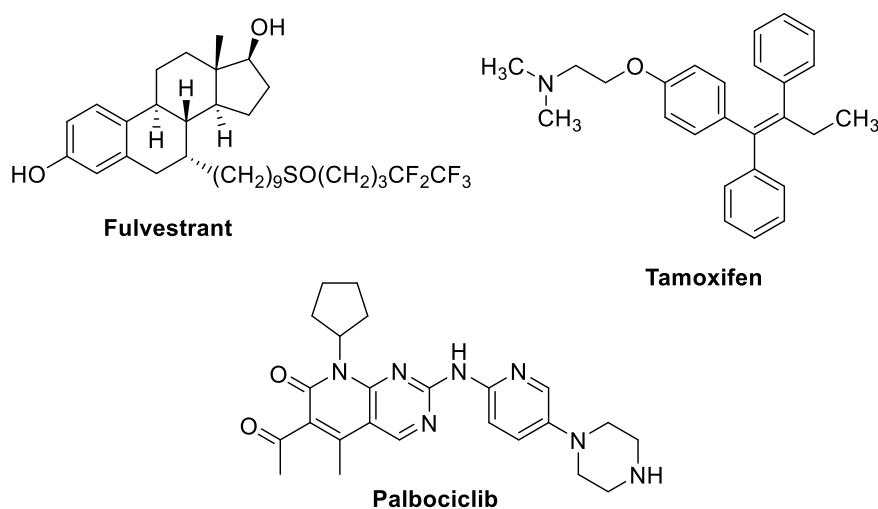
Figure 3 - Chemical structures of Fulvestrant, Tamoxifen and Palbociclib, FDA approved drugs used to treat breast cancer patients in the clinic, diagnosed with the luminal subtype.

Cristofanilli *et al.* demonstrated that a more positive outcome for the association of Fulvestrant and Palbociclib (**Figure 3**) in women with metastatic breast cancer could be achieved, in comparison with the co-administration of Fulvestrant and Placebo [30, 34]. It was also shown that Palbociclib possibly targets a dependence of luminal subtype breast cancer on CDK4 and CDK6, introducing a novel molecular target in patients with endocrine-positive disease [30].

HER2-enriched subtype of breast cancer treatment has a different mechanism of action relatively to luminal cancer since the drugs have different targets. In this case, the most common treatment consists in using a tyrosine kinases inhibitor, such as Lapatinib or a monoclonal antibody, like Trastuzumab (**Figure 4**) [31, 35, 36].

Lapatinib   **Trastuzumab**
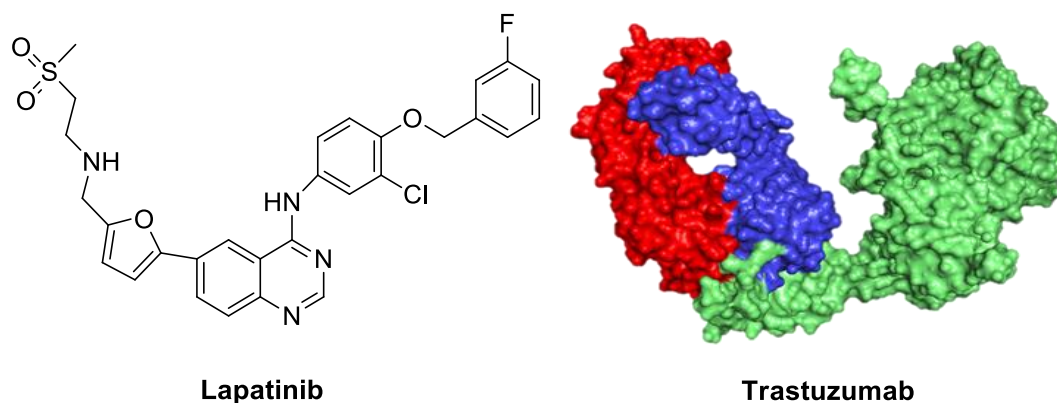
Figure 4 -HER2 targeted therapeutic agents: chemical structure of Lapatinib and 3D structure of Trastuzumab Fab in complex with HER2 extracellular domain (Green: HER2 extracellular domain; Red and blue: Fragment antigen-binding (Fab) of Trastuzumab). Retrieved from Protein Data Dase (PDB) [37].

Contrary, TNBC subtype does not respond to endocrine therapy and has a clinical relevance of being associated with a shorter time to relapse[13]. Since there is no existing targeted therapy for TNBC, cytotoxic chemotherapy is the best option for these patients [38].

In the last 50 years, many classes of anti-tumoral drugs have been developed, known as cytotoxic drugs that directly damage DNA, interfering with the synthesis and replication of DNA processes, and interfering with the function of the mitotic spindle [31].

Cytotoxic drugs are subdivided in accordance with their mechanism of action. The first class is designated as alkylating agents followed by other classes, such as platinum drugs, antimetabolites, topoisomerase inhibitors, anthracyclines and mitotic inhibitors. The mechanism of action of these cytotoxic drugs affects important cell processes that, ultimately, will lead to cell cycle arrest and apoptosis [31].

The mode of action of alkylating agents resides within the covalent binding of an alkyl group, from the drug, to groups N1 and N3 of the adenine residue in the DNA. The outcome is an interstrand cross-linking of the DNA double helix that will trigger the apoptotic process. Cyclophosphamide belongs to this category and is widely used to treat breast cancer (**Figure 5**) [31].

Cyclophosphamide   **Cisplatin**   **Carboplatin**   **Oxaliplatin**
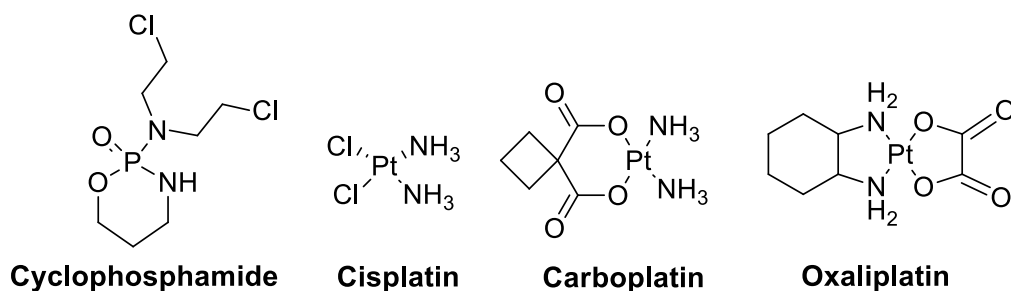
Figure 5 - Cytotoxic drugs: chemical structure of Cyclophosphamide, Cisplatin, Carboplatin and Oxaliplatin, used in the clinic to treat breast cancer patients.

The platinum derived drugs have a similar mode of action to the alkylating agents, by covalently binding the platinum moiety to the DNA bases from the same strand, resulting in interstrand cross-linking and leading to apoptosis. Cisplatin, Carboplatin and Oxaliplatin (**Figure 5**) are examples of platinum derived drugs [31].

Antimetabolites, like Methotrexate (**Figure 6**), are compounds that mimic the structure of purines and pyrimidines and, consequently, cause the inhibition of enzymes that are responsible for the incorporation of nucleic acids into the DNA strand [31].

Methotrexate

Doxorubicin

Paclitaxel
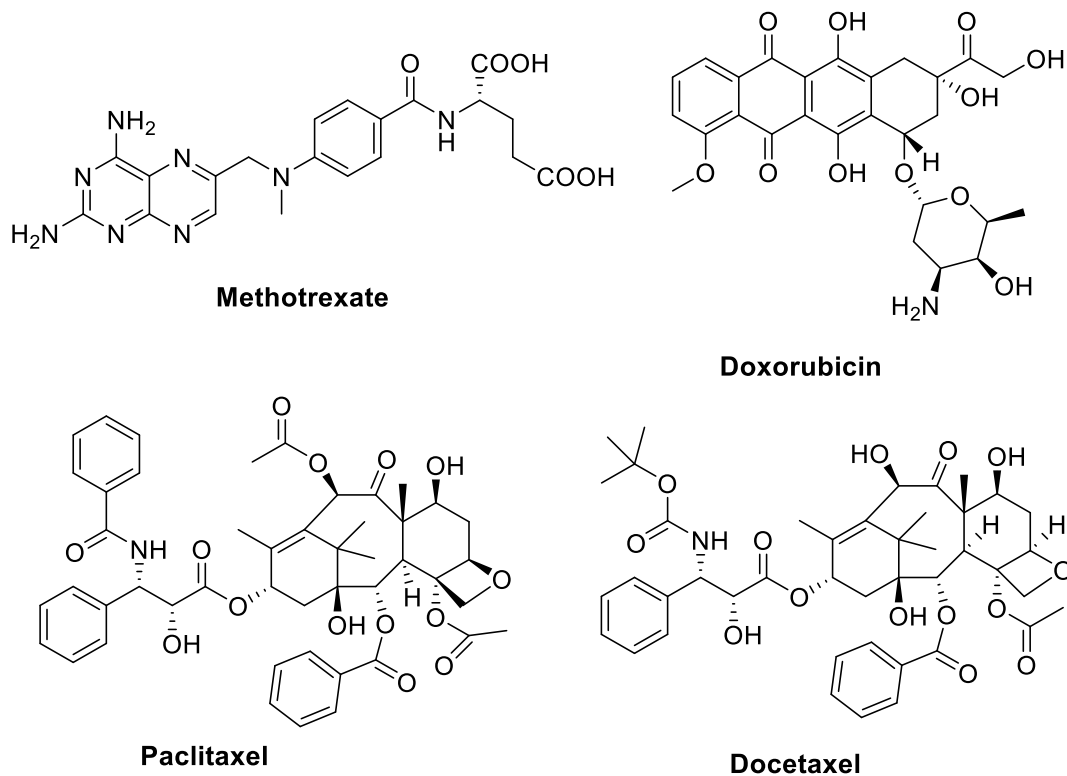
Docetaxel

Figure 6 - Commercially available cytotoxic drugs: chemical structures of the antimetabolite Methotrexate, anthracycline Doxorubicin and mitotic inhibitors, Paclitaxel and Docetaxel.

Another class of cytotoxic drugs are the anthracyclines that are largely used in the clinic. Doxorubicin is an example of the compounds belonging to this class (**Figure 6**) [39]. Even poorly understood, it is believed that the mechanism of action of these drugs resides in their direct linkage to DNA, inhibiting topoisomerase II-mediated DNA repair, leading to cell death.

Paclitaxel and Docetaxel (**Figure 6**) belong to the taxane's family and are considered mitotic inhibitors [31, 40]. These compounds are known as stabilization agents for the microtubules, binding to tubulin and preventing its disassembly, leading to cell death by apoptosis. These agents can be used alone or in combination with drugs differing in their mechanism of action, in solid tumor malignances like breast cancer. Their clinical usage entails serious problems including tumor resistance, risk of hypersensitivity reactions and toxicity.

The treatment administered to the patients will also depend on the cancer stage [27]. If it is an early-stage tumor, surgery after reducing the tumor size with neoadjuvant chemotherapy is recommended. After surgery, residual tumor can be found, and other drugs can be prescribed to continue the treatment, as capecitabine (**Figure 7**).

Capecitabine   **Olaparib**
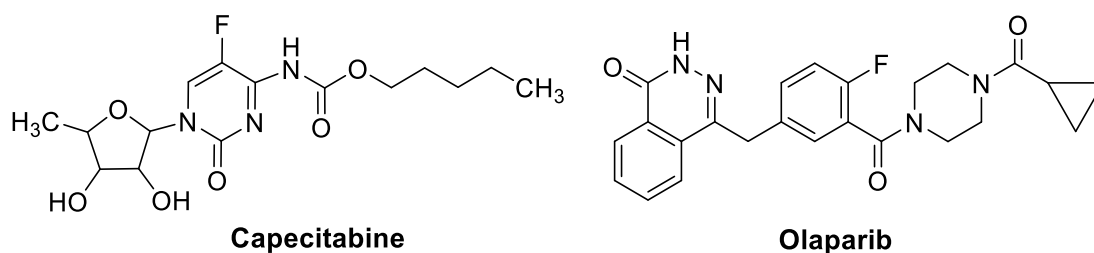
Figure 7 - Chemical structures of Capecitabine, commercialized as Tecentriq®, used after surgery for treatment of residual tumor, and Olaparib, a PARP inhibitor, used in the clinic for the treatment of metastatic TNBC with BRAC mutations.

In 2015, a clinical trial, CREATE-X, was successfully conducted on chemoresistance TNBC patients administering capecitabine jointly with the chemotherapy and nowadays this drug combination is widely used as a standard treatment [41].

For advanced stages, such as metastatic TNBC with BRAC mutations, the standard treatments are the above-mentioned platinum drugs (**Figure 5**) and PARP inhibitors, such as Olaparib (**Figure**

7). In contrast, the same treatment cannot be applied in advanced TNBC expressing programmed cell death ligand 1 (PD-L1). This protein has a higher prevalence in TNBC than in hormone receptor-positive BC subtypes supporting the use of PD-L1 inhibitors, namely Atezolizumab (**Figure 8**) and programmed cell death 1 (PD-1) protein, in antibody monotherapy [42].
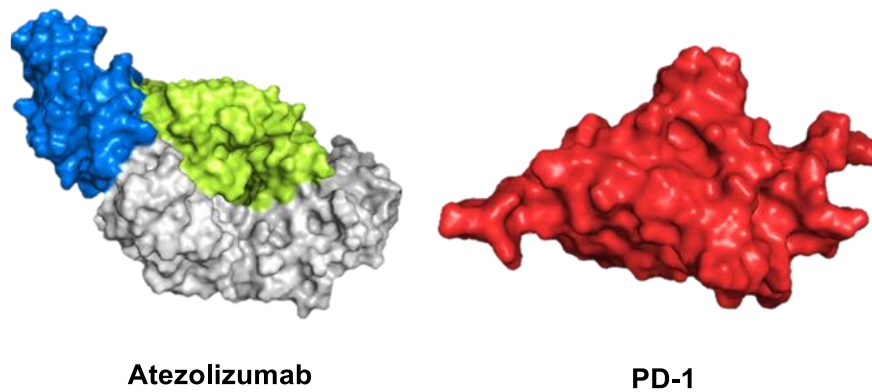
Atezolizumab　　　　**PD-1**

Figure 8 - PD-L1 antibody inhibitors: 3D structures of Atezolizumab Fab in complex with PD-L1 (Blue: human programmed cell death ligand 1, Yellow and grey: Fragment antigen-binding (Fab) of Atezolizumab) and PD-1 (Red: Programmed cell death protein 1) antibodies. Retrieved from Protein Data Base (PDB) [43].

Despite the existent treatments, their poor rate of success and the high TNBC's rate of recurrence demand an urgent development of new, safer and more effective therapies.

2. Chromene-based chromenes

For many years, nature has been used as a source of inspiration for the development of all sort of medicines. Over the years, there has been an increasing interest in the exploitation of chromene-based compounds, due to their natural abundance in plants, such as vegetables, fruits, tea and certain spices and important properties as for example anti-oxidant [44], antimicrobial [44], anti-inflammatory [45], anticancer activity [46], antileishmanial [47], antimalarial [47], antifungal [47] and antiviral [47] activity.

The chromene core can be synthesized through the fusion of a benzene ring with the 5,6-positions of either a 2*H* or a 4*H* pyran ring system originating bicyclic oxygen heterocycles designated as 2*H*-1-benzopyan (or 2*H*-chromene) and 4*H*-1-benzopyran (or 4*H*-chromene) respectively, according to the IUPAC nomenclature (**Figure 9**) [48].
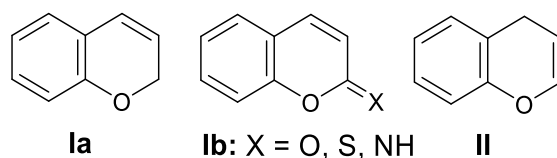
Figure 9 - General structure of **Ia**: 2*H*-Chromene (2*H*-1-benzopyran), **Ib**: chromene-based compound bearing a sp^2 carbon atom in C2 and **II**: 4*H*-chromene (4*H*-1-benzopyran).

Molecule **Ib** is a well-known chromene derivative, where X can be an oxygen atom, resulting in the 2-oxo-2*H*-chromene scaffold, most commonly known as coumarin, or a nitrogen or sulfur atom, as represented in **Figure 9** [48, 49].

2.1. Chromene derivatives as anticancer agents

Regarding to the anticancer activity of natural or synthetic chromene-based compounds, several research studies have been carried out in order to exploit their anticancer potential. A well-known synthetic chromene is EPC2407, also known as Crolibulin™, an example of a compound based on the chromene unit with anticancer activity [50, 51]. This 4*H*-chromene analog progressed to Phase I/II of clinical trials on anaplastic thyroid cancer and is described as a tubulin inhibitor. The activity of this molecule includes antitumoral effect and neovascular endothelial cells disruption, leading to the interruption of the blood flow to the tumor.

Knowing that some cancers, as breast cancer, have become a public health problem in some countries, these studies might represent the beginning for an important breakthrough in cancer therapy [52].

2.1.1. Natural chromenes as anticancer agents

In the 90s, an interesting chromene derivative, isolaxifolin (**Figure 10**), was isolated from root samples *of Derris laxiflora Bentham*, found in south Taiwan, initially explored by aboriginals for medicinal purposes [53]. Unfortunately, the natural abundance of this compound is low, in contrast with apigenin (**Figure 10**), an analogue of isolaxifolin widely distributed in diverse vegetables, fruits and herbs, that presents chemo preventative effects. Nevertheless, the synthesis of isolaxifolin from apigenin was successfully performed, using a low-cost process with a 17% yield, avoiding dull extraction and isolation protocols.
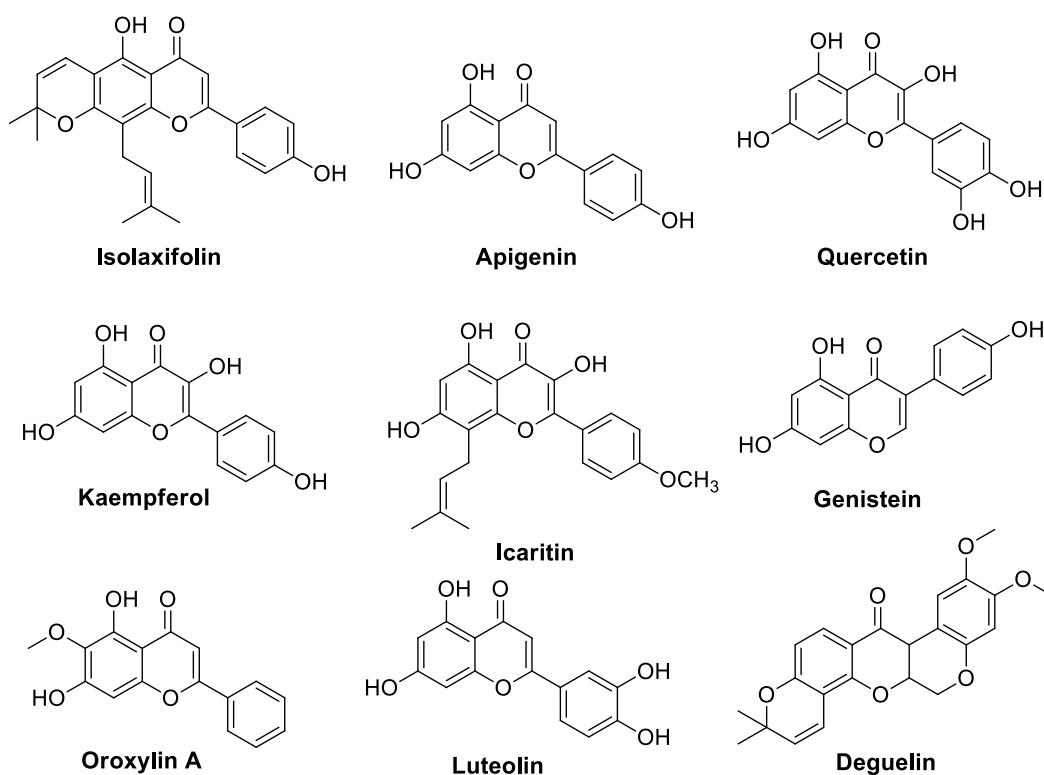
Figure 10 - Chemical structures of several natural chromene-based compounds with anticancer properties.

Chen and coauthors demonstrated in an *in vitro* experiment that isolaxifolin (**Figure 10**) presented cytotoxic effects in breast cancer cell lines MDA-MB-231 and MCF-7, liver cancer cell line HepG2, prostate cancer cell line LNCaP and human colon cancer cell line HCT 116, since it decreased cell viability in 80% at 17.3 µM, 24.2 µM, 24.7 µM, 30.9 µM, and 34.6 µM, respectively [53]. This compound showed no toxicity when tested in a non-neoplastic cell line, at the tested concentrations (LO-2). Isolaxifolin demonstrated a good effect in regulating the latest phases of cell death, in a dose-dependent manner, and stopped cell cycle progression in G_0/G_1 phase in MDA-MB-231 cell line, since the number of cells on that phase increased from 50.4% in untreated cells to 63.3% in cells incubated with 17.3 µM of isolaxifolin, in a dose-dependent manner.

Quercetin (**Figure 10**) is a natural compound widely distributed in plants and fruits, such as red onions, parsley, red grapes and apples, incorporating several biological activities, such as antioxidant, anti-diabetic and anticancer activity [54-56]. This chromene derivative has been extremely exploited due to its biological properties [57]. Lijun Jia *et al.* conducted an *in vitro* study in human breast cancer cell model to assess the effect of quercetin on MCF-7 and MDA-MB-231 cell lines [58]. It was shown that this compound led to the reduction of invading cells and decreased wound closure rate at 30 µM in both cell lines, through transwell invasion and wound healing assays, respectively. The expression of glycolytic proteins like PKM2, GLUT1 and LDHA was also evaluated through Western-blot and the results showed a decreased in the cells protein expression under the effect of quercetin at 30 µM. Furthermore, the effect of this compound was examined in a xenograft mouse model by subcutaneous injection of quercetin (50 mg/kg). The tumor growth was inhibited, and tumor size reduced by approximately 50%, when compared with the control group.

Another study explored the use of nanoparticles incorporating quercetin in an *in vitro* experiment using breast cancer cell model (MCF-7 cells) [59]. The results showed that the proliferation inhibition using the nanoparticle treatment (72 h) was dose- and time-dependent with the inhibition rate of 87% at 100 µM. Additionally, the use of the nanoparticles at 100 µM, in a 72 h treatment, induced late apoptosis in 75.15% of the cells, representing a more efficient treatment when compared to the use of free quercetin (65.97%).

Zhu *et al.* conducted a study to assess the anticancer potential of kaempferol (**Figure 10**), a chromene-derivative commonly found in tea, broccoli, cabbage and also among other plants [60, 61]. This experiment was carried out in a triple negative breast cancer cell model (MDA-MB-231

cells) and showed that kaempferol inhibited cell growth in 50% at 43 µM. This molecule led to the decrease of the number of cells on G_1 phase, from 85.5% to 51.4%, and increased the number of cells on G_2 phase, from 9.3% to 37.5%, arresting the cell cycle in G_2/M phase. Additionally, it was found that kaempferol, at 50 µM, induced the overexpression of apoptotic proteins, such as cleaved caspase 3 and cleaved caspase 9, at different time-points (6 h, 12 h, 24 h and 48 h) [62].

Icaritin (**Figure 10**), a chromene derivative isolated from *Epimedium genus*, is used in Chinese traditional medicine, with important biological properties, namely anticancer activity [63, 64]. Wang *et al.* explored the inhibitory effect of this compound on estrogen receptor-α36 (ER-α36) and EGFR using the triple-negative breast cancer cell model (MDA-MB-231 and MDA-MB-453 cells). Western-blot analysis showed that icaritin treatment reduced ER-α36 and EGFR expression in dose- and time-dependent manner in both cell lines. This compound also demonstrated a growth inhibition rate of 64.2% and 79.3% for MDA-MB-231 and MDA-MB-453 cells, respectively, when used at 5 µM. Finally, the expression of pro-apoptotic proteins, such as PARP, caspase 3 and Bax, was upregulated unlike the expression of Bcl-2 (anti-apoptotic protein), in a dose-dependent manner.

Zhang and coworkers evaluated the anticancer activity of genistein (**Figure 10**), an important natural compound with pharmacological potential, present in most of the edible plants like soybean [54]. The *in vitro* experiment was conducted in liver cancer cell model (HepG2 cells) and cell viability assays demonstrated an half maximal inhibitory concentration (IC_{50}) of 25 µM [65]. The administration of genistein also caused cell cycle arrest in G_2/M phase in a dose-dependent manner, with 34.1% of cells at 50 µM.

Oroxylin A (**Figure 10**) is a natural compound extracted from *Scutellariae radix* with remarkable anticancer activity [66]. Sun *et al.* examined the effects of this compound on MDA-MB-231 cell line (breast cancer cell model), studying the effects on cell proliferation, migration and epithelial-mesenchymal transition. The results showed a reduction of 50% on cell viability when treated with 10 µM for 48 h. For the subsequent experiments, cells were treated with 20 µM for 24 h. The effect of this chromene derivative on cell cycle arrest displayed an increase in cell population in G_1 phase and a decrease in S phase. Furthermore, proteins involved in migration and epithelial-mesenchymal transition were evaluated by qRT-PCR and western-blot. The results showed mRNA and protein expression levels of E-cadherin elevated and downregulation of N-cadherin and vimentin, suggesting an inhibition of proliferation, invasion and migration in MDA-MB-231 cells.

The anticancer effect of luteolin (**Figure 10**), another chromene derivative commonly found in perilla, parsley and other green peppers, was assessed in a human bladder cancer cell model (T24 and 5637 cell lines) [67]. The results obtained from this *in vitro* experiment demonstrated that this compound inhibited cell viability of T24 cells and 5637 cells up to 60% and 40% at 25 μM, respectively. Equally, luteolin showed effect on apoptosis since it increased the number of cells in late apoptosis (25.3% at 25 μM) and induced G_2/M phase arrest in a dose dependent manner. The anti-tumor effect was examined in an *in vivo* experiment using a subcutaneous transplanted BC31 xenograft mouse model. After 5 weeks of treatment with 100 ppm of luteolin, control mice presented a tumor volume of approximately 280 mm^3 and the treated animals a tumor with a volume of 120 mm^3. Additionally, immunohistochemistry of Ki-67, a protein involved in the proliferative process, exhibited less expression on tumors treated with luteolin. These results suggested that this chromene derivative induced apoptosis and blocked proliferative activity in bladder cancer xenograft model.

The extraction of the rotenoid portion from *Mundulea sericea* lead to the isolation of deguelin (**Figure 10**), a natural compound that exhibits chemopreventive and therapeutic activities in several types of cancer, such as colorectal and gastric cancer [68, 69]. Chen *et al.* studied the effect of this compound in human colon cancer model, using SW480, SW620 and RKO cell lines [68]. The results showed that cell viability was inhibited up to 50% at 40.86 nM, 17.73 nM and 13.25 μM, respectively, after 48 h of treatment with deguelin. Western-blot and annexin V-FITC/PI staining assays were performed in SW620 and RKO cells and evidenced the effect of deguelin on apoptosis, since this compound was able to induce an overexpression of apoptotic proteins, such as cleaved caspase-3 and cleaved PARP, in RKO cells and inhibited the expression of anti-apoptotic proteins, like Bcl-2 protein, in SW620 cells. In parallel, the number of apoptotic cells increased in a dose-dependent and time-dependent manner. An *in vivo* experiment was performed in a xenograft five to six-week-old female nude mice model by subcutaneous injection of SW620 cells with subsequent oral treatment with deguelin. The treatment showed low toxicity since deguelin treatment had little effect in body weight over time and suppressed tumor growth of the treated groups (0.702 g) against control groups (1.485 g).

Another study to test deguelin as an anticancer agent was performed in human gastric cancer cell model (MGC-803 and MKN-45 cell lines) [69]. The IC_{50} values obtained after 72 h of treatment were 11.83 and 9.33 μM for MGC-803 and MKN-45 cells, respectively. The effect of this chromene derivative was also evaluated in other aggressiveness parameters and proved to induced cell cycle

arrest at G_0/G_1 phase, in MGC-803 cells and at G_2/M phase at MKN-45 cells, at 10 μM after 48 h of treatment. Furthermore, the mRNA content of deguelin treated cells was assessed, and showed a downregulation of Bcl-2 gene expression and an upregulation of Bax gene expression after 48 h of treatment, with concentrations of 1 μM and 10 μM.

2.1.2. Synthetic chromenes as anticancer agents

Chromene-based compounds have been demonstrated to exhibit potent anticancer properties and the interest in the development of synthetic derivatives has been increasing since several synthetic analogues present a very promising anticancer profile, such as Crolibulin™[50, 51].

Several 3-Amino-1-aryl-1*H*-benzo[*f*]chromene-2-carbonitrile derivatives were synthesized by Ahagh *et al*. and their anticancer potential was evaluated on human colon cancer cell model (HT-29 cells) [70]. The results determined that derivative **1** (**Figure 11**) was the most promising synthetic chromene, with the lowest IC_{50} value (60 μM), after 72 h of treatment. Moreover, this compound affected cell cycle by arresting it in G_1 phase and led to the shifting of early to late apoptosis in HT-29 cells. The expression levels of proteins involved in the apoptotic process were analyzed by Western blot and showed that compound **1** induced expression of caspase 3, 8 and 9, and Bax (pro-apoptotic proteins) and downregulated the expression of Bcl-2 (anti-apoptotic protein). These results suggested an effect of this derivative in the induction of apoptosis and cell cycle arrest.

3-Nitro-2*H*-chromene derivates have been recently exploited as a new class of potent antitumoral agents [71]. An *in vitro* experiment to test the antiproliferative activity of these compounds was conducted using different cancer cell lines, A549 (non-small cell lung cancer), SW1573 (non-small cell lung cancer), HBL-100 (breast cancer), T-47D (breast cancer), HeLa (cervix cancer) and WiDr (colon adenocarcinoma). The results determined that compound **2** (**Figure 11**) possessed the best activity profile towards the six cell lines, since it exhibited the best half maximal growth inhibition concentration (GI_{50}) values, in a range of 0.96 to 2.7 μM.
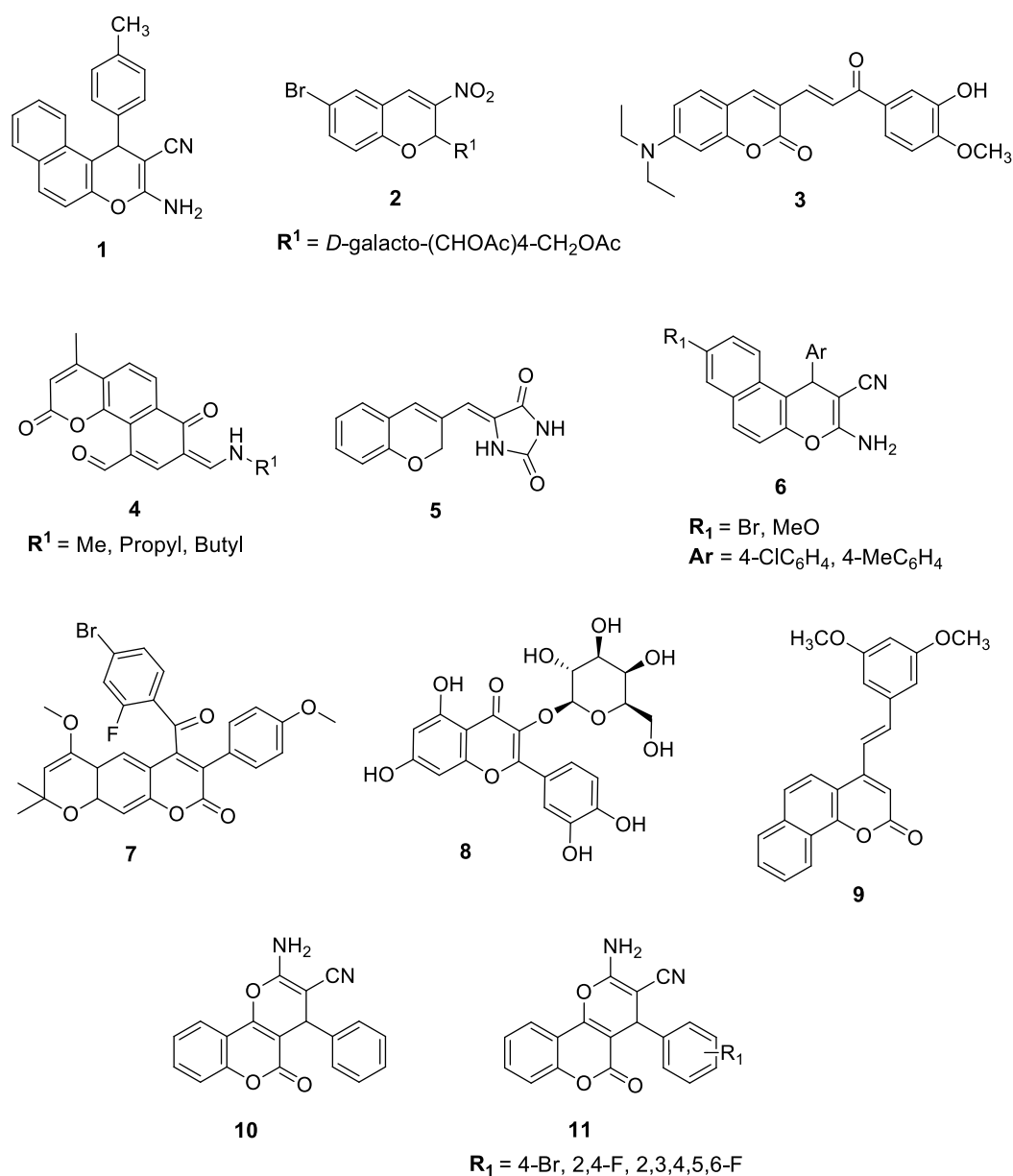
Figure 11 - Synthetic chromene derivatives with anticancer potential, evaluated in several cancer cell models.

Wang *et al.* reported the synthesis of coumarin-chalcone hybrids as thioredoxin reductase (TrxR) inhibitors and analyzed their effect on cell growth inhibition in HCT 116 cell line (colon carcinoma) [72]. The results demonstrated that several synthesized compounds were more active than the used controls, such as xanthohumol, an inhibitor of TrxR. Compound **3** (**Figure 11**) was the most potent compound, since it inhibited 50% of cell growth at 3.60 µM, after 72 h of treatment. Furthermore, the effect of compound **3** was evaluated in the expression of pro and anti-apoptotic proteins, by Western blot technique. The results showed that this compound promoted the

overexpression of Bax and downregulated the expression of Bcl-2 protein levels. It also induced PARP cleavage and mitochondria caspase cascade activation, which led to cell apoptosis.

Sashidhara and coworkers constructed a library of novel benzocoumarin derivatives hosting the natural occurring scaffold of neo-tanshinlactone, known for inhibiting estrogen receptors in human breast cancer cells [73]. The antiproliferative activities of the small library was evaluated using the breast cancer cell model (MCF-7 and MDA-MB-231 cells) and tamoxifen, as a reference compound. The benzocoumarins represented as **4 (Figure 11)** showed promising IC_{50} values in a range of 3.8 to 7.9 µM for MCF-7 cells. Cell cycle of the MCF-7 treated cells with these compounds was analyzed and results demonstrated 70% of the cells in G_0/G_1 phase, demonstrating that these derivatives caused cell cycle arrest. Cell death induction by these compounds was also studied and the number of Annexin V-FITC positive and PI negative cells increased in MCF-7 treated cells, indicating that these cells were undergoing early stages of apoptosis.

A diversity of (2*H*-chromen-3-yl)methylene-azolidinones were synthesized as potential anticancer agents and their effect on cell viability was assessed in several cancer cell models, including human alveolar basal epithelial adenocarcinoma (A549 cells), human chronic myelogenous leukemia (K562 cells), breast cancer (MCF-7 cells), human acute lymphoblastic leukemia (MOLT-4 cells) and in non-cancer cells (mouse embryo fibroblasts, NIH/3T3 cells) [74]. The most promising compound of this *in vitro* study, molecule **5 (Figure 11)**, showed an IC_{50} value of 8.1 µM in MCF-7 cells, exhibiting a cytotoxic effect comparable to cisplatin in this cell line (11.9 µM).

Ahmed *et al.* synthesized a new series of 1*H*-benzo[*f*]chromene derivatives and their effect was evaluated in human breast cancer cell model (MCF-7 cells), human colon cancer (HCT 116 cells) and human liver cancer (HepG2 cells), using two positive controls, Vinblastine and Doxorubicin [75]. The results demonstrated that compounds **6 (Figure 11)** were the most promising examples, showing IC_{50} values in a micromolar range of 0.3 to 1.1 µM. Additionally, the compounds effect in cell death was explored by analysis of the activity of caspases 3 and 7 and showed to enhanced this activity, leading to apoptosis.

Chen *et al.* characterized the anticancer activity of several synthesized chromene derivatives in human leukemia cancer cell model (HL-60 cells), human lung carcinoma (A-549 cells), human hepatic carcinoma (SMMC-7721 cells), human hepatocellular cancer (HepG2 cells) and human cervical carcinoma (HeLa cell) [76]. Compound **7 (Figure 11)** showed to be the most active derivative in HL-60 cells with an IC_{50} value of 16.38 µM, after 48 h of treatment. This derivative

was further investigated in HL-60 cells and showed an inhibitory effect on topoisomerase I even at 0.1 mM. Annexin-V-APC/7-AAD assay of the treated cells demonstrated a growth in the number of apoptotic cells in a dose dependent manner with 66.17% of apoptotic cells at 25 µM after 48 h of treatment. Cell cycle analysis revealed an increase in HL-60 cells in G_1 phase (68.29% at 25 µM), after 48 h of treatment.

The anticancer activity of a well-known flavonoid glycoside, quercetin 3-o-β-d-galactopyranoside **8** (**Figure 11**), was exploited in the breast cancer cell model, using MCF-7 and 4T1 cells [77]. The results showed IC_{50} values of 50 µM and 100 µM for MCF-7 and 4T1 cells, respectively, after 24 h of treatment. It was also demonstrated that this compound induced apoptosis through the decrease of ROS production, suppressing Bcl-2 and overexpressing Bax and Caspase 3 proteins. *In vivo* experiment was carried out using subcutaneous homotransplant mouse model. After 30 days of treatment with the 50mg/kg hyperoside, the control group presented a mean of the tumor volume of approximately 1500 mm³ while the treated group showed a volume of approximately of 750 mm³, supporting the anticancer potential of this compound for the treatment of breast cancer.

A novel class of Benzocoumarin-stilbene-based molecules were synthesized and their anticancer profile was assessed in several cancer cell lines, such as MDA-MB-231 (breast cancer model), 4T1 (breast cancer mouse model), DLD-1 (colorectal adenocarcinoma), PLC/PRF/5 (liver hepatoma), A549 (lung carcinoma), SK-OV-3 (ovarian adenocarcinoma), A-172 (brain glioblastoma) and PANC-1 (pancreatic adenocarcinoma) [78]. From all the compounds tested, chromene **9** (**Figure 11**) demonstrated a good cytotoxic effect against MDA-MB-231 and 4T1 cells with IC_{50} values of 12.5 µM and 11.6 µM, respectively. Caspase 3 and 9 expression was studied by Western blot technique in MDA-MB-231 cells, and the results showed an increase in cleaved caspases 3 and 9 promoting the activation of apoptotic pathway. Furthermore, the antitumor effect of this compound was tested *in vivo*, using syngeneic 4T1 mouse orthotopic breast cancer cell model, at 50 mg/kg and 100 mg/kg, for 32 days of treatment. The results showed an increase of approximately 1250% in tumor size for the control groups while the groups treated with 50 mg/kg and 100 mg/kg demonstrated an increase in tumor size of approximately 800% and 600%, respectively.

In another study, two sets of compounds with chromene-based scaffold, dihydropyranochromenes and chromenopyrimidine-2,5-diones, were synthesized and their effect on MCF-7 cells (human breast cancer model) and HeLa cells (cervical cancer cell model) was

evaluated [79]. From all synthesized compounds, molecule **10** (**Figure 11**) showed the best IC$_{50}$ values of 19 µM and 7 µM in HeLa cells and MCF-7 cells, respectively.

A series of 2-amino-4-aryl-5-oxo-4,5-dihydropyrano[3,2-*c*]chromene-3-carbonitriles were synthesized and their *in vitro* anticancer activity was studied against human cancer cell line (MCF-7 cells), human colon cancer (HCT 116 cells) and liver cancer cell line (HepG2 cells) [80]. The results showed that compounds **11** (**Figure 11**) inhibited 50% of cell growth in a range of 0.2 to 3.1 µM in all studied cell lines. The majority of the tested compounds was capable to increase the number of cells in G$_2$/M phase and decrease significantly the number of cells in G$_1$ cells, causing cycle arrest in G$_2$/M phase. Flow cytometry using Annexin V/PI also displayed indicative results that these compounds increase from 10% to 30% of the total number of apoptotic cells compared to the control cells.

2.1.3. Chromenes in the present work

The compounds that were studied for their anticancer potential in this work are based on the chromene scaffold and were previously synthesized by the organic chemistry group of Doctor Fernanda Proença in the Chemistry Department of the University of Minho.

Different chromene-based compound families were evaluated for their anticancer activity. The first class of chromene-based molecules that were analyzed as potential anticancer agents were recently synthesized by Fabio Conceição during his ongoing PhD thesis work. The newly synthesized 3,5-dihydro-4*H*-chromeno[2,3-*d*]pyrimidin-4-ones **1**, 2,3-dihydro-4*H*-chromeno[2,3-*d*]pyrimidin-4-ones **2**, 2-phenyl-5*H*-chromeno[3,4-*c*]pyridine **3**, 5-(2-hydroxyphenyl)-7-phenylpyrido[2,3-*d*]pyrimidin-4(1*H*)-one **4**, 2-oxo-4-(2-oxo-2-phenylethyl)chroman-3-carbonitrile **5**, 2-amino-4-(2-oxo-2-phenylethyl)-4*H*-chromene-3-carbonitrile **6** and 10-bromo-2,4-diphenyl-4,6a-dihydro-7-oxa-3,4,6-triazabenzo[de]anthracene **7** are represented in **Figure 12**.
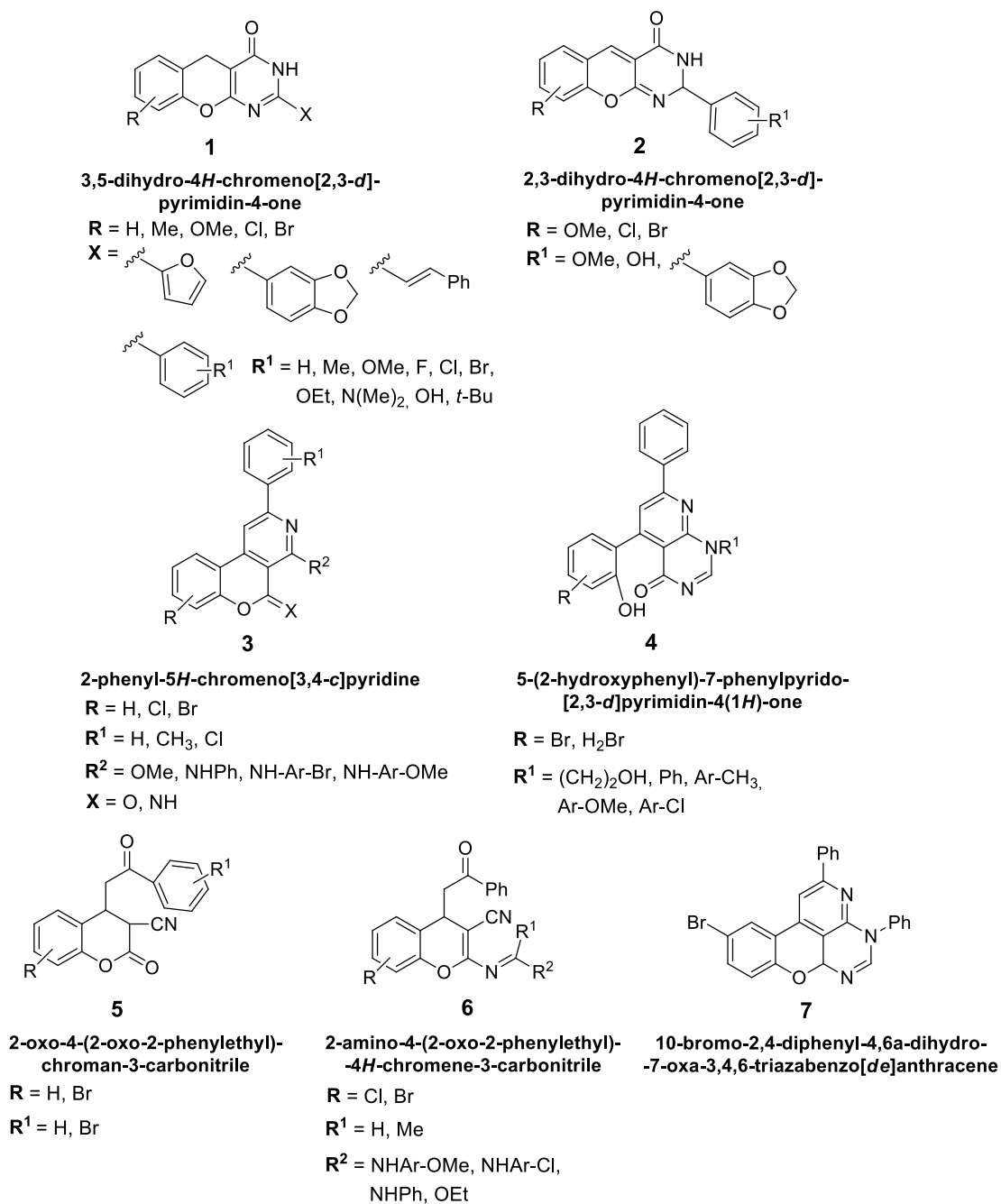
Figure 12 - Chemical structures of the new chromene-based compounds and derivatives explored in this study for their anticancer properties.

Chromeno[2,3-*b*]pyridines **8 (Figure 13)** were synthesized by Diogo Lopes, during his Master's degree thesis in Medicinal Chemistry (2018/2019), under the supervision of Doctors Marta Costa and Fernanda Proença. These compounds were previously screened in the research group for their anticancer activity in three breast cancer cell lines (MCF-7, MDA-MB-231 and Hs578t) and IC_{50} values for the most active compounds were determined. The MCF-10A cell line, a non-tumorigenic

epithelial cell line, was also used to determine the selectivity index of these compounds. In this work, the mechanism of action of the most potent compounds was investigated through the analysis of the protein expression levels of several metabolic and cell death related proteins.
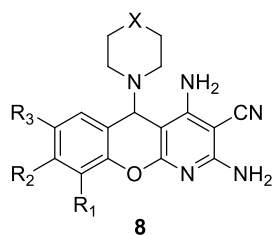
Chromeno[2,3-*b*]pyridines

R^1, **R^2**, **R^3** = H, OMe, Me, Br, Cl, OH
X = N-CH$_3$, N-Ar

Figure 13 - Chromeno[2,3-*b*]pyridines **8**: a family of new chromene derivatives studied in this work, investigated for their mechanism of action.

Aims

Chromene derivatives are an important class of compounds and well represented in nature. The biological activity of natural chromene-based structures led to the development of synthetic analogues, some of them displaying remarkable bioactivities as pharmaceuticals. The continuous effort in drug discovery revealed numerous chromenes with significant anticancer properties in many different cancer cell models, with several molecular targets involved in cancer progression.

Inspired by the collaboration of the Oncology research group of the ICVS (Marta Costa and Fátima Baltazar) and the Organic Chemistry research group of the Chemistry Center (Fernanda Proença), several newly synthesized chromene-based compounds were screened for their potential as anticancer agents, using the breast cancer cell model.

The FD-chromene-based compounds were proposed for a full-screening, in order to analyze their anticancer potential and mechanism of action. This work included:

a)   *In vitro* evaluation of the anticancer activity in several breast cancer cell lines, by cell viability determination (IC_{50}) and assessment of the toxicity of the most active compounds, using a non-tumorigenic breast cell line (MCF-10A);

b)   *In vitro* characterization of the anticancer effect of the compounds with best selectivity index, through the analysis of several cancer aggressiveness parameters as cell proliferation, migration, cell cycle and apoptosis and more specific assays to assess the mechanism of action.

c)   *In vivo* toxicity studies using the *Caenorhabditis elegans* model and *in vivo* efficacy studies to evaluate the ability of the most promising compounds to inhibit tumor growth and angiogenesis, using the Chick Chorioallantoic membrane (CAM) model.

The expectations for this work englobe the identification of one or two lead compounds and the characterization of their mechanism of action. Hopefully, these new lead compounds may represent a promising novelty in BC treatment.

The study of the anticancer potential of another family of compounds, herein designated as DL-chromene-based compounds, was previously initiated within our research group. A full screening of their anticancer potential was performed in the BC model, using several cells lines (MCF-7, Hs578t and MDA-MB-231) and the non-tumorigenic breast cell line (MCF-10A) for toxicity evaluation [81]. Several cancer aggressiveness features were characterized in this study and to further investigate the potential of these chromenes several assays were performed within the scope of this master thesis. In this work, the mechanism of action of DL-chromene-based

compounds was further characterized, by analysis of protein expression levels associated to regulated cell death and cell metabolic pathways, through Western-blot technique.

Chapter II – Materials and Methods

Biological assays

1. Cell lines and culture conditions

Three human breast cancer cell lines Hs578t (basal-like), MDA-MB-231 (basal-like) and MCF-7 (luminal), and a non-neoplastic breast cell line MCF-10A, were obtained from ATCC (American Type Culture Collection). The Hs578t basal-like cancer cell line was cultured in Dulbecco's modified Eagle medium, 4.5 g/L Glucose (DMEM, Biochrom) supplemented with 10% heating activated Fetal Bovine Serum (FBS, Biochrom) and 1% antibiotic solution (Penicillin-Streptomycin, Gibco). MDA-MB-231 and MCF-7 breast cancer cell lines were cultured in Dulbecco's modified Eagle medium, 4.5 g/L Glucose (DMEM, Gibco) supplemented with 10% heating activated Fetal Bovine Serum (FBS, Gibco) and 1% antibiotic solution (Penicillin-Streptomycin, Gibco). The non-neoplastic breast cell line MCF-10A was cultured in Dulbecco's Modified Eagle Medium:Nutrient Mixture F-12 (DMEM/F12, Gibco) supplemented with 5% heating activated Fetal Bovine Serum (FBS, Gibco), 1% antibiotic solution (Penicillin-Streptomycin, Gibco), 1% steroid hormone (Hydrocortisone, Sigma-Aldrich), 0.1% peptide hormone (Insulin, Sigma-Aldrich) and 0.01% protein complex (Cholera Toxin, Gibco). Cells were grown in a humidified incubator at 37 $^\circ$C and 5% CO_2.

For all assays, sub-confluent cells were grown on the incubator for the performed experiments. These cells were first rinsed with phosphate-buffer saline (PBS 1x) and then detached from the flasks using trypsin (TrypLE™ Express, Gibco) at 37 $^\circ$C. To inactivate Trypsin, DMEM 10% FBS or DMEM 5% FBS (MCF-10A) were added to the flask. Then, the cells were centrifuged at 900 rpm, at 4 $^\circ$C for 5 minutes and resuspended in medium. To count the cells, 10 µL of resuspended cells were transferred to a microtube along with 20 µL of Trypan Blue (Trypan Blue Solution 4%, Gibco). The Trypan Blue is used as a dye exclusion test for the determination of the number of viable cells. The principle of this method resides on the fact that living cells sustain their membranes intact, excluding exclusion dyes as Trypan Blue. Considering this, live cells will display a clear cytoplasm, while death cells present blue cytoplasm since their membranes are disrupted. Cells were counted in a Neubauer chamber for posterior density population calculation.

2. Cell viability assays

2.1. Sulforhodamine B

The sulforhodamine B assay was used to assess cell cytotoxicity. The principle of this assay resides on the ability of the protein dye sulforhodamine B to bind to protein basic amino acid residues of trichloroacetic acid-fixed cells. Under acidic conditions, this dye can bind to the amino acid residues, while under basic conditions it can be extracted from cells and solubilized for measurements. This method is appropriate and sensitive to measure drug-induced cytotoxicity. Moreover, it is inexpensive, and the endpoint is colorimetric, nondestructive, and indeterminately stable.

For the screening and IC_{50} values determination of the compounds in several breast cancer cell-lines (Hs578t, MDA-MB-231, MCF-7, MCF-10A), the respective cells were plated in 96-well plates, with a density of 3000 cells per well (100 µL). Cells adhere for 18 to 20 h (overnight) and where then exposed to the compounds at different concentrations, for a total of 72 h of treatment. Controls were performed using DMSO at 0.3%.

After 72 h of incubation with different concentrations, the culture medium was removed and cells were fixated with 50 µL of cold 10% Trichloroacetic acid (TCA) for 1 hour, at 4°C. Afterwards, plates were washed, two to three times, with distilled water to eliminate TCA excess and dried overnight at room temperature. Cells were stained with 50 µL of 0.4% sulforhodamine B for 30 minutes, at room temperature. To remove SRB excess, the plates were rinsed with 1% acetic acid and let to dry overnight. To dissolve SRB crystals, 100 µL of Tris-base buffer (10 mM) were added and the plate was placed in an agitator at room temperature until a homogenous color was obtained in each well. Spectrophotometric measurement of absorbance was read at 490 nm, using 690 nm as background absorbance (Tecan Infinite M200). GraphPad Prism 6 software was used for the calculations of the IC_{50} values from at least three independent experiments, each one in triplicate, applying a sigmoidal dose-response (variable slope) non-linear regression, after logarithmic transformation.

3. Protein extraction and Western-Blot

MCF-7 or Hs578t cells were grown overnight (18-20 h) in 6-well plates in a humidified incubator at 37 °C and 5% CO_2. Then, cells were treated with the respective compounds at their IC_{50} value concentration or 0.3% DMSO (controls) for 24 h and 48 h. After this treatment period, cells were washed with PBS 1x and treated with lysis buffer (50 mM Tris pH 7.6, 150 mM NaCl, 5 mM EDTA, 1 mM Na_3VO_4, 10 mM NaF, 1% NP-40, 1% Triton-X100 and 1/7 protease inhibitor cocktail (Roche Applied Sciences)). Cells were collected by scraping and incubated for 15 minutes on ice and then centrifuged at 13000 rpm for 15 min at 4 °C. The supernatant was collected for protein concentration determination using the Bradford method.

Thirty µg of total protein of each sample were separated on 12% polyacrylamide gel (100 V for 90 min) and transferred to a nitrocellulose membrane (100 V for 30 minutes). Membranes were blocked with 5% milk in TBS 1x for 1 hour before overnight incubation with primary antibodies at 4 °C (Table 2). After washing 5 minutes (twice) and a further 15 minutes (once) with 0.1% Tween 20, blots were incubated for 1 hour with the respective secondary antibodies, at room temperature (Table 2). Once more, washing with TBS/0.1% Tween 20 was performed and immunoreactive bands were detected with chemiluminescent WesternBrightTM Sirius (Advansta, USA) on ChemiDoc XRS + system (BioRad, for DL-based compounds) or Sapphire Biomolecular Imager (Azure Biosystems, for FD-based compounds).

Table 2 - Primary and secondary antibodies used in the Western blot assays.

Antibody designation	Label	Reference	Dilution
Rabbit anti-PARP	Cell signaling	#9542	1:500 5% BSA
Mouse anti-Caspase 9	Cell signaling	#9508	1:1000 5% BSA
Mouse anti-Caspase 8	Santa Cruz Biotechnology	sc-81656	1:1000 5%BSA
Rabbit anti-Caspase 3	Cell signaling	#14220	1:1000 5% BSA
Rabbit anti-Bcl-XL	Cell signaling	#2764	1:500 5% BSA
Rabbit anti-Bad	Cell signaling	#9239	1:1000 5%BSA
Rabbit anti-Bid	Cell signaling	#2002	1:500 5% BSA
Rabbit anti-BIM	Cell signaling	#2933	1:500 5% BSA
Mouse anti-Hif-1α	BD Biosciences	#610958	1:500 5% BSA

Mouse anti-Hif-2α	Abcam	ab8365	1:1000 5% BSA
Mouse anti-Hexokinase 2	Abcam	ab104836	1:1000 5% BSA
Rabbit anti-c-Myc	Cell signaling	#5605	1:1000 5% BSA
Rabbit anti-CAIX	Abcam	ab15086	1:1000 5% BSA
Mouse anti-Glut1	Abcam	ab15309	1:500 5% milk
Mouse anti-GAPDH	Santa Cruz	sc32233	1:1000 5% milk
Mouse anti-LDHA	Santa Cruz	sc137243	1:1000 5% BSA
Rabbit anti-β-tubulin	Abcam	ab6046	1:10000 5% BSA
Goat-anti-rabbit IgG-HRP	Cell signaling	#7074	1:1000 5% BSA
Horse-anti-mouse IgG-HRP	Cell signaling	#7076	1:1000 5% milk

4. Migration assay

Cell migration event was assessed by the wound-healing assay that mimics the cell migration during wound-healing *in vivo*. This method consists in performing a scratch in a confluent well of the plate, simulating a wound in a cell monolayer, and then capturing the images at different regular time-points during cell migration. In the end of the experiment, the taken images are compared to quantify the respective rates, evaluating the effect of the new compounds on cell migration.

Hs578t cells were plated in 6-well plates at a density of 9.0×10^5/well (2 mL) and grown overnight at 37 $^\circ$C in a 5% CO_2 humidified atmosphere. Next, two scratches were made with a 200 µL pipette tip on the cell monolayer of each well. Then, cells were gently washed with 500 µL PBS 1x to remove floating cells. Treatment of the cells with the compounds at the respective IC_{50} and $\frac{1}{2}IC_{50}$ or 0.5% DMSO (control) for 72 h was performed. The images were taken at 0, 12, 24, 48 and 72 h of treatment, at four specific wound sites, with an Olympus IX51 inverted microscope equipped with an Olympus DP20 Digital Camera System using 100x magnification.

Assessment of the migration distances was performed with the MeVisLab platform and the percentage of cell migration normalized to the control was evaluated with the GraphPad Prism 6 software. Three independent experiments were performed for each compound.

5. Proliferation assay

Cell proliferation was evaluated by 5-bromo-2'-deoxyuridine (BrdU) assay (Roche Applied Sciences). This assay is a colorimetric immunoassay based on the quantification of BrdU, a pyrimidine analog, incorporated in cells during DNA synthesis.

Hs578t cells were plated in 96-well plates at a density of 8000 cells/well (100 µL) and grown overnight at 37˚C in a 5% CO_2 humidified atmosphere. The adherent cells were treated with compounds **1.9**, **1.26** and **7** at IC_{50} and ½ IC_{50} concentrations and the controls were treated with 0.5% DMSO, for 24 and 48 h. After incubation, cells were labeled with 5 µL/well of BrdU labeling solution (final concentration of 20 µM) and reincubated for 6 h, enabling BrdU to replace thymidine during DNA synthesis. Then, cells were fixed, and DNA was denatured through incubation with 200 µL of FixDenat solution for 30 minutes at room temperature. After removal of this solution, 100 µL of Anti-BrdU-POD antibody were added during 90 minutes at room temperature. The antibody binds to the recently incorporated BrdU in cells' DNA. The wells were rinsed three times with 200 µL of PBS 1x followed by addition of 100 µL of substrate solution (tetramethyl-benzidine). This solution allowed the detection of the immune complexes, acting until color development (5 minutes) at room temperature. The colorimetric reaction was stopped by adding 25 µL/well of 1 M H_2SO_4. The reaction product was quantified by measuring the absorbance at 450 nm in a microplate reader (Tecan Infinite M200). A blank control was used in each experimental time point, without cells, performing all previously described steps. The results were evaluated with GraphPad Prism 7 software.

6. Cell cycle analysis

Hs578t cells were plated in 6-well plates 8.0×10^4 – 2.0×10^5 cells/well (2 mL) and incubated overnight at 37 ˚C in 5% CO_2 humidified atmosphere. Then, cells were treated with the compounds, **1.26** and **7**, at the respective IC_{50} concentration or 0.5% DMSO (controls) for 24 and 48 h. The culture medium and PBS 1x (500 mL), used to wash the wells, were collected to the respective tubes and 300 µL Accutase® (Grisp) solution was added to the wells to detach the cells, for 10-15 minutes at room temperature. After centrifugation at 1000 rpm for 5 minutes, ethanol solution (70% v/v) was added to fix the cells for 30 minutes at 4˚C. PBS 1x was used twice to rinse the ethanol followed by centrifugation (1200 rpm, 6 minutes, 4˚C) and removal of the supernatant. Fixated cells were labeled with a solution containing PBS 10x (100 µL/mL), PI (50 µg/mL,

Invitrogen), RNase A (20 mg/mL, Invitrogen), Triton-X100 (1 µL/mL) in distilled water. Samples were incubated for 1 hour in the dark at 50 °C and then PI signal was measured using a FACS LSRII flow cytometer (BD Biosciences®) with a 488 nm excitation laser, captured and FACS Diva was used as the acquisition software. The percentage of cells in each phase was analyzed using the FlowJo 7.6 (Tree Star®) software.

7. Cell death assessed by Annexin/PI assay

Hs578t cells ($8.0x10^4$ – $2.0x10^5$ cells/well) were plated in 6-well plates and incubated overnight at 37 ˚C in 5% CO_2 humidified atmosphere to adhere in DMEM medium. Cells were treated with IC_{50} concentrations of the compounds **1.26** and **7** or 0.5% DMSO (control) for 24 and 48 h. Both adherent and floating cells were collected and centrifuged at 1000 rpm, 5 min at 4 ˚C. Then, the supernatant was removed, and the pellet was resuspended in 300 µL Binding Buffer. To this solution, 8 µL of FITC annexin V (BD Pharmingen) and 30 µL of PI (50 ug/mL, P1304MP, Invitrogen), were added. Next, samples were incubated for 15 minutes at room temperature, in the dark. PI signal was measured using a FACS LSRII flow cytometer (BD Biosciences®) with 488 nm excitation laser. The annexin V signal was collected through a 488 nm blocking filter, a 550 nm ion-pass dichroic with a 525 nm band pass.

Signals were captured and FACS Diva was used as the acquisition software. The percentage of cells in each phase was analyzed using the FlowJo 7.6 (Tree Star®) software.

8. Immunofluorescence Assay

Hs578t cells ($7.0x10^4$ – $9.0x10^4$/well) were cultured in 12-well culture plate and adhered overnight at 37 ˚C in 5% CO_2 humidified atmosphere. Cells were treated with IC_{50} concentration of the compounds **1.26** and **7**, paclitaxel (0.5µM) or 0.5% DMSO for 48 h.

Cells were fixed with methanol for 20 minutes at -20 ˚C, washed twice with PBS Tween 0.05% and blocked for 30 minutes in 5% BSA, at room temperature. Cells were incubated 2 h with the primary antibody β-tubulin (Abcam, ab6046, 1:200), at room temperature. After washing three times with PBS Tween 0.05% (5 minutes each), cells were incubated with the corresponding fluorescence conjugated secondary antibody (BD Biosciences, CD11b, 1:500) for 1 hour. Cell nuclei were labeled with 4',6-Diamidino-2-Phenylindole, Dihydrochloride (DAPI), that binds strongly

to adenine-thymine rich regions in DNA. Cells were visualized using a fluorescence microscope (Olympus Widefield Upright Microscope BX61) and images were taken using the objective 10x.

9. Chick chorioallantoic membrane (CAM) assay

This assay was performed to test the *in vivo* efficacy of compounds **1.26** and **7**, on tumor progression and angiogenesis. For this purpose, eggs were incubated at 37 °C (day 0). Then, on the 3rd day of embryo development, a small window was cut in the eggshell to detach the CAM membrane from the eggshell and the eggs were incubated again at 37 °C. On the 9th day of embryo development, $2.0x10^6$ Hs578t breast cancer cells were mixed with 10 μL of Matrigel, to form a gel and graft the cells on the top of the CAM, and again incubated at 37 °C. On the 12th day of embryo development, the shell windows were opened again, and the formed tumors photographed *in ovo* and 20 μL of the IC_{50} solution of each compound were added over the tumor and the window closed again. On the 17th day of development, the eggs were opened, and the tumors were photographed *in ovo*. After that, the embryos were sacrificed at -80 °C for 20 min and the CAM was removed from the egg and photographed *ex ovo*. The images were obtained using a stereomicroscope (Olympus S2 x 16) and a digital camera (Olympus DP71) and the tumor perimeters were determined using ImageJ.

10. Statistical analysis

All graphs and statistical analysis were performed with the GraphPad Prism 6 software. Statistical significance was assessed by the t-test and results are presented as normalized means ± SD.

The results of viability studies and CAM assays are expressed as means ± standard deviation (SD) and were analyzed using one-way ANOVA with GraphPad Prism 7® software (San Diego, CA, USA). Differences between groups were considered significant for $*p < 0.05$, $**p < 0.01$, $***p < 0.001$ and $****p < 0.0001$. All assays were performed in triplicate.
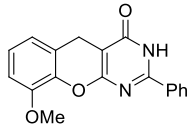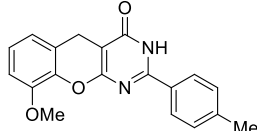
Chapter III – Results and Discussion
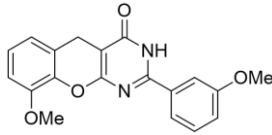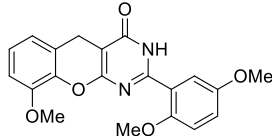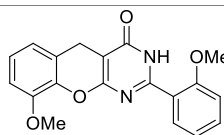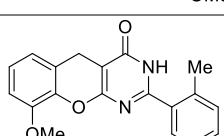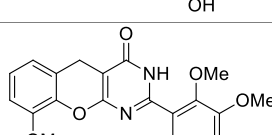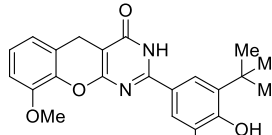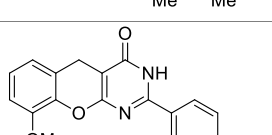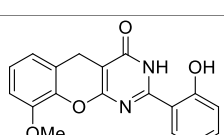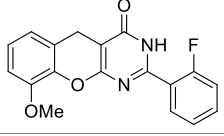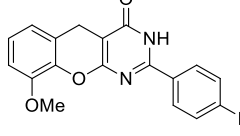
Part I – Anticancer potential of FD-chromene-based compounds
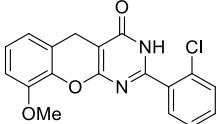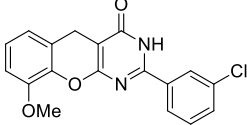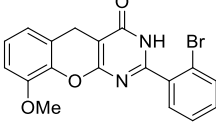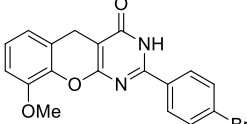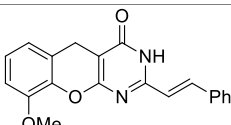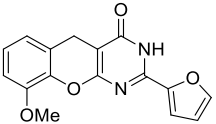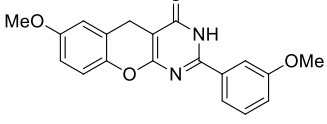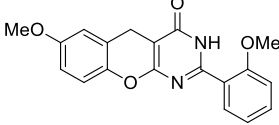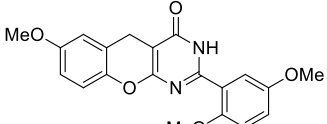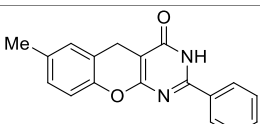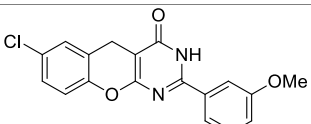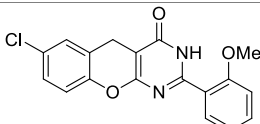
1. Viability screening of the synthesized compounds

All the compounds synthesized by Fábio Conceição were tested for their biological activity in breast cancer cell lines. Initially, a range of 57 compounds were evaluated for their ability to reduced cell viability in Hs578t, MDA-MB-231 and MCF-7 (for compounds **1, Table 3**) or in Hs578t (for compounds **2-7, Tables 4-9**), using SRB assay. To proceed with this study, cells were treated with 10 and 30 μM concentrations of this set of compounds, for 72 h. The concentrations used for this first screening were chosen according to previous results obtained in the research group [82, 83]. The percentage of cell survival was calculated by measuring the SRB incorporation in viable cells. The different sub-families of FD-chromene-based compounds were organized using different tables (**Tables 3-9**). Each sub-family has the same central core, but a diverse substitution pattern around this nucleus and this organization facilitates the evaluation of the influence of specific atoms or groups on the cytotoxic activity. The compounds belonging to FD-**1** and FD-**2** families are characterized by a pyrimidinone ring incorporated in the 4*H*-chromene and 2*H*-chromene core, respectively, in C2-C3 position (**Table 3** and **4**). While FD-**3** molecules incorporate a pyridine moiety in C3-C4 and also 2-imino or 2-oxo groups in C2 (**Table 5**). Compounds FD-**4** present a similar scaffold to the above described molecules, but in this case no intramolecular cyclization occurred leading to the chromene nucleus (**Table 6**). Compounds FD-**5** and FD-**6** (**Table 7** and **8**) display an identical nucleus as FD-**3**, substituted with 2-oxo or 2-imino groups in the C2 position, respectively. Molecule FD-**7** presents a rigid tetracyclic structure with pyrimidine and pyridine rings linked in C2-C3 and C3-C4 positions (**Table 9**).
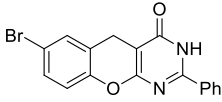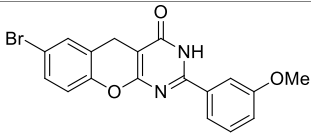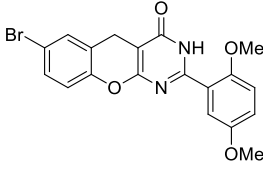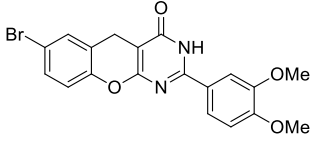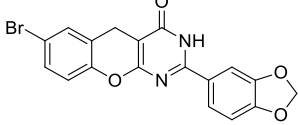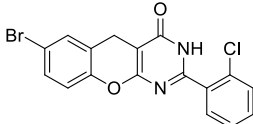
Table 3 - Cell viability results of FD-chromene-based compounds FD-**1.1** - **1.34** in Hs578t, MDA-MB-231 and MCF-7 breast cancer cell lines, after 72 h of treatment with two concentrations (10 and 30 μM).

FD-compounds		Cell viability (%)					
		Hs578t		MDA-MB-231		MCF-7	
		10 μM	30 μM	10 μM	30 μM	10 μM	30 μM
	1.1	91.13	75.79	91.76	89.18	n.d.	
	1.2	86.84	63.27	99.17	91.07	n.d.	

Structure	Compound						
8-OMe chromeno, 2-(3-methoxyphenyl)	1.3	99.3	85.3	n.d.		n.d.	
8-OMe chromeno, 2-(2-methoxyphenyl)	1.4	86.0	80.2	n.d.		n.d.	
8-OMe chromeno, 2-(2,5-dimethoxyphenyl)	1.5	72.69	73.95	87.06	88.43	n.d.	
8-OMe chromeno, 2-(2,5-dimethoxyphenyl)	1.6	74.70	61.92	93.74	98.43	n.d.	
8-OMe chromeno, 2-(2-Me-5-OH-phenyl)	1.7	75.90	67.25	101.55	101.84	n.d.	
8-OMe chromeno, 2-(2,3-dimethoxyphenyl)	1.8	88.2	84.8	n.d.		n.d.	
8-OMe chromeno, 2-(3,5-di-tert-butyl-4-hydroxyphenyl)	1.9	30.02	18.70	68.14	58.56	59.82	43.49
8-OMe chromeno, 2-(4-NMe2-phenyl)	1.10	97.41	87.52	109.97	103.13	n.d.	
8-OMe chromeno, 2-(2-OH-phenyl)	1.11	71.81	62.79	89.21	81.14	n.d.	
8-OMe chromeno, 2-(2-F-phenyl)	1.12	95.34	60.76	81.17	71.18	n.d.	
8-OMe chromeno, 2-(4-F-phenyl)	1.13	97.47	84.40	105.25	97.77	n.d.	

37

(structure)	**1.14**	81.69	72.51	92.53	90.05	n.d.
(structure)	**1.15**	72.02	49.85	80.80	76.91	n.d.
(structure)	**1.16**	66.84	40.59	92.00	80.75	78.41	52.39
(structure)	**1.17**	97.72	84.40	83.73	80.38	n.d.
(structure)	**1.18**	99.75	97.94	99.18	92.52	n.d.
(structure)	**1.19**	99.8	90.7	n.d.	n.d.
(structure)	**1.20**	88.0	77.0	n.d.	n.d.
(structure)	**1.21**	87.5	65.6	n.d.	n.d.
(structure)	**1.22**	95.9	96.5	n.d.	n.d.
(structure)	**1.23**	96.0	73.3	n.d.	n.d.
(structure)	**1.24**	54.7	33.9	n.d.	n.d.
(structure)	**1.25**	91.7	92.0	n.d.	n.d.

Structure	Compound						
6-Br chromene pyrimidinone, 2-Ph	**1.26**	40.17	21.07	62.35	52.06	39.19	36.73
6-Br chromene pyrimidinone, 2-(3-OMe-phenyl)	**1.27**	76.6	34.0	n.d.		n.d.	
6-Br chromene pyrimidinone, 2-(2,5-diOMe-phenyl)	**1.28**	94.12	93.64	102.59	95.04	n.d.	
6-Br chromene pyrimidinone, 2-(3,4-diOMe-phenyl)	**1.29**	86.08	78.54	85.32	77.84	n.d.	
6-Br chromene pyrimidinone, 2-(benzodioxole)	**1.30**	78.41	38.70	88.17	64.96	80.01	57.34
6-Br chromene pyrimidinone, 2-(2-Cl-phenyl)	**1.31**	96.6	84.0	n.d.		n.d.	
chromene pyrimidinone, 2-Ph	**1.32**	76.3	65.4	n.d.		n.d.	
chromene pyrimidinone, 2-(3,5-di-tert-butyl-4-OH-phenyl)	**1.33**	80.2	81.0	n.d.		n.d.	

*The results were obtained from at least three independent experiments, each one in triplicate and the data are presented as mean values.

The viability tests for compounds FD-1 (Table 3) showed that chromenes **1.9**, **1.24**, **1.26** and **1.27** were the most active molecules, in Hs578t cell line. Compounds **1.1-1.19**, bearing the methoxyl group in C9 of the chromene moiety showed in general no capacity to reduce cell viability, although a variety of substituents (H, OH, Me, OMe, NMe2, F, Cl, Br) were introduced in the aromatic moiety of the substituent linked to the pyrimidinone unit. The only exception was observed for chromene **1.9**, incorporing a substituted aromatic group, with two tert-butyl units and a hydroxyl group, in the pyrimidinone core, leading to an excellent reduction of cell viability in Hs578t cell line. Chromenes **1.20-1.23**, bearing the methoxyl or methyl group in C7 of the chromene moiety were not active in this cell line. Halogenated compounds **1.24-1.31** (Cl and Br) in the C7 position of the

39
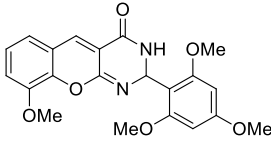
chromene unit were also tested as anticancer agents, with a variety of aromatic substituents in the pyrimidinone moiety (H, OMe, -OCH$_2$O-, Cl) and chromenes **1.24**, **1.26** and **1.27** demonstrated the potential to reduce cell viability. These compounds presented a phenyl group (**1.26**) or 3-methoxy substituent in the aromatic moiety (**1.24** and **1.27**). Compounds **1.32** and **1.33**, unsubstituted examples in the aromatic ring of the chromene unit, led to high viability percentages and did not demonstrate the capacity to inhibit cell viability. Chromene **1.33** incorporated the same aromatic moiety in the pyrimidinone core as molecule **1.9** but without the 9-OMe substituent in the chromene unit, which proved to be essential for the anticancer activity. Molecule **1.32** has the same scaffold as compound **1.26**, however is missing the 7-Br atom in the chromene unit, leading to a total loss of the anticancer activity.
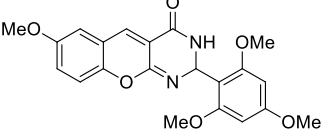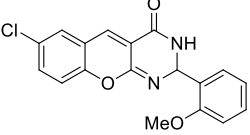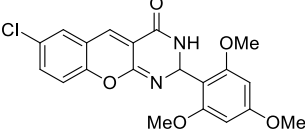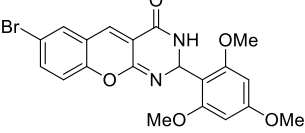
These results showed that the biological activity of this compounds is dependent on very slight modifications in the substituents on both the chromene and pyrimidinone unit, making it very difficult to identify a common pattern that leads to enhanced anticancer activity.

The biological activity of compounds **1.1-1.2**, **1.5-1.7**, **1.9-1.18**, **1.26** and **1.28-1.30** was also tested in other two breast cancer cell lines, MDA-MB-231 (triple negative) and MCF-7 (luminal). Even though MDA-MB-231 is a TNBC cell line as Hs578t cell line, the cell viability results proved that this set of compounds had poor or no anticancer activity. For MCF-7 cells, only four compounds were tested, including **1.9** and **1.26**. The results showed similar cell viability percentages between this cancer cell line and Hs578t.

The FD-**2** compounds (**Table 4**) have a similar structure as FD-**1** chromenes. The only difference is the position where the C-C double bond is located, leading to an 4*H* (FD-**1**) or 2*H* chromene (FD-**2**).

Table 4 - Cell viability results of FD-chromene-based compounds FD-**2.1** – **2.5** in Hs578t breast cancer cell line, after 72 h of treatment with two concentrations (10 and 30 μM).

		Cell viability (%)	
FD-compounds		Hs578t	
		10 μM	30 μM
	2.1	94.8	86.0

		10 µM	30 µM
	2.2	100.3	96.5
	2.3	80.2	90.5
	2.4	96.9	79.5
	2.5	98.4	83.0
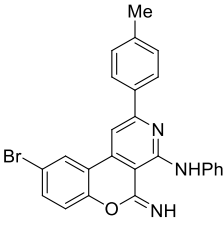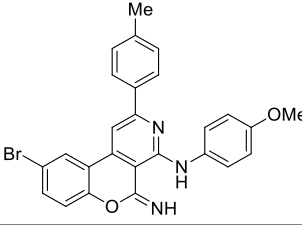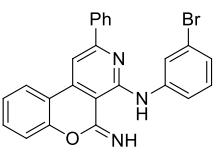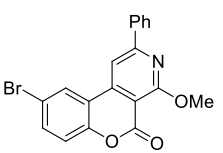
*The results were obtained from at least three independent experiments, each one in triplicate and the data are presented as mean values.

None of the FD-**2** compounds showed anticancer activity, even with halogenated substituents in the chromene moiety. Compound **2.3**, which is the 2*H*-analogue of chromene **1.24**, did not demonstrate the capacity to decrease cell viability.

Chromenes belonging to the FD-**3** compounds (**Table 5**) also incorporate a third heterocyclic unit, linked to the chromene core, but in this case in C3-C4 position and not in C2-C3 as the previous two compound series (FD-**1** and FD**2**).

Table 5 - Cell viability results of FD-chromene-based compounds FD-**3.1** – **3.6** in Hs578t breast cancer cell line, after 72 h of treatment with two concentrations (10 and 30 µM).

FD-compounds		Cell viability (%)	
		Hs578t	
		10 µM	30 µM
	3.1	89.5	92.3
	3.2	92.0	67.1

41
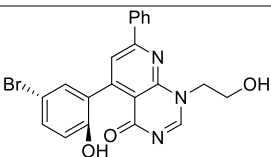
	3.3	99.9	97.2
	3.4	101.0	97.5
	3.5	111.2	101.2
	3.6	95.7	97.7
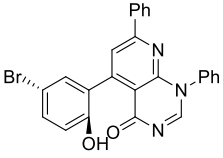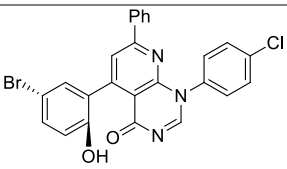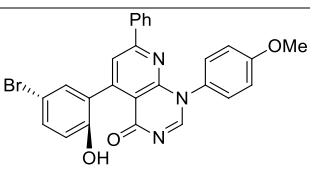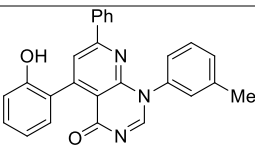
*The results were obtained from at least three independent experiments, each one in triplicate and the data are presented as mean values.

FD-**3** compounds did not exhibit any anticancer activity in the tested cell line. The substitution of the 2-imino group (**3.1-3.5**) by a 2-oxo group (**3.6**) did also not lead to the desired anticancer activity.

Compounds FD-**4** show a similar structure as the previous ones, but in this case no intramolecular cyclization occurred to form the chromene unit, leading to this set of compounds with a more flexible structure (**Table 6**).
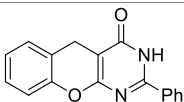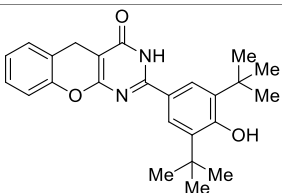
Table 6 - Cell viability results of FD-chromene-based compounds FD-**4.1** – **4.5** in Hs578t breast cancer cell line, after 72 h of treatment with two concentrations (10 and 30 µM).

		Cell viability (%)	
FD-compounds		Hs578t	
		10 µM	30 µM
	4.1	87.4	87.3
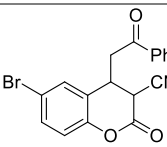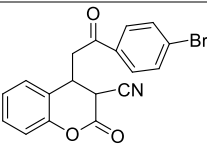
		80.6	46.9
	4.2	80.6	46.9
	4.3	56.9	38.3
	4.4	101.9	52.9
	4.5	102.9	100.0

*The results were obtained from at least three independent experiments, each one in triplicate and the data are presented as mean values.

Compound **4.3** presented a reasonable anticancer activity at 10 and 30 µM concentrations, contrary to the rest of the chromenes of this subset. This activity may be favored by a second halogenated substituent, introduced in the aromatic moiety linked to the pyrimidinone unit.
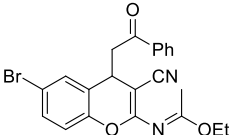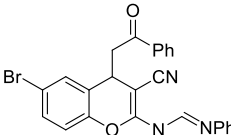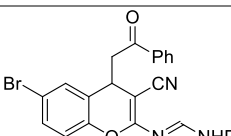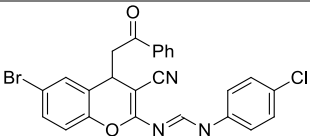
The FD-**5** (Table 7) and FD-**6** (Table 8) compounds have similar core structures, but differ in the substitution in C2, with compounds FD-**5** incorporating a 2-oxo group and compounds FD-**6** a 2-imino group.

Table 7 - Cell viability results of FD-chromene-based compounds FD-**5.1** – **5.2** in Hs578t breast cancer cell line, after 72 h of treatment with two concentrations (10 and 30 µM).

		Cell viability (%)	
FD-compounds		Hs578t	
		10 µM	30 µM
	5.1	99.7	95.1
	5.2	107.7	104.5

*The results were obtained from at least three independent experiments, each one in triplicate and the data are presented as mean values.

Table 8 - Cell viability results of FD-chromene-based compounds FD-**6.1** – **6.4** in Hs578t breast cancer cell line, after 72 h of treatment with two concentrations (10 and 30 μM).
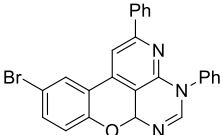
FD-compounds		Cell viability (%)	
		Hs578t	
		10 μM	30 μM
	6.1	97.7	91.4
	6.2	96.1	89.9
	6.3	85.0	93.9
	6.4	99.1	91.9

*The results were obtained from at least three independent experiments, each one in triplicate and the data are presented as mean values.

These compounds (**Tables 7** and **8**) did not present any anticancer activity in Hs578t cells, despite the presence of halogenated substituents in the chromene moiety, contrary to chromenes **1.24**, **1.26** and **1.27**. In the case of compounds FD-**5**, the introduction of a second Br atom in the phenyl group linked to the C=O unit (**5.2**) did not lead to an enhanced anticancer profile, when compared to molecule FD-**5.1**. For compounds FD-**6**, variations in the substituent pattern of the nitrogen atom linked to C2, from smaller (**6.1**) to bulkier aromatic substituents (**6.2**-**6.4**), did also not lead to the capacity to reduce cell viability.

Compound **7** (**Table 9**) has a rigid and planar tetracyclic structure, with two phenyl groups in the pyridine and pyrimidine rings, and a 7-halogenated substituent in the chromene moiety, leading to a good capacity to reduce cell viability.

Table 9 - Cell viability result of FD-chromene-based compound FD-**7** in Hs578t breast cancer cell line, after 72 h of treatment with two concentrations (10 and 30 μM).

FD-compounds	Cell viability (%)		
	Hs578t		
		10 μM	30 μM
(structure)	**7**	50.4	32.6

*The results were obtained from at least three independent experiments, each one in triplicate and the data are presented as mean values.

From this first screening, we selected the compounds with the best anticancer potential for the determination of the $IC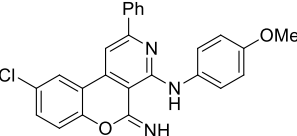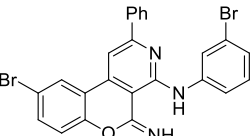_{50}$ values and to assess the respective dose-response curves. Hence, we recruited compounds **1.9**, **1.24**, **1.26**, **1.27**, **4.3** and **7** based on their induced low survival rates of the tested cancer cell lines. Furthermore, the effect of compounds **1.9** and **1.26** on cell survival was also tested in a non-neoplastic cell line, MCF-10A, in order to determine the *in vitro* toxicity of these compounds and selectivity towards cancer cell lines. The use of a non-neoplastic cell line to test the toxicity is important since most of the conventional therapies, such as chemotherapy, involve severe side-effects associated with the drugs scaffold [84-89].

2. Dose response curves and IC_{50} determination

The IC_{50} values of the most promising compounds was determined by SRB assay. Hs578t cells were treated with 7 different concentrations of the selected compounds: **1.9**, **1.24**, **1.26**, **1.27**, **4.3** and **7** using the range of 40, 30, 10, 5, 1, 0.1 and 0.05 μM. In addition, IC_{50} values of compounds **1.9** and **1.26** were also determined for MCF-10A cells, with a concentration range of 60, 45, 30, 10, 5, 1 and 0.1 μM. Doxorubicin (**Figure 6**), a well-known cytotoxic drug, and Quercetin (**Figure 10**), a natural occurring chromene, were used in this assay as reference compounds for breast cancer treatment. The results of the IC_{50} determinations are summarized in **Table 10** and the dose response curves for the most active FD-chromene based compounds are presented in **Figure 14.**

Table 10 - IC$_{50}$ values of chromenes **1.9**, **1.24**, **1.26**, **1.27**, **4.3** and **7** and reference compounds, for Hs578t and MCF-10A cell lines, after 72 h of treatment.

FD-compounds[a]	Breast cell lines		
	Hs578t	MCF-10A	SI[c]
	IC$_{50}$ (µM) ± SD[b]	IC$_{50}$ (µM) ± SD[b]	
1.9	9.08 ± 0.10	> 60	> 5.61
1.24	13.10 ± 0.05	n.d.	n.d.
1.26	4.50 ± 0.29	> 60	> 12.33
1.27	20.23 ± 0.06	n.d.	n.d.
4.3	26.28 ± 0.08	n.d.	n.d.
7	8.63 ± 0.04	n.d.	n.d.
Doxorubicin[d]	0.52 ± 0.01	1.54 ± 0.08	1.96
Quercetin	50.54 ± 0.12	n.d.	n.d.

[a] Each compound was tested at least in triplicate and the data are presented as mean values. [b] Standard Deviation. [c] Selectivity index of Hs578t *vs* MCF-10A. [d] Previously determined by the research group in reference[83].
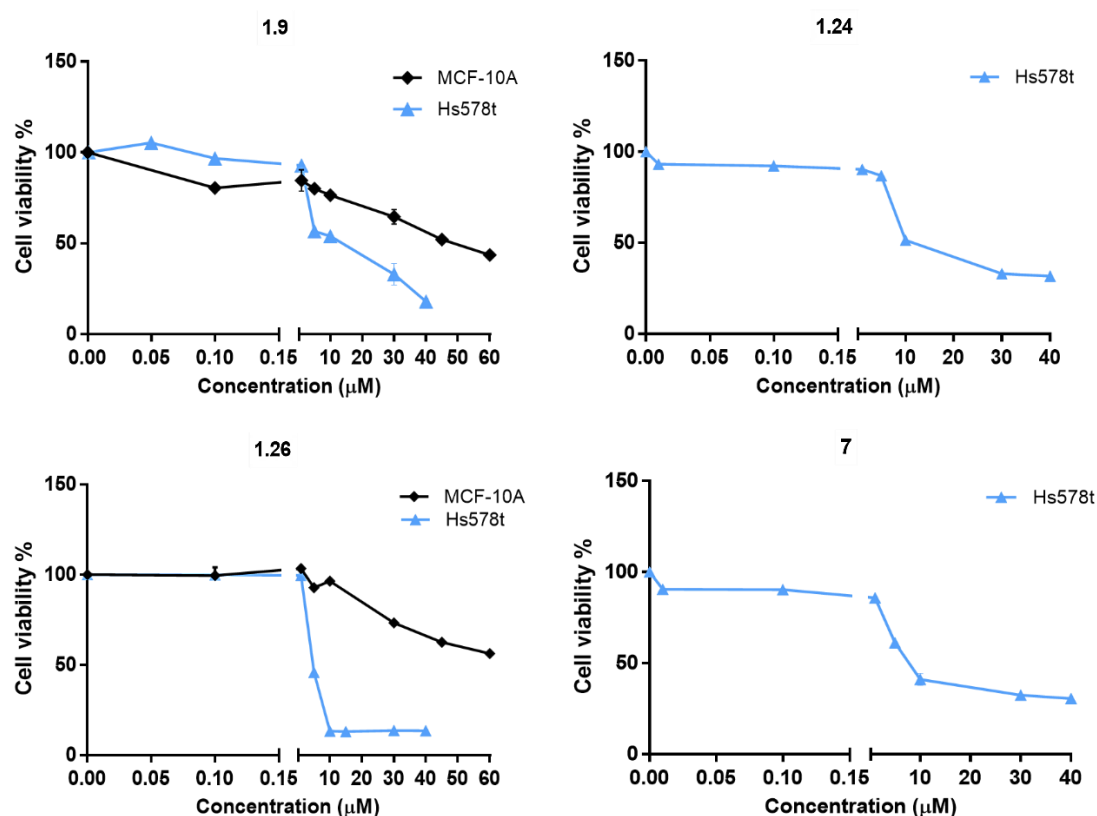
Figure 14 - Dose response curves: effect of FD-compounds **1.9** and **1.26** on Hs578t and MCF-10A cells and of FD-compounds **1.24** and **7** on Hs578t cells, for total cell biomass (72 h of treatment). Results are expressed as mean ± SD.

The FD-chromene-based compounds **1.9**, **1.26** and **7** presented the lowest IC$_{50}$ values (micromolar range) from the set of the tested compounds, in Hs578t cell line. Two of these

chromene derivatives, **1.9** and **1.26**, were also tested in MCF-10A cell line, displaying an outstanding selectivity index (SI) towards cancer cell line Hs578t, when compared with the commercial drug, Doxorubicin (**Table 10**). These compounds exhibited a very promising anticancer activity and selectivity for the tested TNBC cell line.

From these set of compounds, the presence of a halogenated group in the chromene moiety seemed to enhance their anticancer potency, as can be seen for compounds **1.26** and **7** (**Table 10**) with IC_{50} values of 4.50 ± 0.29 and 8.63 ± 0.04 µM, respectively. The chromene derivative **1.9** ($IC_{50} = 9.08\pm0.10$ µM), even not substituted with the same group in the chromene unit and pyrimidinone core as **1.26** and **7**, presented also an increased anticancer potential. The above mentioned three compounds, led to the lowest IC_{50} values in Hs578t cells, and therefore were selected to pursue to further studies to characterize their mechanism of action.

3. Combinatorial potential of compounds 1.9, 1.26 and 7 with doxorubicin: IC_{50} determination.

The compounds that exhibited the best IC_{50} values (**Table 10**) were selected for a combinatorial drug assay with the commercial drug used as reference in this work, Doxorubicin, in Hs578t cells. The drug's IC_{50} value is very low (nanomolar) in this breast cancer cell line, however its SI is poor, meaning that doxorubicin is cytotoxic for non-neoplastic cells as MCF-10A cell line. Regarding this information, the goal of this assay was to combine doxorubicin and our compounds (low micromolar IC_{50}; low toxicity) to potentially bypass the side effects associated with doxorubicin usage in the clinic and to increase the activity of the studied compounds [90-96].

In this experiment, Hs578t cells were treated with a fixed concentration of doxorubicin, equivalent to half of its IC_{50} value (**Table 10**) and with a range of concentrations (30, 10, 1, 0.1, 0.01, 0.005 and 0.001 µM) of compounds **1.9**, **1.26** and **7**. The results of the determined IC_{50} values are summarized in **Table 11**.

Table 11 - IC$_{50}$ values of FD-compounds **1.9**, **1.26** and **7** in combination with ½ IC$_{50}$ of doxorubicin for Hs578t cancer cell line, after 72 h of treatment.

FD-Compounds[a]	Cell viability (%)
	IC$_{50}$ (µM) ± SD[b]
1.9	3.42 ± 0.24
1.26	2.32 ± 0.10
7	1.44 ± 0.06

[a] Each compound was tested at least in triplicate and the data are presented as mean values. [b] Standard Deviation.

All the compounds showed a significantly decreased in their IC$_{50}$ value when combined with doxorubicin, especially compound **7**, which demonstrated the highest decrease in the IC$_{50}$ value. Although the results seemed very promising, the interaction between the compounds and doxorubicin is unknown and need to be further investigated [97-101].This assay needs also to be performed in a non-tumorigenic cell line (MCF-10A cells) to determine if the SI of the tested combinations is favorable. Nevertheless, these results are very promising for this TNBC cell line and represent a possible breakthrough for future therapies, optimizing the dosage concentration administered to the patients when doxorubicin is administered and reducing possible side effects of the conventional chemotherapy.

4. Effect of FD-chromene-based compounds on cell proliferation

In this study, the inhibitory effect of the selected compounds on cell proliferation was assessed by the BrdU assay. Hs578t cells were treated with ½ IC$_{50}$ and IC$_{50}$ values of the compounds, for 24 h and 48 h. This assay measures the capability of BrdU incorporation during DNA synthesis through posterior detection using anti-BrdU antibodies. The results summary is presented in **Figure 15**.
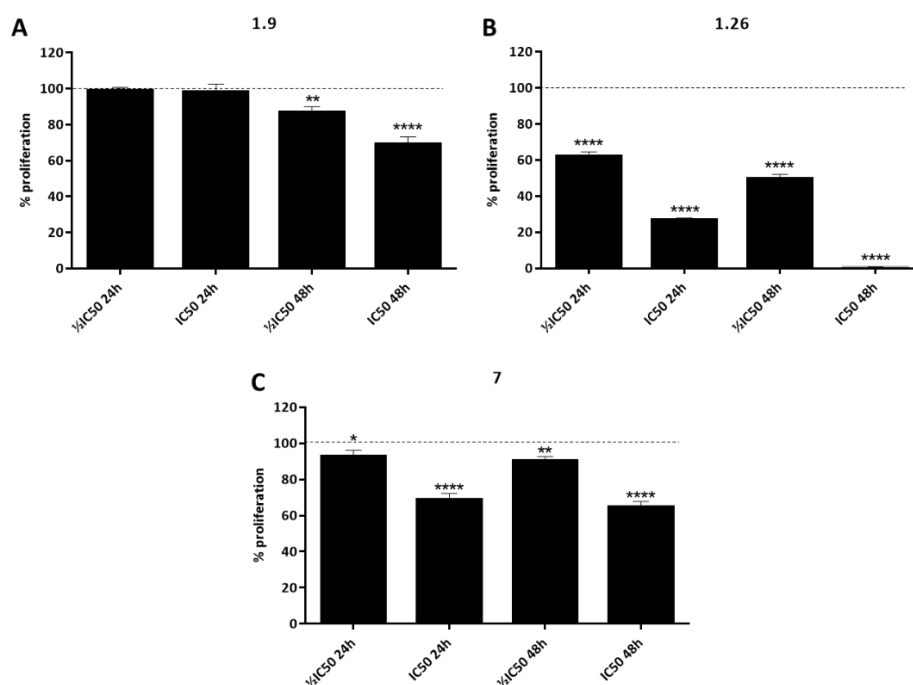
Figure 15 - Effect of FD-compounds **1.9 (A)**, **1.26 (B)** and **7 (C)** on Hs578t cells proliferation, after 24 h and 48 h of treatment. Results are presented as mean ± SD of at least three independent experiments. **** $p<0.0001$, **$p<0.004$, *$p<0.05$ compared to control (0.5% DMSO).

The results indicate that all the selected compounds for this experiment have evident inhibitory effect on Hs578t cells proliferation. Chromene **1.9 (Figure 15A)** presented a different proliferation inhibition profile than chromene **1.26** and **7** since there were no significant differences at 24 h of treatment in comparison to the control (0.5% DMSO). After 48 h of treatment with compound **1.9**, cell proliferation reduced 13% and 30% in cells treated with ½ IC_{50} and IC_{50}, respectively. As seen, the inhibitory effect of this compound relies more strongly on the time of treatment, with a more evident effect for the IC_{50} concentration.

Compound **1.26 (Figure 15B)** displayed the best activity of the studied chromenes at 24 h and 48 h of treatment, in a dose- and time-dependent manner. For this chromene, after 24 h of treatment, cells treated with ½ IC_{50} and IC_{50} suffered a reduction of the proliferation rate of approximately 40% and 70%, respectively. At 48 h of treatment, cell proliferation was reduced up to 50% and 99% in cells treated with ½ IC_{50} and IC_{50} concentrations, respectively.

Similar to chromene **1.26**, compound **7 (Figure 15C)** also inhibited cell proliferation in a dose- and time-dependent manner, since the proliferation rate was reduced in approximately 8% and 30% (24 h of treatment), and in 10% and 35% (48 h of treatment), in cells treated with ½ IC_{50} and IC_{50},

respectively. In this case, the most impacting variable was the compound's concentration and not the time of exposure to the treatment.

Attending to these results, it is possible to conclude that chromenes **1.9** and **1.26** affect cell proliferation in a dose- and time-dependent manner, the latter in a more evident manner. Chromene **7** affects Hs578t cell proliferation rate in a dose-dependent manner.

5.   Effect of FD-chromene-based compounds on cell migration

Migration and invasion are two important features acquired by malignant cells and are crucial for cancer progression and metastasis [7, 102, 103]. The effect of the four most promising compounds on Hs578t cells migration ability was evaluated through the wound-healing assay. In this study, cells were treated with the respective IC_{50} value of each compound for 72 h. Plate images were successively taken at specific timepoints (12 h, 24 h, 48 h and 72 h of treatment) and the progression of scratch closure for each molecule is presented in **Figure 16.**
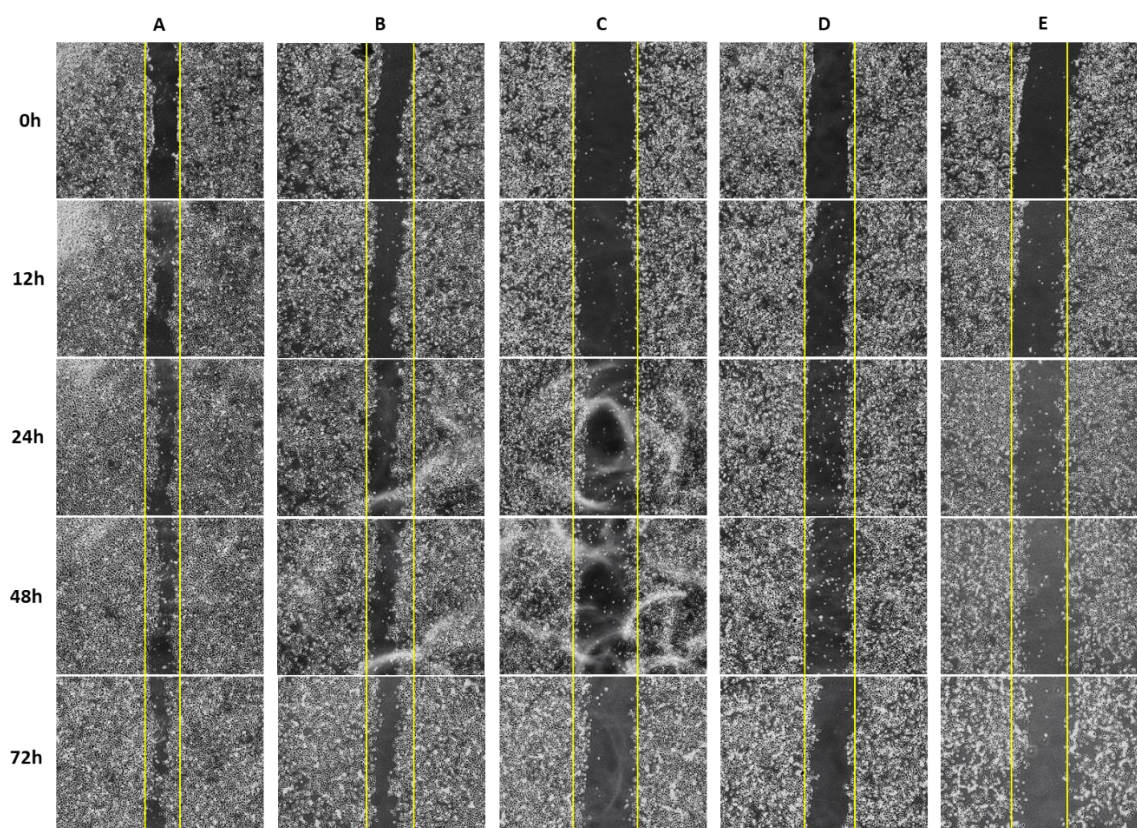
Figure 16 - Representative images of control (0.5% DMSO) (**A**) and effect of FD-compounds **1.9** (**B**), **1.24** (**C**), **1.26** (**D**) and **7** (**E**) on Hs578t cell migration (12 h, 24 h, 48 h and 72 h of treatment with the respective IC_{50} of each compound) by wound healing assay.

As presented in **Figure 16**, the wound-healing assay was successfully performed, since the inserted wound in the non-treated cells was reduced significantly overtime.

In general, all chromene-derivatives tested in this study showed capacity to inhibit wound-healing, although chromene **1.26** outstands with the most effective profile (**Figure 16D**). The treatment with this compound allowed a significant reduction of the cell migration rate to approximately 23%, relatively to the control (0.5% DMSO) after 72 h of treatment. For the cells treated with **1.24** and **7**, the migratory rate decreased to nearly 50% and 60%, respectively, after 48 h of treatment (**Figures 17B** and **17D**), followed by an increase at the 72 h timepoint, possibly associated to cells' ability to recover.
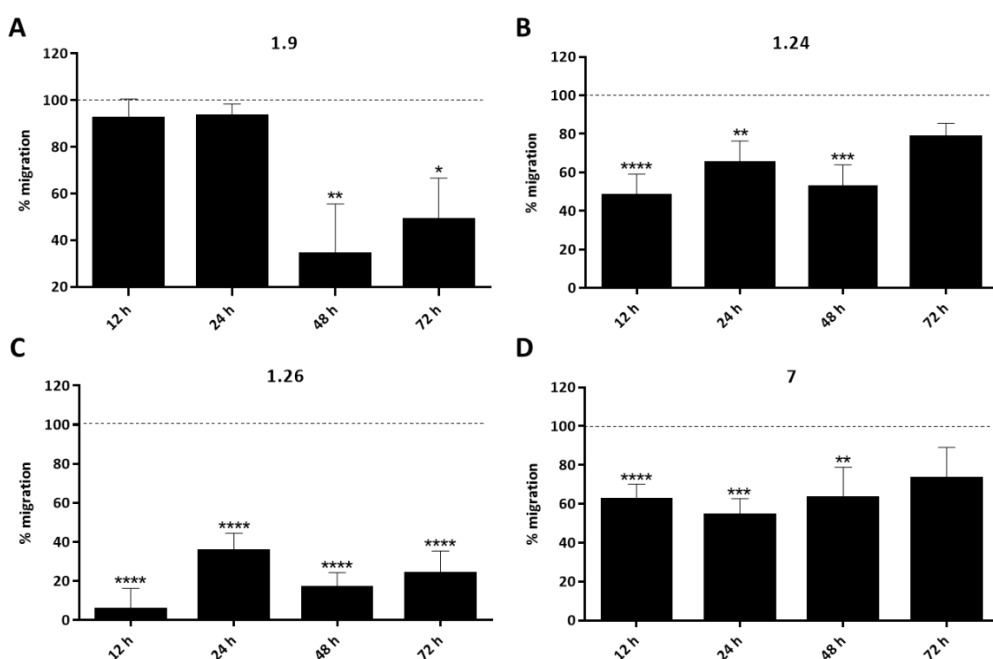
Figure 17 - Effect of FD-compounds **1.9 (A)**, **1.24 (B)**, **1.26 (C)** and **7 (D)** on Hs578t cell migration, measured at regular timepoints (12 h, 24 h, 48 h and 72 h) of treatment. Results are presented as mean ± SD of at least three independent experiments. **** $p<0.0001$, ***$p<0.0007$, **$p<0.01$, *$p<0.05$ compared to control (0.5% DMSO).

Chromene **1.9** displayed a different dynamic of action since cell migration rate remained at around 90% after 12 h and 24 h of treatment. Then, the cell migration rate abruptly decreased to 34% at 48 h of treatment and increased to nearly 50% at the last timepoint. This result can be related to the slower activity profile, associated to this compound, also observed in other studies, such as the proliferation assay (**Figure 17A**).

6. Effect of FD-chromene-based compounds on regulated cell death

Chromenes and derivatives are known for their anticancer activity through diverse mechanisms of action, affecting cell viability, metabolic pathways and other features of the tumorigenic events [54, 64, 75, 104]. These natural or synthetic compounds can also induce cell cycle arrest and/or cell death through apoptosis [105, 106].

Apoptosis is a rational and active decision made to sacrifice specific cells for the greater well-being of an organism, unlike necrosis which is a more traumatic cell death [107]. Both external and internal death signals are transmitted through signaling pathways which leads ultimately to the activation of a type of serine proteases, the caspases, responsible for the execution of cell destruction. There are three pathways by which these proteases can be activated, the extrinsic and intrinsic pathways and the less known intrinsic endoplasmic reticulum pathway. The first two pathways are represented in **Figure 18**.
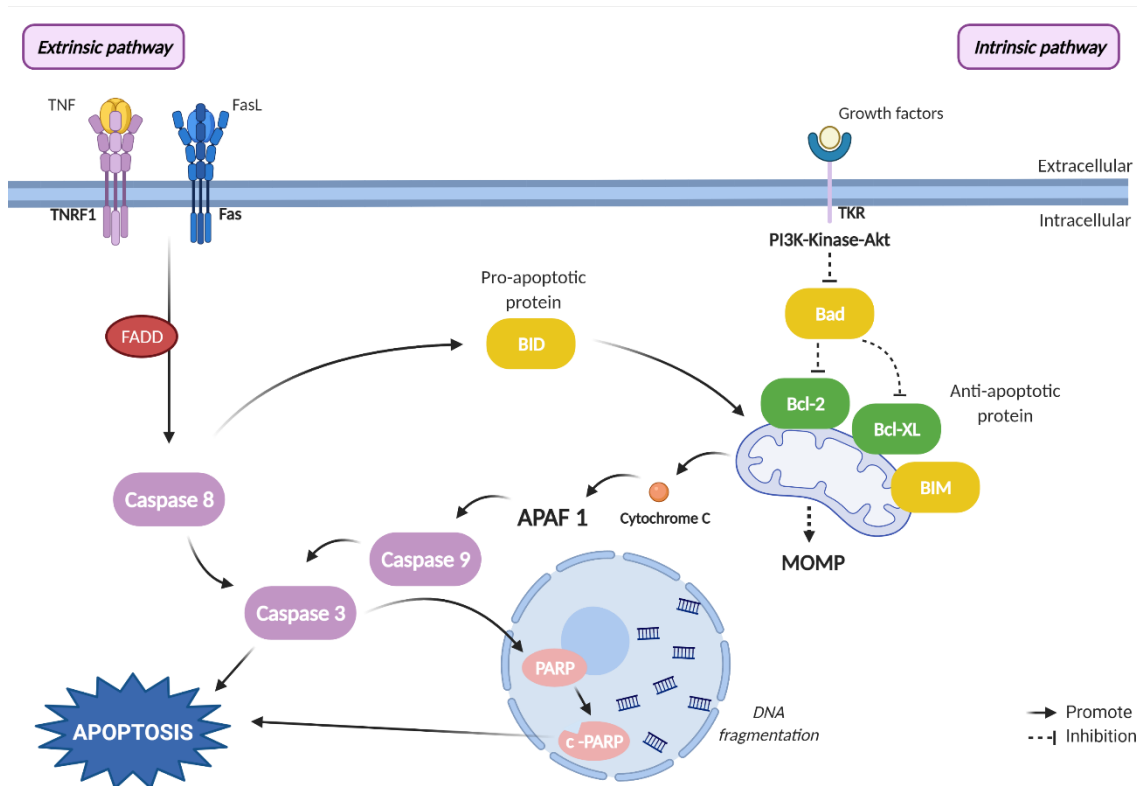
Figure 18 - Representative image of the two major apoptotic pathways, extrinsic and intrinsic, in mammalian cells. (Adapted from [108, 109])

The extrinsic pathway initiates when TNF and Fas ligands bind to the death receptors, type 1 TNF receptor (TNFR1) and to a related protein called Fas respectively, present in the cell membrane

[110]. The activation of this pathway recruits caspase 8, which initiates apoptosis by cleavage of downstream executioner caspase 3.

Most stimuli induce apoptosis via intrinsic pathway or mitochondrial pathway. The key event on this pathway is the mitochondrial outer membrane permeabilization (MOMP) [111]. Once this process occurs, several proteins are released into the cytosol, including cytochrome c, which assumes a lethal function by activating the caspases cascade. The activation of caspase 9, an initiator and an effector protein, will lead to the cleavage and, consequently, activation of caspase 3 that unleashes several catabolic mechanisms affecting cell stability [110, 112, 113].

Finally, the less studied third pathway revolves around the injuries that cellular stressing conditions cause to the endoplasmic reticulum, like hypoxia, glucose starvation and free radicals [110]. These conditions cause the unfolding of proteins and the reduction of the protein synthesis rate within the cell, causing dissociation of TNF receptor associated factor 2 (TRAF2) from procaspase 12, activating the caspase cascade.

The expression levels of the proteins involved in cell death events were analyzed through Western-blot technique. In this study, Hs578t cells were treated with IC_{50} concentrations of the compounds **1.9**, **1.24**, **1.26** and **7**, during 24 h and 48 h.

Generally, all compounds induced cell death through apoptosis on Hs578t cells since the expression levels of pro-apoptotic proteins, such as PARP, caspase 8 and 9, were evident at 24 h and 48 h of treatment, as showed in **Figure 19A**.

A
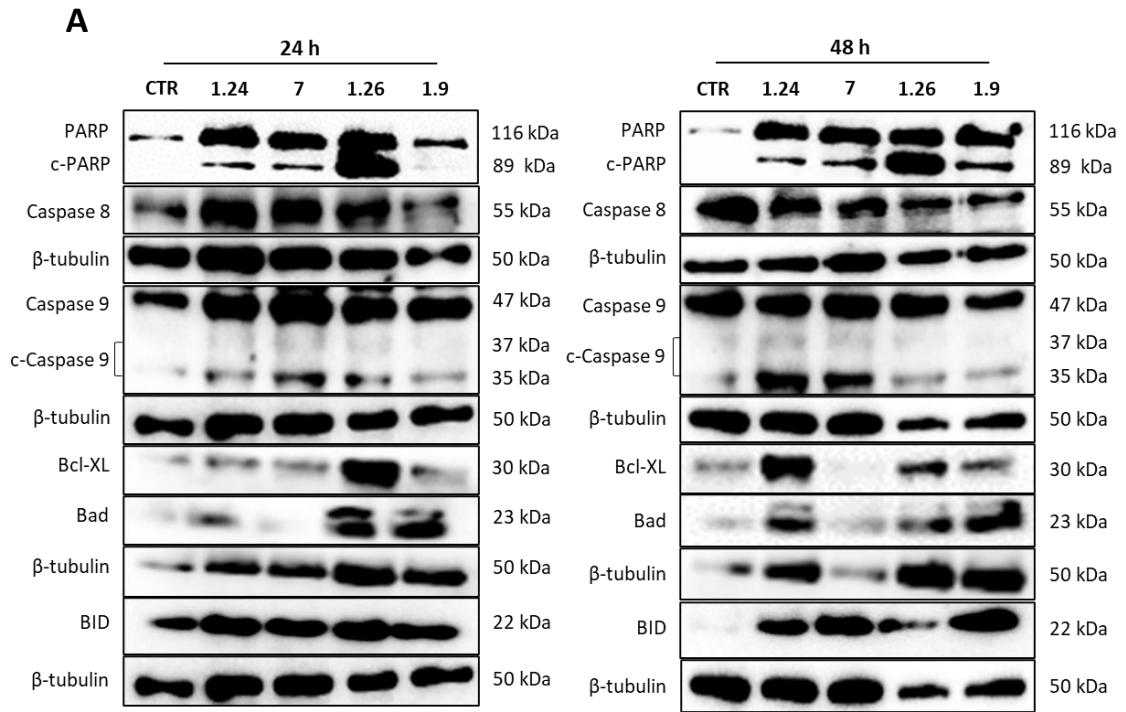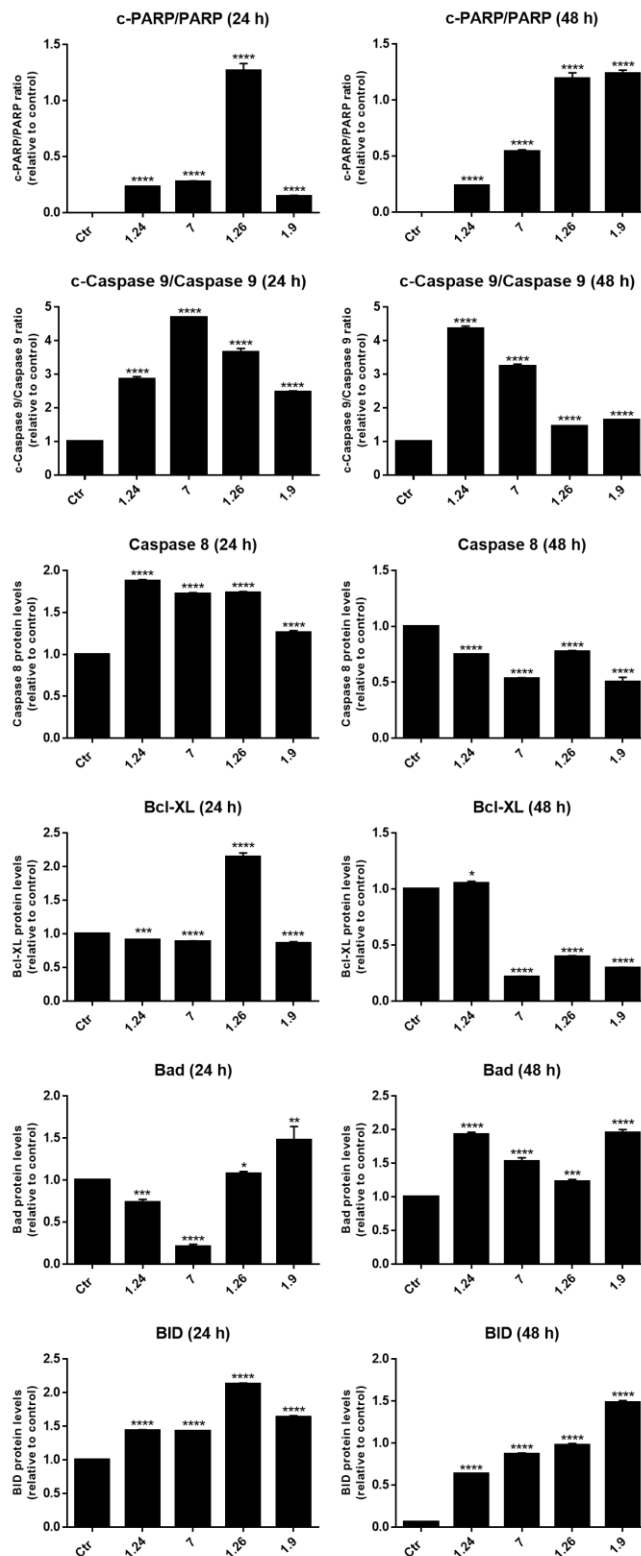
Figure 19 – A) Representative immunoblots of Hs578t cells treated for 24 h and 48 h, with FD-compounds **1.9**, **1.24**, **1.26** and **7**. Similar blots were obtained from at least 3 independent experiments. **B)** Quantification of the c-PARP/PARP and Caspase 9 ratios and the protein levels of Caspase 8, Bcl-XL, Bad and BID, after 24 and 48 h of incubation of Hs578t cells with FD-compounds **1.9**, **1.24**, **1.26** and **7**. Values are mean ± SEM of 3 independent experiments. **** p<0.0001, ***p<0.001, **p<0.007, *p<0.02 when compared with control by the Student's t-test.

The caspase cascade activation is the main mechanism involved in regulated cell death [114]. The initiators caspase 8 and 9 are two members of the cysteine proteases family and are responsible for triggering the extrinsic and intrinsic apoptotic pathways, respectively. Both pathways converge to the cleavage and consequent activation of the downstream caspase C3 (executioner), as represented in **Figure 18** [115]. The quantification of the protein levels of the performed immunoblot results for C8 and C9 (**Figure 19B**) showed that all the compounds tested induced their expression after 24 h of treatment. For the second timepoint (48 h), a significant decrease in the C8 expression was observed, although more significant for compounds **1.9** and **7**. Regarding the expression levels of C9, all the tested chromenes provoked a significant increase in comparison to control cells (0.5%DMSO), however chromene **1.24** and **7** in a more evident manner.

The poly ADP-ribose polymerase (PARP) plays a key role in DNA repair single-strand breaks and, when activated, represents an important death marker in apoptosis [116, 117]. PARP activation involves its cleavage promoted by a setting of proteases belonging to the Interleukin-1ß-converting enzyme (ICE) family. As observed in **Figures 19A** and **19B**, the protein levels of PARP and cleaved PARP increased after 24 h of treatment. All the compounds contributed to the increase of c-PARP/PARP ratio, being this increase even more evident for chromene **1.26**. At 48 h, this ratio also increased for all the tested compounds, especially for the cases where compounds **1.26** and **7** were applied.

Concerning Bcl-2 family proteins, Bcl-XL, BID and Bad are involved in the regulation of the intrinsic apoptotic pathway (**Figure 18**), through the balance of the pro (BID and Bad) and anti-apoptotic (Bcl-XL) proteins within the mitochondria. Once these proteins are activated by intrinsic stimuli, their interaction promote the formation of the MOMP complex. This event triggers a cascade of events that culminates in the activation of caspase 3, leading to cell death [118]. Regarding the expression levels of the anti-apoptotic protein Bcl-XL (**Figure 19B**), at the first timepoint, the compounds were capable to reduce the effect of this protein, with the exception of compound **1.26**, that promoted a significant increase on this protein levels expression. After 48 h of treatment, the levels of Bcl-XL were significantly reduced when cells were treated with chromenes **1.9**, **1.26** and **7**.

The quantification results for the protein levels related to the pro-apoptotic Bad expression levels (**Figure 19B**) demonstrated an increase when cells were treated with compounds **1.9** and **1.26**, after 24 h of treatment. However, for compounds **1.24** and **7** a decrease on the proteins levels

was observed. At the following timepoint, all the tested compounds were capable to induce the overexpression of the protein, when compared to the control cells. Bad is a pro-apoptotic protein and a downstream signal of PI3K-Kinase-Akt pathway. In most mammalian cells, the pro-apoptotic protein Bad is associated by affinity to Bcl-XL (anti-apoptotic) and the activation PI3K-Kinase-Akt pathway causes Bad phosphorylation, promoting its dissociation from Bcl-XL. The free Bcl-XL suppresses apoptosis and promotes cell survival [119]. In view, chromenes **1.9**, **1.26** and **7** were able to activate the expression of pro-apoptotic protein Bad and inhibit the expression of anti-apoptotic protein Bcl-XL, past 48 h of treatment. At the same timepoint chromene **1.24** significantly prompted Bad expression as well.

Lastly, the pro-apoptotic protein BID is activated by the initiator C8 of the extrinsic pathway but exercises its role in the intrinsic pathway (**Figure 18**). This activation results from its cleavage and consequent association with the mitochondria membrane, promoting the MOMP [120]. The results (**Figure 19B**) showed that levels of BID increased significantly for chromenes **1.9**, **1.24**, **1.26** and **7**, for both timepoints, in comparison to control cells treated with 0.5% DMSO.

In general, all the tested compounds in this work induced regulated cell death in Hs578t cells at studied timepoints. Chromenes **1.9**, **1.26** and **7** exhibited an interesting effect over the protein expression patterns analyzed in this section, since these three molecules promoted the overexpression of several pro-apoptotic proteins and suppressed the expression of the anti-apoptotic protein Bcl-XL. Chromene **1.24** also induced apoptosis, although demonstrated a less effective capacity to reduce anti-apoptotic protein levels of Bcl-XL after 48 h of treatment, when compared to the remaining compounds (**Figure 19B**).

To further validate the ability of the studied chromenes to induce apoptosis, flow cytometry was performed using annexin V-FITC and PI (V/PI) staining. This staining is widely used to determine if cells are viable, in apoptotic or necrotic stages, through the integrity of the plasma membrane [121, 122]. Apoptosis involves a variety of processes that compromises cell membrane integrity, causing the loss of phospholipid asymmetry. The early apoptotic cells membrane integrates a particular molecule, phosphatidylserine, in the outer membrane that is capable to interact with annexin V [123]. The propidium iodide (PI) is a nuclear stain and a good cell viability indicator since it can be excluded in living cells, depending on the cell membrane permeability [124]. The combination of both allows the distinction between viable cells, early apoptotic, late apoptotic, and necrotic cells.

Chromenes **1.26** and **7** were selected to perform this experiment since they exhibited the most promising anticancer activity (**Table 10**). Their previous results from Western-blot technique demonstrated a high potential to mediate cell death through apoptosis, verified by the overexpression of pro-apoptotic proteins and suppression of the anti-apoptotic protein (**Figures 19A and 19B**). Briefly, Hs578t cells were treated with IC_{50} concentrations of each compound or 0.5% DMSO (control), for 24 h and 48 h. Then, cells were collected and stained with annexin V-FITC and PI, and the results are presented in **Figure 20**.
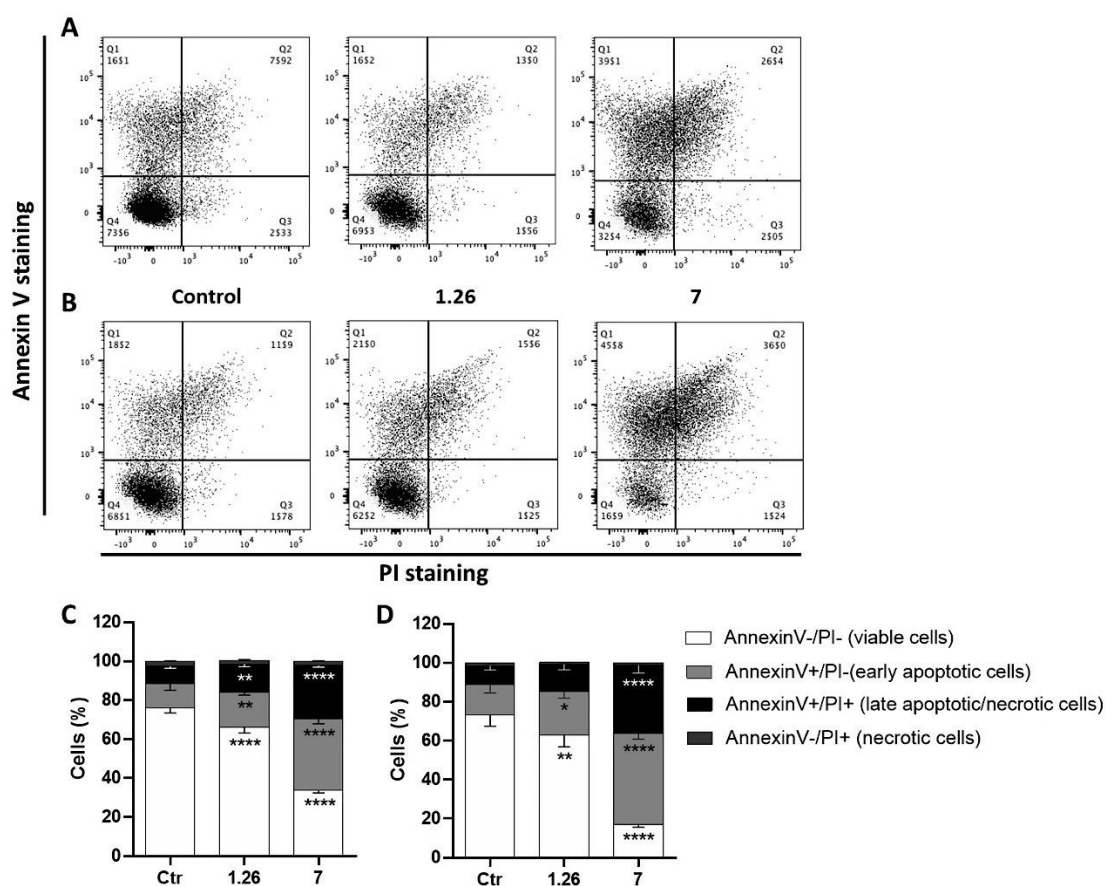
Figure 20 - Flow cytometry analysis of the viability of Hs578t cells assessed by annexin V/PI assay. Representative dot plots of Hs578t cells untreated (control) or treated for **(A)** 24 h and **(B)** 48 h with IC_{50} concentrations for FD-compounds **1.26** and **7**. Graphical representation after quantification of the percentage of cells in each quadrant of the dot plot for **(C)** 24 h and **(D)** 48 h. The results were obtained using the non-treated cells as control and mean ± SEM. Annexin V/PI data was analyzed by two-way ANOVA and Bonferroni post hoc test, **** $p<0.0001$, ** $p<0.002$, * $p<0.03$.

Analysis by flow cytometry revealed a significant decrease in cell viability for cells treated with chromenes **1.26** and **7** after 24 h and 48 h (**Figure 20**). Additionally, the treatment of Hs578t cells with chromene **7** demonstrated an increase in the percentage of early and late apoptotic cells, in

comparison to the control cells for both timepoints. The increase in the percentage of early apoptotic cells of approximately 50%, caused by the treatment with this compound, was remarkable at the 48 h timepoint. The viability of this cell line was also affected by the treatment with chromene **1.26**. This result was supported by the increase of the percentage of early apoptotic cells verified at 24 h and 48 h, accompanied by the decrease in viable cells. Moreover, this compound also promoted the significant increase of late apoptotic cells at 24 h.

The gathering of the information provided in **Figures 19A, 19B** and **20** suggest that apoptosis is the mechanism by which the tested chromenes induced cell death in Hs578t cells. Both chromenes **1.26** and **7** induced a similar effect in cell death, although compound **7** seems to potentiate even more this regulated cell death mechanism.

Many studies associated with the effect of chromene derivatives in different cancer cell lines (HL-60, MCF-7, MDA-MB-231) have proven the ability to induce cell death through apoptosis [125-128]. For example, a study conducted in the research group showed that a 4*H*-chromene derivative triggered programmed cell death in MCF-7 cell line [28]. Moreover, novel chromene derivatives fused with the imidazo[1,2-*a*]pyridine nucleus were also synthesized by these research group and demonstrated a good anticancer activity in HCT 116 cells, leading to the activation of apoptotic mechanisms [129].

7. Effect of FD-chromene-based compounds on cell cycle

The duplication of the genetic material and cell division events are ensured by the cell cycle, a highly regulated process that involves four phases, G_1, S, G_2 and M [130]. In cancer cells, the cell cycle activity is characterized as aberrant, with unscheduled cell division leading to uncontrolled cell growth. This overactivity is resultant from upstream mutations in signaling pathways or genetic lesions within genes encoding cell cycle proteins [131].

There are multiple research articles focusing on potential chromene derivatives as anticancer agents for several human cancer cells, including breast cancer, presenting cell cycle arrest capability [28, 126, 127, 129, 132]. Alblewi *et al.* confirmed the effect of the newly synthesized 2-substituted 4*H*-benzo[*h*]chromene and 7*H*-benzo[*h*]chromeno[2,3-*d*] pyrimidine derivatives on MCF-7, HCT 116 and HepG2 cell lines by arresting cell cycle in G_2/M phase [44]. In 2015, another

study was conducted with novel biomolecules inspired in the chromene unit that also demonstrated HTC-116 cell cycle arrest induction by the treatment with the respective compounds [129].

To evaluate the effect on cell cycle of chromenes **1.26** and **7**, the two most promising compounds of the analyzed set, Hs578t cells were stained with PI, and analyzed by flow cytometry after 24 and 48 h of treatment, for determination of the DNA content (**Figure 21**).
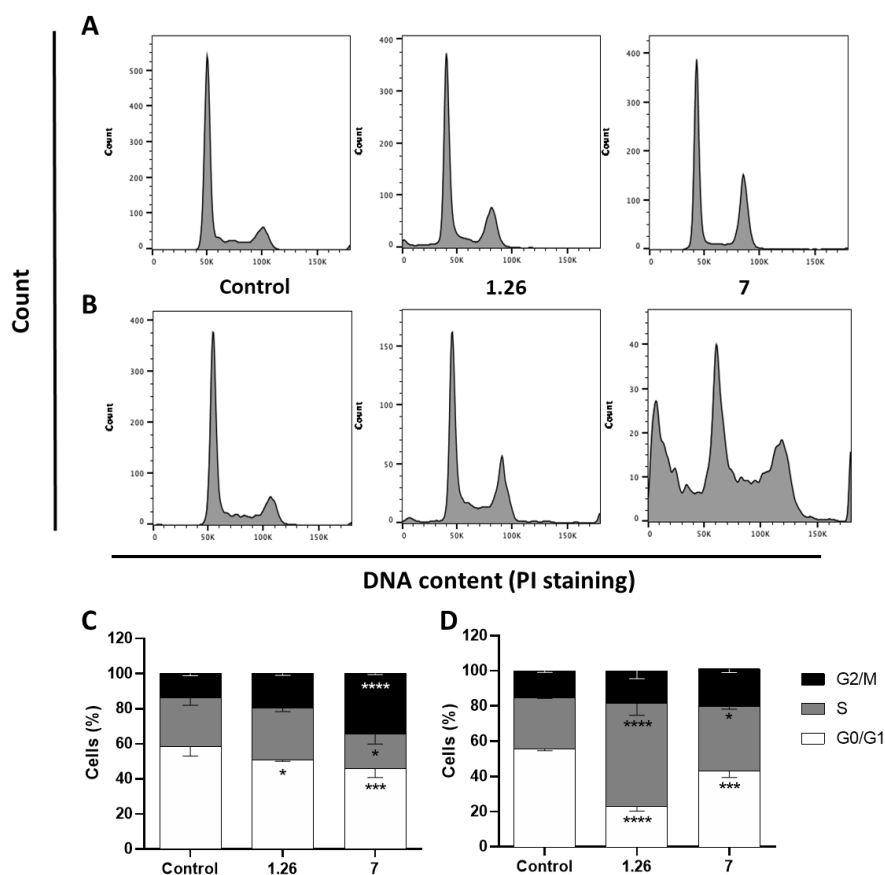
Figure 21 - Flow cytometry analysis of the DNA content of Hs578t cells. Cell cycle profile of Hs578t cells untreated (control) or treated for **(A)** 24 h and **(B)** 48 h with the IC_{50} values of FD-compounds **1.26** and **7**. Graphical representation after quantification of the cells in different phases of cell cycle **(C)** after 24 h and **(D)** 48 h of treatment. Data was analyzed by two-way ANOVA and Bonferroni post hoc test. ****$p<0.0001$, ***$p=0.0007$, *$p<0.05$ compared to control.

As presented in **Figure 21**, both chromenes **1.26** and **7** were able to arrest cell cycle in Hs578t cells. Regarding to the effect of chromene **1.26**, this molecule was able to induce a decrease in the G_0/G_1 cell population, while exhibiting no significant effect in S and G_2/M cell fractions. A severe reduction of G_0/G_1 population was registered at 48 h, while an impressive accumulation of cells in phase S occurred. These results corroborate the cell cycle arrest inducing profile of this compound (**Figures 21B** and **21D**).

Chromene **7** initially caused an increase of G_2/M cell population in comparison to the control cells, followed by a decreased of cells in phases S and G_0/G_1. At the second timepoint, it was noticed a slight cell accumulation at S phase, as observed in **Figure 21**.

8. Effect of FD-chromene-based compounds on metabolic key points

Carcinogenesis is a process that involves several steps in order to transform a normal cell into a cancerous cell [7, 133]. The cellular metabolism reprogramming is a hallmark of cancer and a key factor in carcinogenesis since it is needed to satisfy the altered cell energy demands [134-137]. The metabolic signaling pathways in cancerous cells are severely modified. Breast cancer cells are characterized by a high glycolytic flux and low mitochondrial oxidative phosphorylation activity [138].

Glycolysis can occur in the presence (aerobic) or absence (anaerobic) of O_2, and the resulting product is lactate and CO_2, respectively [136]. Even under fully oxygenated conditions, tumor cells present an increased glucose uptake and lactate production ("aerobic" glycolysis). This phenomenon is known as the Warburg effect and, in spite the low ATP yield (2 ATP) against the production of 36 ATP molecules per molecule of glucose in aerobic glycolysis, there are some advantages in glycolysis for the cancer cells, such as the reduction of reactive oxygen species (ROS) resulting from mitochondrial oxidative phosphorylation, and consequently decrease in oxidative stress (**Figure 22**).
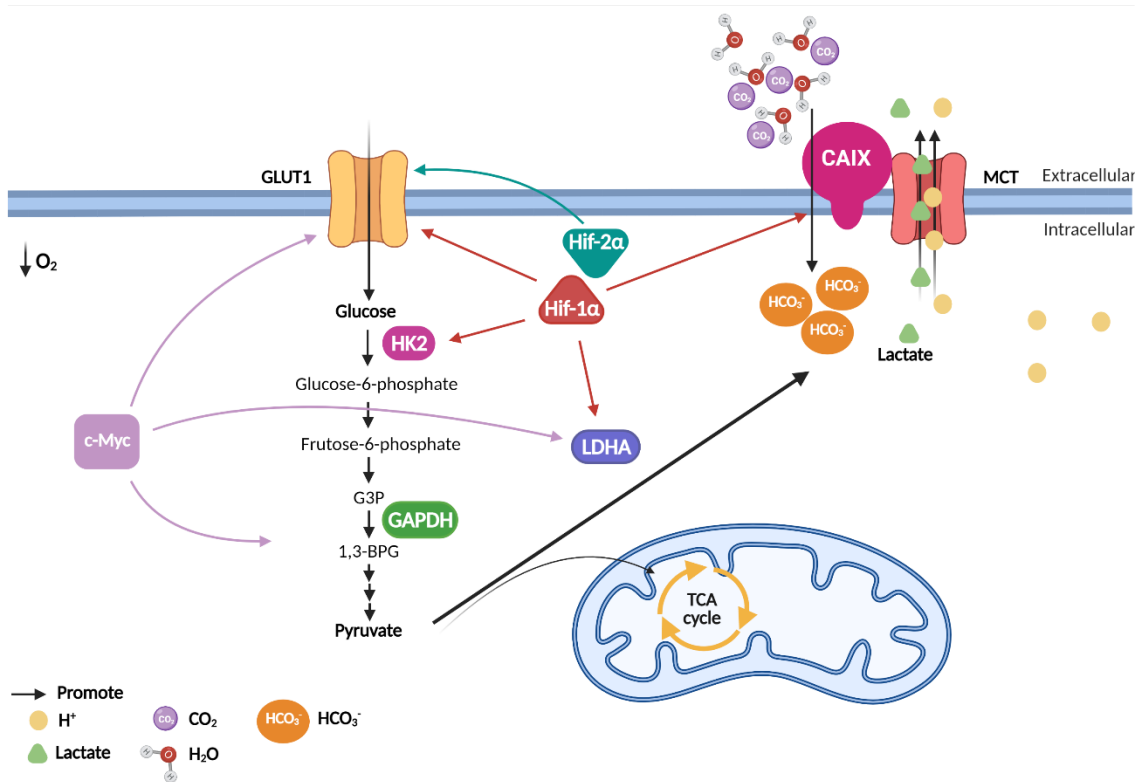
Figure 22 - Representative image of the main proteins involved in glucose metabolism and their interaction network. Hif-1α, hypoxia-inducible factor 1; Hif-2α, hypoxia-inducible factor 2; Glut-1, glucose transporter 1; HK2, hexokinase 2; c-Myc, transcription factor Myc; GAPDH, Glyceraldehyde 3-phosphate dehydrogenase; LDHA, lactate dehydrogenase A; CAIX, carbonic anhydrase IX [139-141].

In this study, the effect of the compounds **1.9**, **1.24**, **1.26** and **7** on metabolic signaling pathways was evaluated by Western-blot, after treatment of Hs578t cells with the respective IC_{50} values, for 24 h and 48 h (**Table 10**). Representative immunoblots demonstrate that, in general, all the tested compounds affect the expression of several important metabolic proteins at the studied timepoints (**Figure 23A**).

A
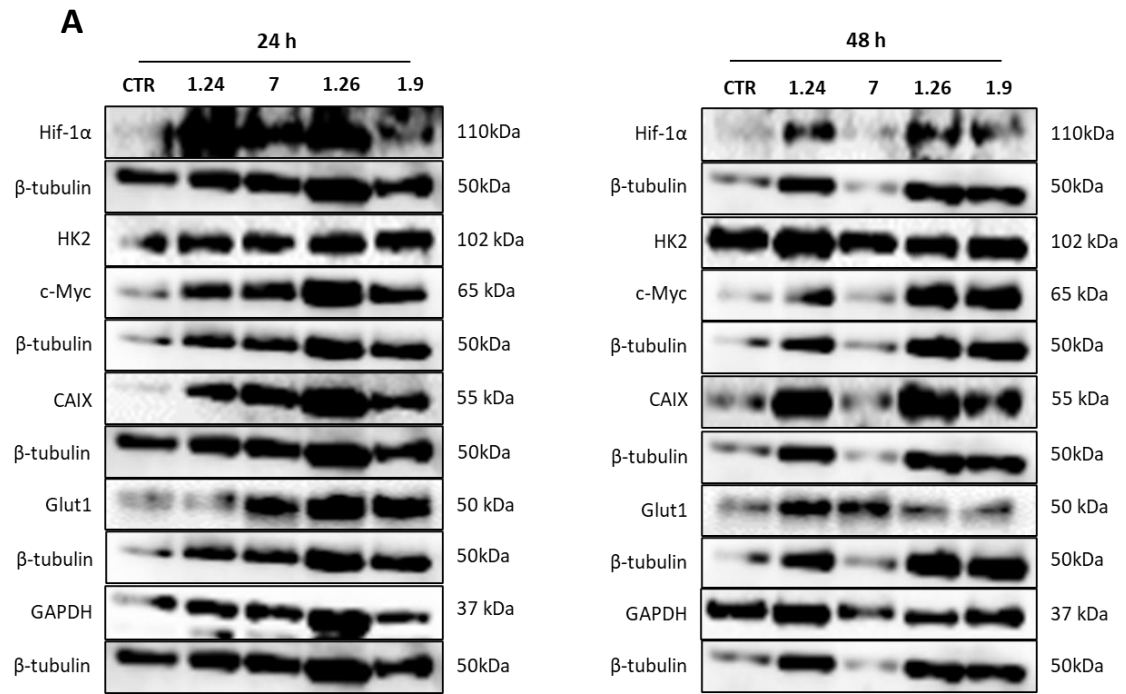
B
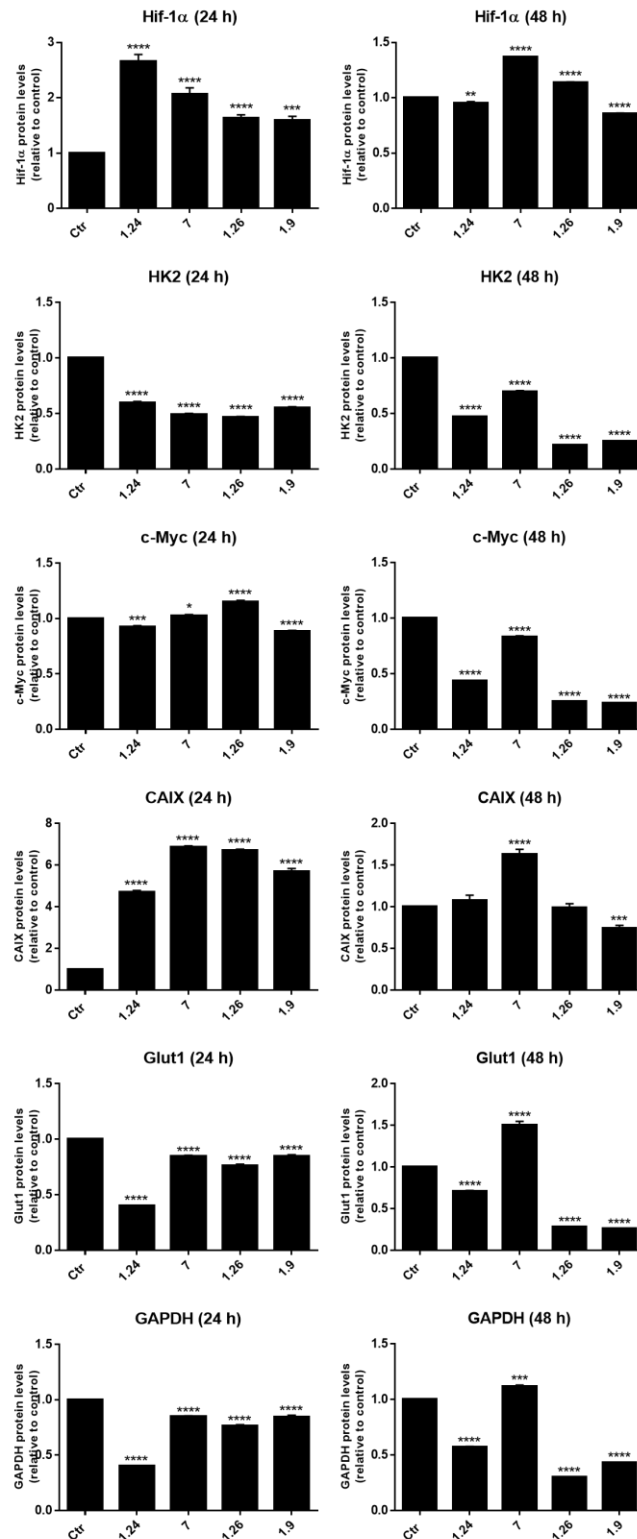
Figure 23 - A) Representative immunoblots of Hs578t cells treated for 24 h and 48 h, with FD-compounds **1.9**, **1.24**, **1.26** and **7**. Similar blots were obtained from at least 2 independent experiments. **B)** Quantification of the levels of Hif-1α, HK2, c-Myc, CAIX, Glut1 and GAPDH proteins after 24 h and 48 h of incubation of Hs578t cells with FD-compounds **1.9**, **1.24**, **1.26** and **7**. Values are mean ± SEM of 2 independent experiments. **** $p<0.0001$, ***$p<0.001$, **$p<0.007$, *$p<0.02$ when compared with control by the Student's t-test.

The protein hypoxia-inducible factor α (Hif-1α) is a transcription factor essential to regulate cell metabolism, survival and proliferation [142]. Under hypoxia conditions, Hif-1α is responsible for the expression of glycolytic genes, including glucose transporter 1 (Glut1), proangiogenic genes and genes involved in pH regulation [143]. After 24 h of treatment, all the tested compounds increased the expression levels of Hif-1α, especially compounds **1.24** and **7**. At the second studied timepoint (48 h), the expression levels of Hif-1α were significantly decreased in cells treated with chromene **1.9** and **1.24** relatively to the control cells (**Figure 23B**).

Other important proteins involved in metabolic pathways were also analyzed, namely the hexokinase 2 (HK2). It has been reported that higher expression levels of this protein are commonly associated to several human carcinomas, suggesting a major role of this protein in cancer development. HK2 catalyzes the conversion of glucose to glucose-6-phosphate, which corresponds to the first step of glycolysis, in a rate-limiting reaction [144]. All the incubation conditions led to a significant decrease in HK2 expression levels after 24 h and 48 h, comparing to control cells (**Figures 23A** and **23B**), suggesting a possible effect of the studied chromenes on HK2 expression levels.

c-Myc is an oncogenic transcription factor directly regulating glycolytic genes, such as Glut1, glyceraldehyde-3-phosphate dehydrogenase (GAPDH) and lactate dehydrogenase (LDH), during the glycolysis [139, 145]. It is upregulated in one-third of breast cancers and it is involved in important cellular processes, like cell growth, cell cycle control, metabolism, adhesion, differentiation, and apoptosis [113]. The protein level quantification demonstrated that, after 24 h of treatment, c-Myc expression levels remained similar (**1.24** and **7**), were higher (**1.26**) or even decreased (**1.9**) comparing to control cells. At 48 h, c-Myc expression levels declined in all conditions, however in a less apparent way for cells treated with compound **7** (**Figure 23B**). Nevertheless, these chromenes seemed to disturb c-Myc expression in a time-dependent manner.

Another crucial protein for the tumorigenic process is the carbonic anhydrase IX (CAIX). Several studies support its role in cell survival, proliferation, invasion, metastasis and resistance to radiotherapy and chemotherapy, and its depletion in hypoxic conditions could affect the viability of several types of cancer cells in vitro [146]. This enzyme catalyzes the interconversion of carbon dioxide (CO_2) and water (H_2O) and the carbonic acid (HCO_3), maintaining the intracellular pH while acidifying the extracellular environment [147, 148]. At 24 h, the results summarized in **Figure 23B** showed that this protein was overexpressed in all conditions, when compared to control cells.

However, after 48 h, chromenes **1.24** and **1.26** induced similar expression levels as the control cells. Chromene **1.9** exhibit the best activity for this set of compounds, since CAIX levels were reduced, while cells treated with chromene **7** increased CAIX levels. As a conclusion, chromene **1.9** demonstrated a possible effect this cell line by making CAIX levels decrease in a time-dependent manner.

Glut1 is a protein with high affinity for glucose and it is frequently overexpressed in cancer cells to increase intracellular glucose rates (Warburg effect) (**Figure 22**) [149-151]. In several types of cancer, namely breast cancer, a higher expression of Glut1 is associated to a poor prognosis [152]. Regarding the expression pattern of this transporter (**Figures 23A** and **23B**), Glut1 levels were significantly reduced in all conditions for both timepoints, except for cells treated with chromene **7**, that increased its levels after 48 h. This raise in Glut 1 expression could be associated with a similar expression pattern observed for Hif-1α and CAIX expressions, at the same timepoint (**Figure 23B**).

GAPDH is an important metabolic enzyme once it catalyzes the redox reaction by converting glyceraldehyde-3-phosphate (G3P) to 1,3-bisphosphoglycerate (1,3-BPG), reducing NAD^+ into NADH. It has been considered a house-keeping enzyme, although accumulative evidence suggests non-enzymatic roles, with diverse functions and distinct subcellular distribution, and its upregulation seems associated with to cancer development [153]. GAPDH expression levels were assessed since it represents a key enzyme in the glycolytic process. The results presented in **Figure 23B** showed a reduction of its expression levels at 24 h in cells treated with all the molecules, although more evidently for chromene **1.24**, in comparison to control. At 48 h of treatment, cells treated with chromene **7** increased GAPDH expression levels, while cells treated with the remaining chromenes decreased its expression. Again, the expression pattern for cells treated with chromene **7** is similar to those observed for previous analyzed proteins, Hif-1α and CAIX.

Interestingly, the effect of chromenes **1.9**, **1.24**, **1.26** and **7** on the expression pattern of c-Myc, Glut 1 and GAPDH proteins at 48 h has multiple similarities, indicating a possible effect of our compounds on c-Myc expression, since this transcription factor regulates Glut1 and GAPDH expression levels.

In general, these results indicate that all the tested compounds interfered with critical metabolic players, particularly chromene **1.9**, that promoted the decrease of the expression levels of several glycolytic or glycolytic-related proteins. Chromenes **1.24** and **1.26** also exhibited an interesting

activity, while compound **7** displayed the poorest activity. Taking all into consideration, these results demonstrated a very promising biological activity of the synthesized molecules.

9. Effect of FD-chromene-based compounds on the microtubule network

The cellular cytoskeleton is an essential component with important key roles such as cell division, polarity, and migration. All these features are altered in cancer cells and, therefore, the study of the microtubule network became one of the focus of cancer researchers in the development of target drugs [154]. Microtubule-target drugs disrupt microtubule dynamics in two distinct ways, through stabilization and destabilization of the microtubules. Paclitaxel, or Taxol, belongs to the group of microtubule-stabilizing agents (MSAs), while vinblastine and colchicine are microtubule-destabilizing agents (MDAs) [155]. To assess the effect of chromenes **1.26** and **7** on the microtubule network, Hs578t cells were treated with their respective IC_{50} concentrations (**Table 10**) for 24 h. The MSAs agent Paclitaxel (C = 0.5 µM) was used as a reference compound. The results are summarized in **Figure 24**.

Control   **Paclitaxel**

1.26   **7**
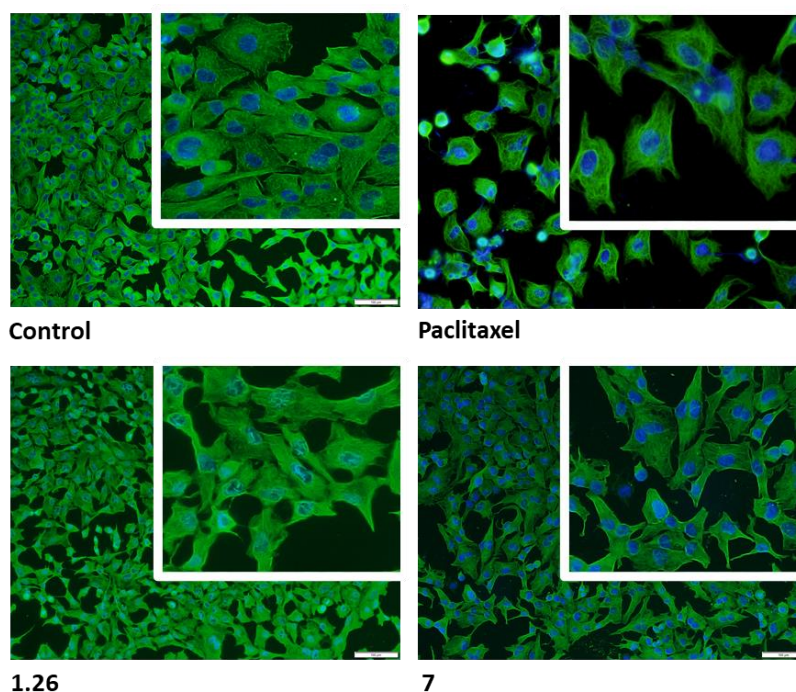
Figure 24 - Effect of FD-compounds **1.26** and **7** on the microtubule network of Hs578t cells. Control (vehicle), Paclitaxel (0.5 µM) and cells treated with compounds chromenes **1.26** and **7** at the IC_{50} values for 24 h were stained with β-tubulin and counterstained with 4,6-diamidino-2-phenylindole (DAPI). Microtubules and unassembled tubulin are shown in green. DNA, stained with DAPI, is shown in blue. Representative images were obtained using Olympus Wide field Upright Microscope BX 61, magnification 10X. Paclitaxel-treated cells were obtained using magnification 10X and 40X.

The images regarding cells treated with 0.5 µM of Paclitaxel showed a higher definition of the tubulin filaments when compared to the control cells (0.5% DMSO), corroborating the stabilization properties of this drug (**Figure 24**).

In 2004, Zeigler *et al*. managed to describe in detail the morphological alterations that occur in the nuclei, cell membrane and cytosol, and in the mitochondria during cell death through apoptosis or necrosis [156]. The most noticeable events occur in the nuclei, cell membrane and cytosol, such as the chromatin condensation and nuclear fragmentation, and the loss of contact with neighboring-cells. Further in the process, the appearance of protrusions in the cell membrane, also known as blebs, is very common. Considering the previous statement, cells treated with chromenes **1.26** and **7** for 24 h suffered morphologic alterations comparing to the control cells, as described in the study by Zeigler *et al.* The cells treated with chromene **1.26** started to detach from neighboring cells, presenting a more elongated shape and the formation of blebs were also visible (equally observed in cells treated with paclitaxel). Shrinkage of the nuclei with possible condensation of chromatin was also detected. A similar morphological behavior was detected for cells treated with chromene **7**, which also acquired a more elongated cell shape and reorganization of the microtubules, associated to a possible chromatin condensation and visible shrinkage of the nuclei.

In 2001, Coleman *et al.* conducted a research relating cell morphological changes during apoptosis with caspases cascade activation [157]. In this study, the authors reported the determinant role of ROCK, a protein responsible for contractile force generation, on membrane blebbing event mediated by caspase cascade activation. Considering the previous results, the protuberances exhibited in treated cells (**Figure 24**) may be associated to the overexpression of caspase 9 and 8, reported in **Figures 19A** and **19B**.

10. *In vivo* toxicity study of the FD-chromene-based compounds using *Caenorhabditis elegans* model

The mammalian models used in laboratory share many features with humans, such as organs and development pathways and, for this reason, these models are recurrently used in toxicology assays [158]. Nevertheless, the United States National Research Council pointed out the need to replace the use of traditional animal models for non-mammalian models in toxicity assays, such as *Caenorhabditis elegans* (*C. elegans)*. This nematode gathers several features that make it an engaging model [159, 160]. The most striking advantages in the use of this model are the ability to be handled using *in vitro* techniques and the high degree of conservation of several biological processes between *C. elegans* and mammalian species [159-161]. Several studies supported a positive correlation between the toxicity in *C. elegans* and median lethal dose (LD_{50}) in rodents, indicating this model as an intermediate between *in vitro* and mammalian studies [158].

To analyze the *in vivo* toxicity of the most promising FD-chromene-based compounds, a collaboration with Patrícia Maciel's group (ICVS) was established to test chromenes **1.9**, **1.26** and **7** using *C. elegans* model. To achieve this goal, the group performed a food clearance-based assay, where the rate of consumption of bacteria (OD_{50}) over time represented a good prediction factor of this nematodes development, health and fertility. The compounds were tested at several concentrations, diluted in a DMSO solution, up to the highest soluble concentration possible: 100 μM for chromenes **1.9** and **1.26** and 50 μM for chromene **7**, comparing to the treatment vehicle of 1% DMSO and toxic dose of 5% DMSO (**Figure 25**).

The study showed no statistical differences in the rate of food consumption for the tested days 3-5, for the nematodes treated with the synthetized chromenes (ANOVA, followed by the Games-Howell post hoc test, **Figure 25**). In fact, the compounds seemed to be well tolerated, even at significantly higher concentrations than those used for the *in vitro* assays, representing a good indicator for non-toxicity in mammalian models.
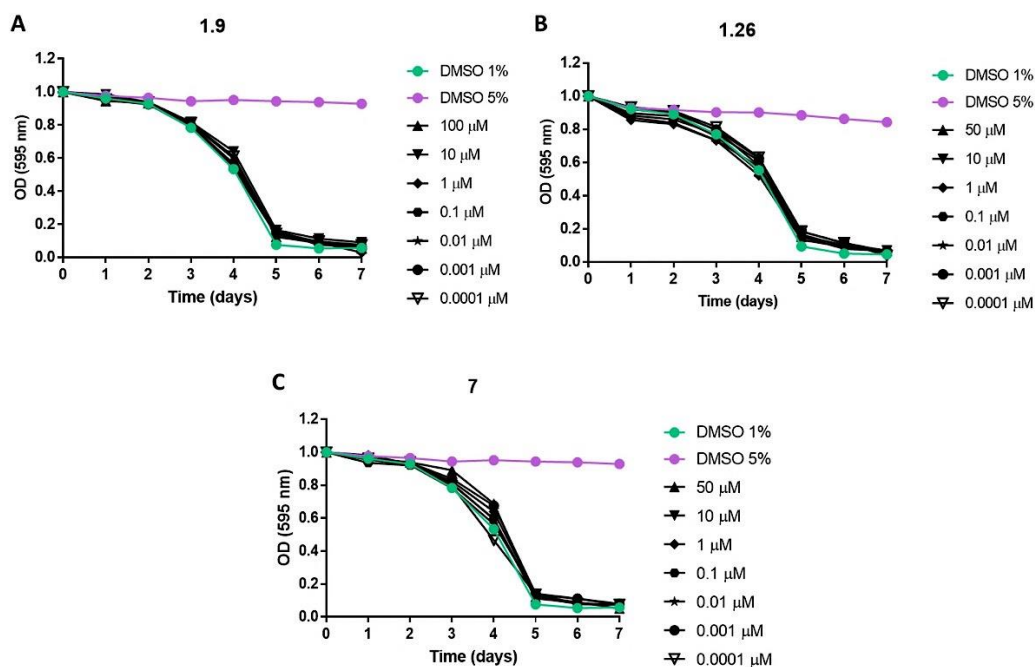
Figure 25 - Analysis of the *in vivo* toxicity of compounds **1.9**, **1.26** and **7**. Toxicity was assessed in wild-type *C. elegans* through daily evaluation of food consumption (optical density 595 nm) of animals treated with different concentrations of each compound. Animals treated with 1% DMSO and 5% DMSO were used as non-toxic and toxic controls, respectively. Curves in the graphs represent daily optical density (OD) values, normalized for the OD at day 0, being concentrations of each compound measured in quintuple. **(A) 1.9; B) 1.26; C) 7**. Graphic represented with Mean ± SEM. Nonlinear regression, sigmoidal, 4PL, X is log(concentration), profile likelihood, P<0.05.

11. *In vivo* efficacy assessment of FD-chromene-based compounds using the chick chorioallantoic membrane assay

Considering the promising anticancer profile and the results obtained from the *in vivo* toxicity study, chromenes **1.26** and **7** were selected for further evaluation of their capacity to inhibit tumor growth, using the chick chorioallantoic membrane (CAM) model.

This model is a very useful technique for early pre-clinic *in vivo* efficacy studies for multiple fields of research, including oncologic and drug development, due to the rapid development cycle of the chick embryo and easy accessibility to the CAM [162]. Several studies described the efficiency of the obtained tumor growth in nodule-form, independently from the tumor cells lines our tissues, enabling to process data referent to the tumor size and weight [163].

The nourishing nature of CAM is one of the advantages of this model since it allows the stimulation of grafted cells (**Figure 26**). The immunodeficiency of the host during the first 18 days of development also allows the implementation of tumor cells without triggering an immune

response [162-164]. At last, this model holds an additional ethical advantage in comparison to several mammalian *in vivo* models, since CAM does not possess nervous terminations and the assays terminates before the development of pain perception on the chick's brain, being an attractive option for *in vivo* experiments in early pre-clinical studies [162, 163].
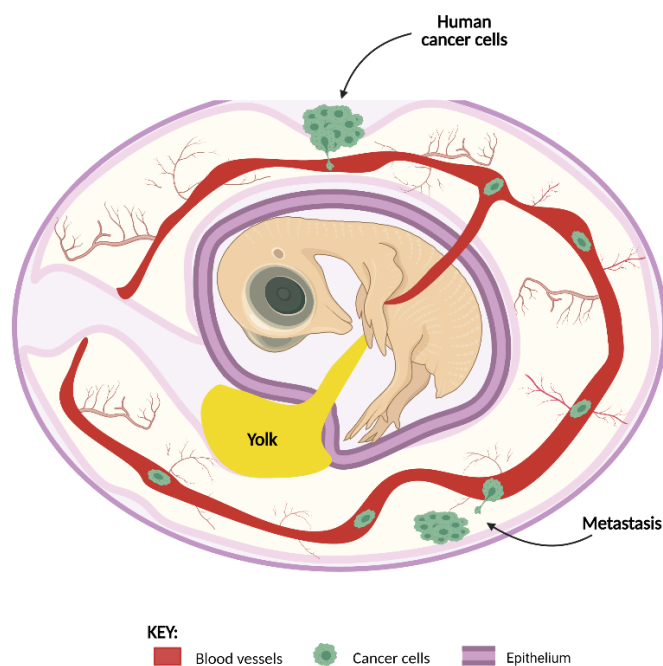
Figure 26 - Representative image of CAM model and tumor progression. Cancer cells are inserted on the CAM of the chick embryo, invading the epithelium and basement membrane and further move through the connective tissue into the vasculature. Metastasis can occur on the lower CAM, liver and/or lung (Adapted from [165]).

In this study, Hs578t cells were seeded on the CAM and the resultant tumors were treated with 2x IC_{50} concentrations of each compound or 0.5% DMSO (control group), in order to evaluate tumor regression. The concentration of compounds to be used in this assay was previously optimized by our research group and in this work, the respective 2x IC_{50} concentrations were used since the results with *C. elegans* revealed a safe profile for even higher values. The results presented in **Figure 27B** demonstrated a significant regression in the tumors progression treated with chromenes **1.26** and **7**, comparing to the control group. Chromene **7** proved to be the most effective compound, since treatment caused a regression in the tumors' perimeter of approximately 12.4%, while treatment with chromene **1.26** caused a reduction of 6.3%. Nevertheless, both compounds displayed a significant *in vivo* efficacy profile in tumor regression.
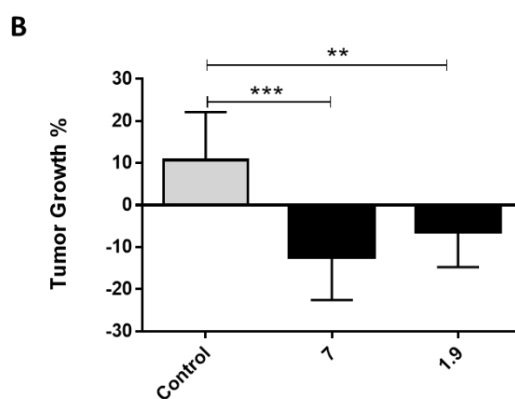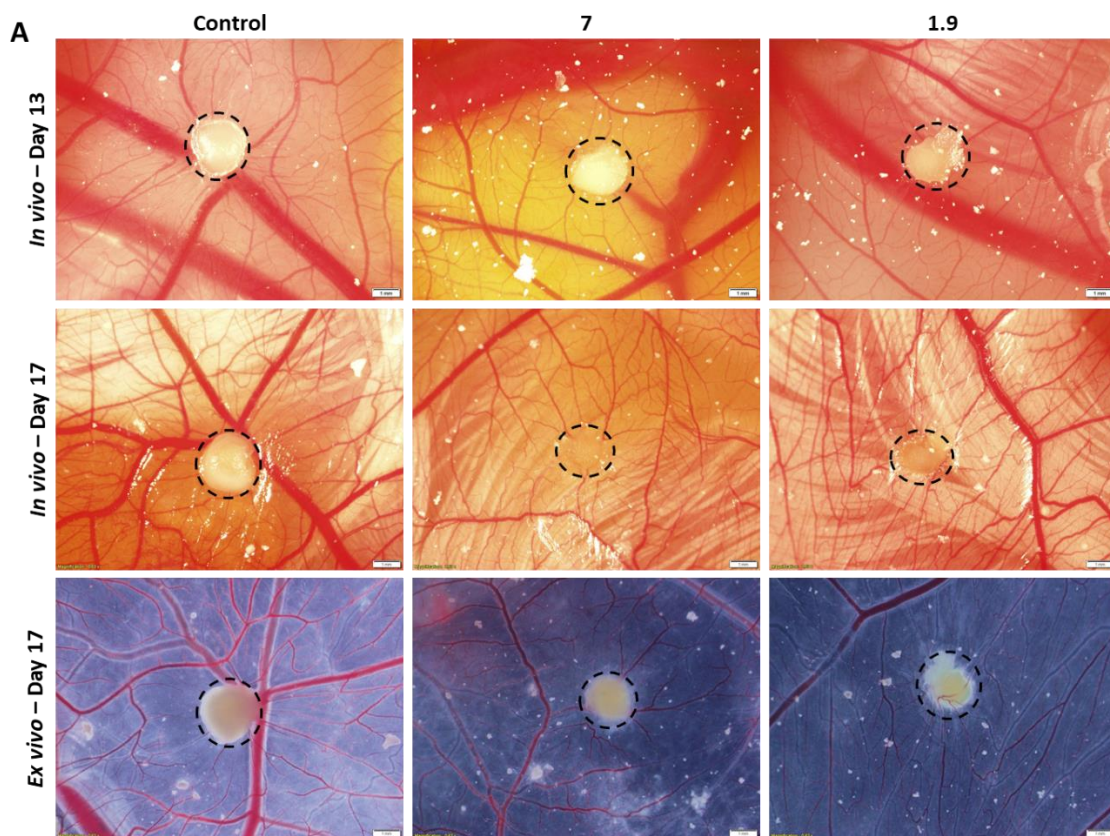
Figure 27 - Effect of chromenes **1.26** and **7** in Hs578t tumor progression. **A)** *In ovo* pictures at day 13 of embryo development and *in ovo* and *ex ovo* pictures at day 17; representative images were taken at 20x in a Zeiss stereomicroscope. **B)** Graphical representation of tumors growth. Data was analyzed by one-way ANOVA and the results are representative for a media of at least 10 eggs per group; ****p<0.0001, **p<0.005 treated group vs control.

This model is also used to study *in vivo* angiogenesis and the efficacy of natural or synthetic molecules as proangiogenic or antiangiogenic agents [166]. In 2019, a study was conducted showing the effect of naphthopyrans, which are chromene derivatives, on angiogenesis though the disruption of the vasculature in the CAM [167].

As visualized in **Figure 27A**, after four days of tumor development, the formation of blood vessels is noticeable in the control group, whereas the treated groups experienced a decreased in blood vessels formation, suggesting a possible inhibition of angiogenesis by chromene **1.26** and **7**. However, a more specific assay is needed to determine this capacity.

Part II – Anticancer potential of DL-chromene-based compounds

Chromeno[2,3-*b*]pyridines **8 (Figure 13)**, were synthesized by Diogo Lopes, during his Master's degree thesis in Medicinal Chemistry (2018/2019), under the supervision of Doctor Marta Costa and Professor Fernanda Proença [168]. The synthetized compounds were previously screened in the research group for their anticancer activity in three breast cancer cell lines (MCF-7, Hs578t and MDA-MB-231) and in MCF-10A cell line, a non-tumorigenic epithelial cell line, used to determine the selectivity index of the compounds, shown in **Table 12** [81].

Table 12 - IC$_{50}$±SD values (µM) for chromeno[2,3-*b*]pyridines **8** in MCF-7, Hs578t, MDA-MB-231 and MCF-10A cell lines.

8.1: R$_1$= R$_2$=H, R$_3$=Br
8.2: R$_1$= Me, R$_2$=R$_3$=H
8.3: R$_2$= OMe, R$_1$=R$_3$=H
8.5: R$_1$= R$_2$=H, R$_3$=OMe
8.6: R$_1$= R$_2$=H, R$_3$=OH
8.7: R$_1$= R$_2$=H, R$_3$=Cl

8.8: X=N—⟨ ⟩—Cl (Cl)

8.9: X=N—⟨ ⟩—CF$_3$
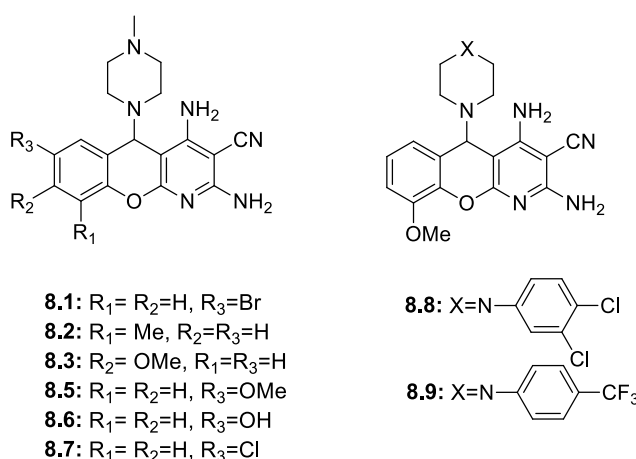
DL-compounds[a]	Breast cell lines			MCF-10A IC$_{50}$ (µM) ± SD[b]	SI[d]
	MCF-7 IC$_{50}$ (µM) ± SD[b]	Hs578t IC$_{50}$ (µM) ± SD[b]	MDA-MB-231 IC$_{50}$ (µM) ± SD[b]		
8.1	3.47±0.36	14.92±0.22	8.52±0.03	41.32±0.22	10.9/1.8/3.9
8.2	15.16±0.16	10.62±0.15	20.59±0.08	24.42±0.54	0.6/1.2/0.2
8.3	2.96±0.15	n.d.	22.30±0.13	28.66±0.035	8.7/0.3
8.4	5.01±0.12	4.67±0.15	8.86±0.04	11.89±0.19	1.4/1.5/0.3
8.5	8.420±0.001	n.d.	19.40±0.14	20.99±0.06	1.5/0.08
8.6	15.54±0.04	16.77±0.01	16.66±0.21	24.12±0.11	0.6/0.4/0.5
8.7	9.63±0.28	n.d.	11.16±0.05	27.63±0.25	1.9/1.48
8.9	8.51±0.02	n.d.	20.42±0.27	29.49±0.03	2.5/0.45

Quercetin	55.87±0.22	50.54±0.12	>75μM	n.d	n.d
Doxorubicin[c]	1.32±0.04	0.52±0.006	0.35±0.01	1.54±0.078	0.17/2.0/3.4

[a] Each compound was tested at least in triplicate and the data are presented as mean values. [b] Standard Deviation. [c] Previously determined by the research group in reference [28]. [d] Selectivity index of MCF-7 / Hs578t/MDA-MB-231 *vs* MCF-10A.

The IC_{50} values for the most promising DL-chromene-based compounds were previously determined in the research group, after a careful screening of a library of 20 compounds at 10 and 30 μM. Compounds **8.1** and **8.3** presented a promising anticancer activity and high selectivity for MCF-7 cell lines. Chromene **8.4** also presented an interesting IC_{50} value for this cell line, although with a lower SI value. This compound showed the lowest IC_{50} value for triple negative breast cancer cell line Hs578t and for MDA-MB-231 cell line compound **8.1** demonstrated to be the most active chromene. For the most active compounds, the SI was superior than 1, indicating a higher affinity towards cancer cell lines than to the non-tumorigenic cell line.

These compounds exhibited a promising anticancer profile for MCF-7 cells in terms of their capacity to decrease cell viability. Therefore, experiments to unravel the mechanism of action of these chromenes were conducted using this cell line. From the compounds presented in **Table 12**, the three most potent compounds (**8.1**, **8.3** and **8.4**) were selected and their effect on regulated cell death through apoptosis and on important metabolic pathways was assessed using Western-blot technique.

1. Effect of DL-chromene-based compounds on regulated cell death

The mechanism of action of DL-chromene-based compounds was exploited through the analysis of the expression levels of several proteins involved in the apoptotic process, through Western-blot technique. Compounds **8.1**, **8.3** and **8.4** were tested in the luminal breast cancer cell line, MCF-7, at the respective IC_{50} concentration values (**Table 12**) or 0.5% DMSO (controls) for 24 and 48 h of treatment. The immunoblots and the respective protein quantification results are presented in **Figures 28A** and **28B**, respectively.

A

B
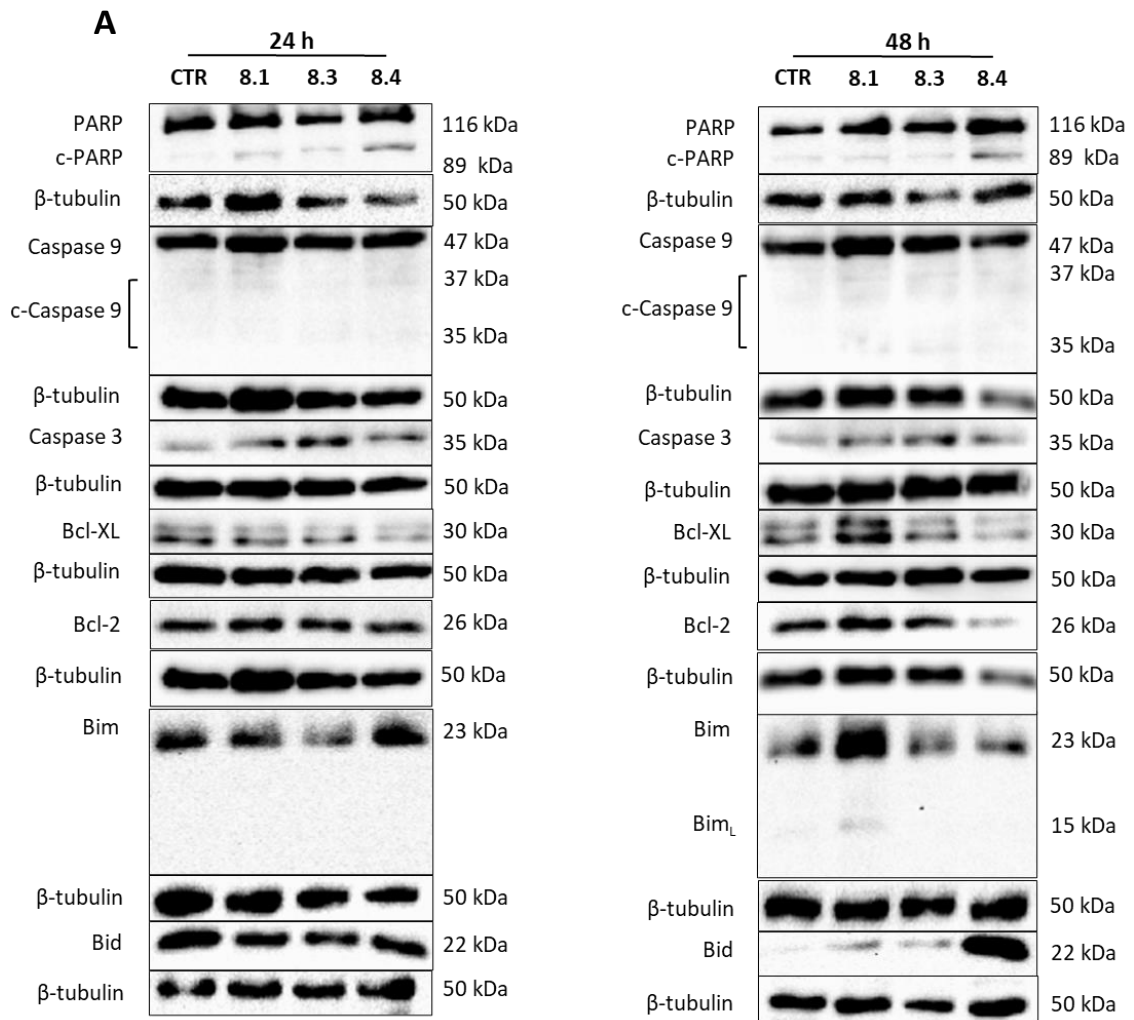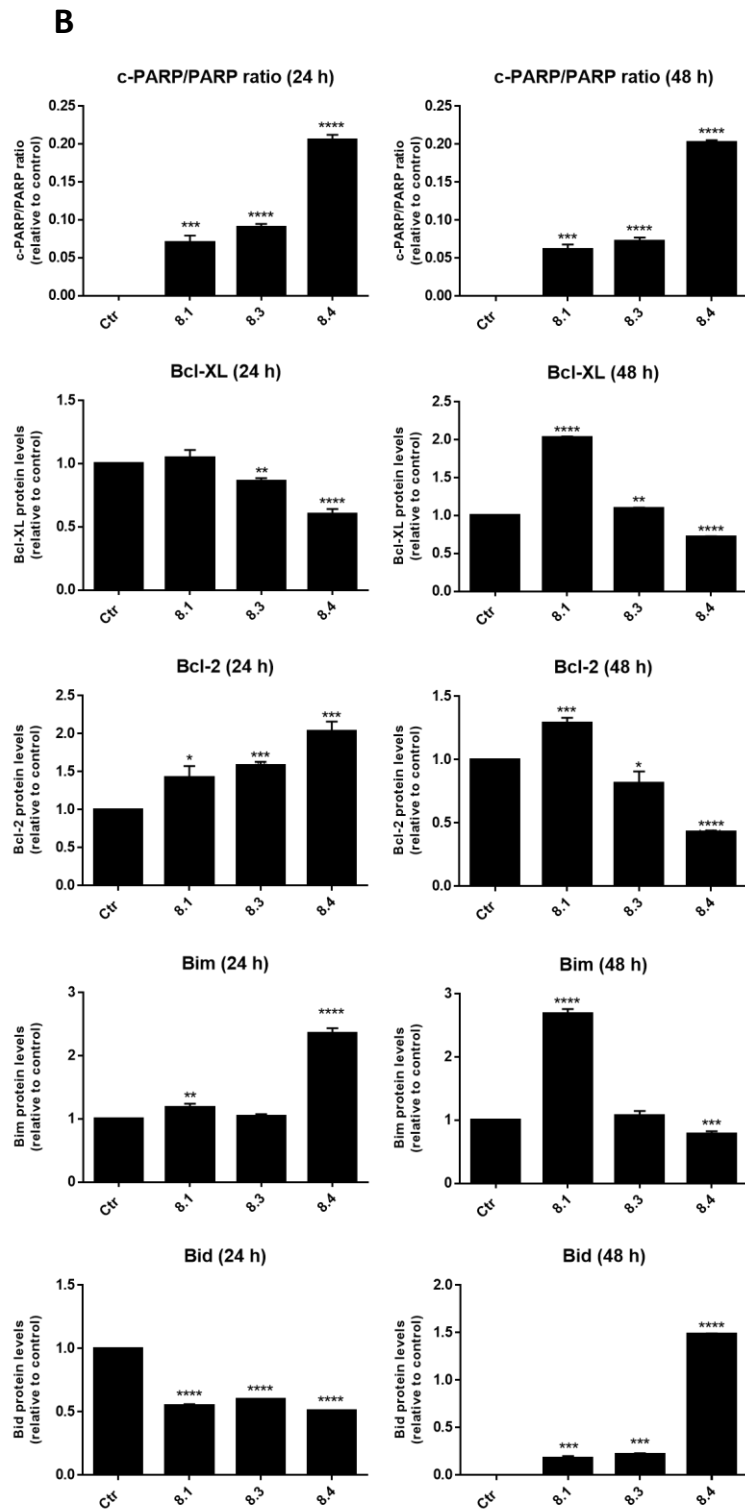
Figure 28 - **A)** Representative membranes of MCF-7 cells treated for 24 h and 48 h with compounds **8.1**, **8.3** and **8.4**. **B)** Quantification of c-PARP/PARP ratio and the levels of Bcl-XL, Bcl-2, Bim and Bid proteins after 24 and 48 h of incubation of MCF-7 cells with compounds **8.1**, **8.3** and **8.4**. Values are mean ± SEM of 3 independent experiments. **** p<0.0001, ***p<0.001, **p<0.007, *p<0.04 when compared with control by the Student's t-test.

The apoptotic event can occur through several signaling pathways, depending on the stimuli, that can be disrupted in cancer cells, leading to tumor progression [169]. In this study, the effect of our compounds on the apoptotic signaling pathways (previously mentioned and represented in (**Figure 18**) was evaluated.

As shown in **Figure 28A** and **28B**, chromene **8.4** seemed to induce regulated cell death through apoptosis. At 24 h of treatment, the expression levels of cleaved PARP are evident. However less significant, chromenes **8.1** and **8.3** triggered PARP cleavage as well. After a 48 h, the same expression pattern was observed for all three compounds.

Regarding the expression levels of caspase 9 and 3, the immunoblots (**Figure 28A**) displayed slight expression levels of cleaved C9 and although cleaved C3 fragments were not detected, it is noteworthy the higher expression of the total protein in all treated conditions, after 48 h of treatment.

The levels of Bcl-2 family proteins, Bcl-xL, Bcl-2, Bim and Bid involved in the regulation of the intrinsic apoptotic pathway, as mentioned before, were assessed as well. The expression levels of anti-apoptotic proteins Bcl-xL and Bcl-2 were significantly reduced in cells treated with chromene **8.4** (**Figures 28A** and **28B**), after 48 h, while chromenes **8.1** and **8.3** caused a rise in both anti-apoptotic proteins.

The levels of pro-apoptotic protein Bim were enhanced in cells treated with chromene **8.4** after 24 h, compared to the remaining chromenes. At 48 h, chromene **8.1** led to the increase of Bim protein expression levels, where the isoform Bim-L is also visible (**Figures 28A** and **28B**). Although the levels of Bid in cells treated with our chromenes were reduced in comparison to control cells (24 h), after 48 h the increase in Bim levels were evident on cells treated with the chromene **8.4**, as in cells treated with **8.1** and **8.3** but in a less significant extent.

In general, an interesting protein expression pattern was observed with the overexpression of several pro-apoptotic proteins and suppression of anti-apoptotic proteins leading to cell death through apoptosis. Cells treated with chromene **8.4** presented high expression levels of caspase 9 and Bid proteins, suggesting that this chromene may induce apoptosis through the activation of the extrinsic pathway (**Figure 18**). To corroborate this assumption, the expression levels of caspase 8 needs to be assessed in a future experiment.

2. Effect of the DL-chromene-based compounds on metabolic key points

Since metabolic reprogramming of cancer cells was identified as a hallmark of cancer, the study of metabolic proteins and pathways involved in glucose uptake and glycolysis became the focus of several cancer researchers for the development of target therapies [170]. Some critical proteins related to glucose metabolism were explored as possible therapeutic targets after treating cells with the most promising compounds.

In this study, the effect of the compounds **8.1**, **8.2** and **8.3** on metabolic signaling pathways (previously mentioned and represented in **Figure 22**) was evaluated by Western-blot, after treatment of MCF-7 cells with the respective IC_{50} values for 24 h and 48 h of (**Table 12**). The obtained results are represented in **Figures 29A** and **29B**.

B
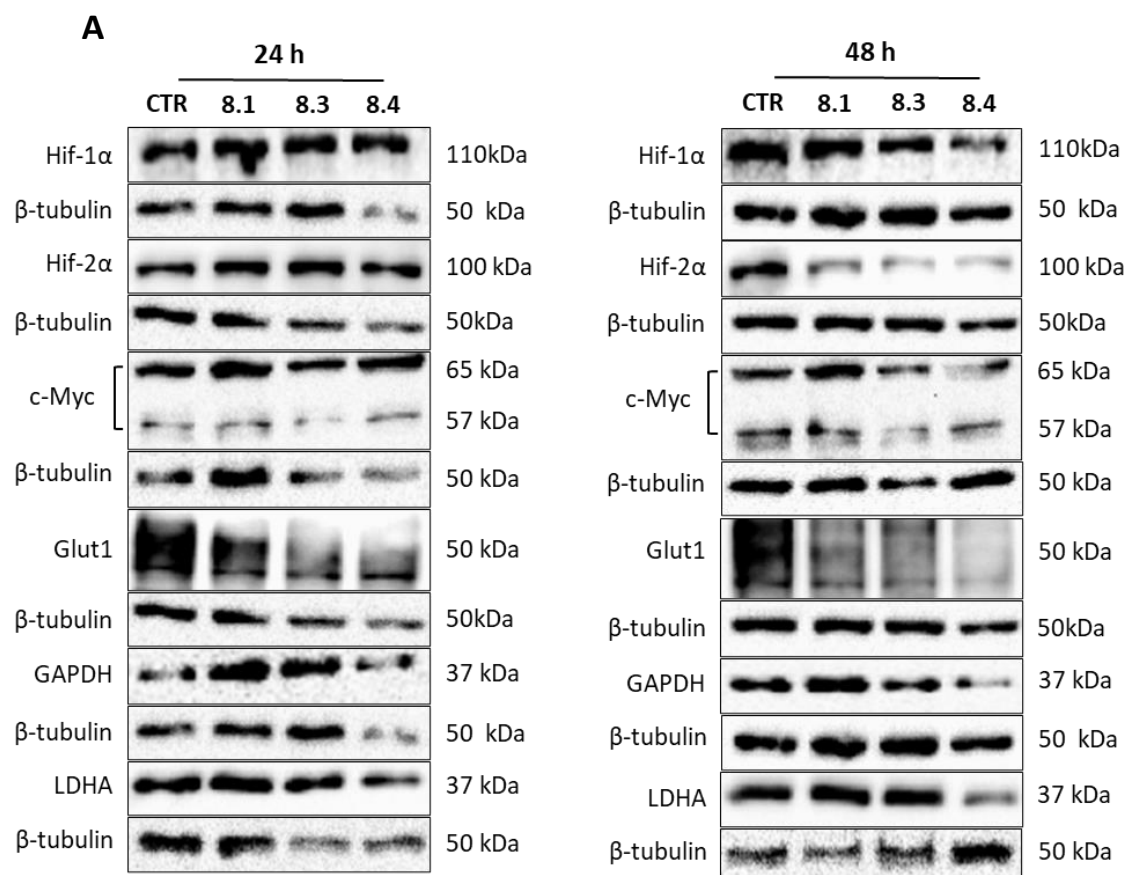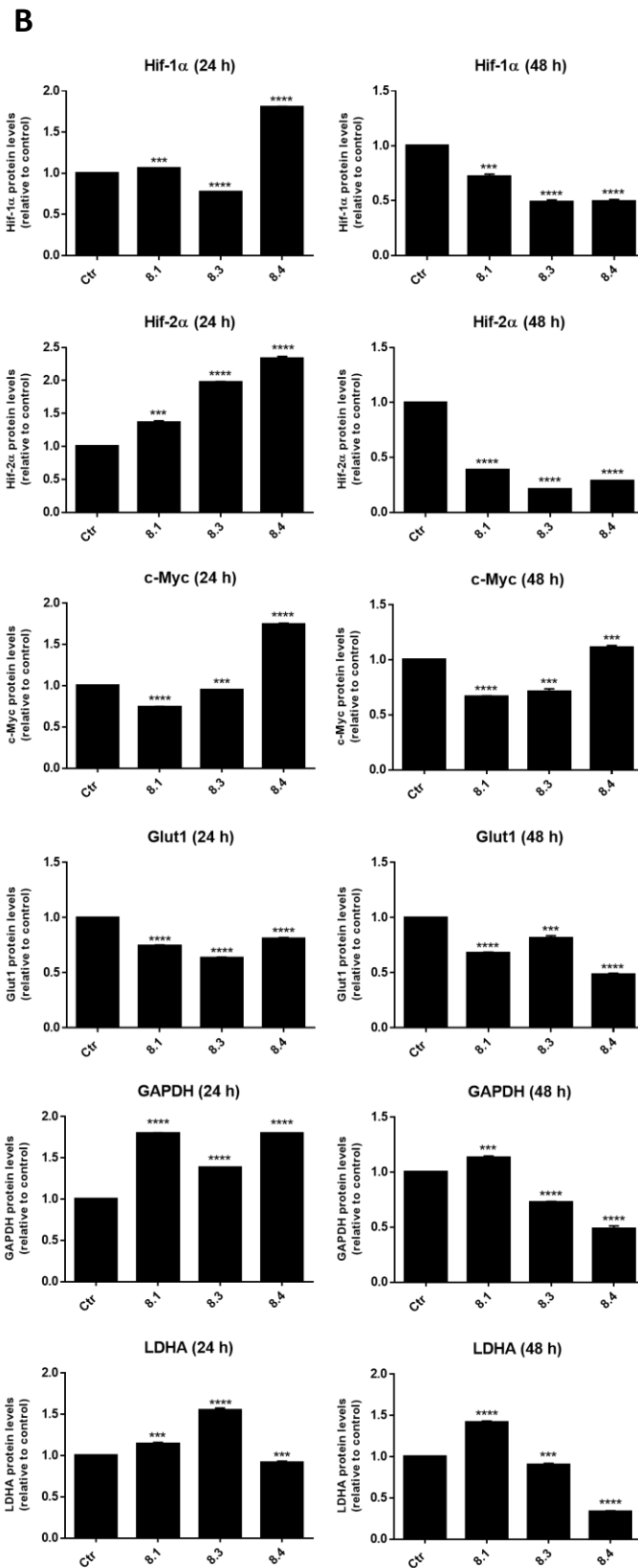
Figure 29 - **A)** Representative membranes of MCF-7 cells treated for 24 h and 48 h with chromenes **8.1**, **8.3** and **8.4**. **B)** Quantification of the levels of Hif-1α, Hif-2α, c-Myc, Glut1, GAPDH and LDHA proteins after 24 h and 48 h of incubation of MCF-7 cells with compounds **8.1**, **8.3** and **8.4**. Values are mean ± SEM of 3 independent experiments. **** p<0.0001, ***p<0.001 when compared with control by the Student's t-test.

As observed in **Figures 29A** and **29B**, chromenes **8.1**, **8.3** and **8.4** seemed to exhibit a significant effect on the analyzed proteins at 24 h and 48 h of treatment, given the protein expression patterns alterations, specifically when cells were treated with chromene **8.4**.

Expression levels of Hif-1α and Hif-2α were measured after treating cells with the selected compounds. Chromene **8.4** led to a significant increase of Hif-1α levels, after 24 h. At the same timepoint, Hif-2α levels increased significantly in all conditions in comparison to the control. The expression of these two proteins decreased abruptly after 48 h, proposing that the studied chromenes may affect the activity of these transcription factors.

The oncogenic transcription factor, c-Myc, was also evaluated and the results showed that cells treated with chromene **8.4** experienced a significant increase in its expression at 24 h and 48 h of treatment. While chromenes **8.1** and **8.3** induced a reduction of c-Myc levels for both timepoints (**Figure 29B**).

Glut1 levels were decreased at 24 h and 48 h of treatment in all conditions, but in a more evident manner in cells treated with chromene **8.4**. These results are in accordance with the previous analyses since Hif-1α regulates Glut1 expression and therefore supporting a possible effect of these chromenes on Hif-1α expression.

GAPDH and LDHA, two important glycolytic enzymes, displayed a decline in their expression levels after cells were treated with chromenes **8.3** and **8.4** for 48 h. Compound **8.1** caused an increase in their levels compared to control cells, for both timepoints.

Regarding the metabolic key points of cancer cells, chromene **8.4** exhibited the best activity by decreasing the expression levels of several important glycolytic proteins studied. Chromene **8.3** also demonstrated a similar activity but in a more moderate manner. Both compounds induced a reduction on Hif-1α, Hif-2α, GAPDH and LDHA expression levels.

Part II, regarding the anticancer activity of the DL-compounds, has been included in a research article entitled "Unravelling the anticancer potential of functionalized chromeno[2,3-*b*]pyridines for breast cancer treatment" [81]. This project was developed in this research group and evaluated the anticancer activity of these compounds. As previously mentioned, the DL-compounds showed a higher effect in MCF-7 cell line. The most promising compounds were chromenes **8.1**, **8.3** and **8.4**, exhibiting IC$_{50}$ values in the low micromolar range. These molecules were able to induce cell cycle arrest, cell death through apoptosis, microtubule destabilization and inhibited cell

proliferation. Their toxicity was assessed as well using the *C. elegans* model, proving their safe profile. The selected molecules presented important bioactive features, potentiating their use as anticancer drugs.

Chapter IV - Conclusion

In the past years, the search for more effective and selective drugs for cancer therapy has become the focus of several researchers since current treatments present several side effects and low efficacy. In order to overcome these difficulties, natural and novel synthetic compounds have been exploited due to their anticancer properties and low toxicity, including chromene-based compounds.

Our research group successfully synthesized two distinct families of compounds that presented promising anticancer activity in the breast cancer cell model.

Regarding to FD-chromene-based family, chromenes **1.26** and **7 (Figure 30)** displayed the best anticancer profile with low micromolar IC_{50} values in Hs578t cell line.

1.26   **7.1**
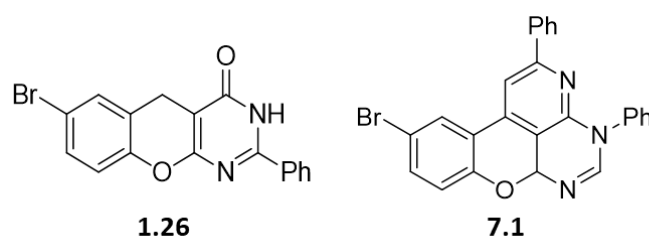
Figure 30 - Most promising compounds of the FD-chromene-based family.

These compounds were able to inhibit cell proliferation and migration, to induce regulated cell death through apoptosis, cell cycle arrest at S phase, cell morphological modifications and alteration in the expression of important glycolytic proteins, as Hif-1α, HK2, c-Myc and Glut1. These molecules also presented no toxicity *in vivo* using the *C. elegans* model, suggesting a safe profile. Additionally, *in vivo* tumor regression and inhibition of angiogenesis events were also verified after treatment with these two compounds, demonstrating an effective anticancer profile.

Although several studies need to be further performed to determine the exact target(s) by which chromenes **1.26** and **7** exert their mechanism of action, the promising anticancer profile demonstrated in this work reenforces their potential use in TNBC therapy.

The anticancer activity of DL-chromene-based compounds was previously determined by our group, using several BC cell lines. Chromenes **8.1**, **8.3** and **8.4 (Figure 31)** exhibited the best activity in MCF-7 cells, with IC_{50} values in low micromolar range, and higher selectivity compared to the reference molecule (doxorubicin).
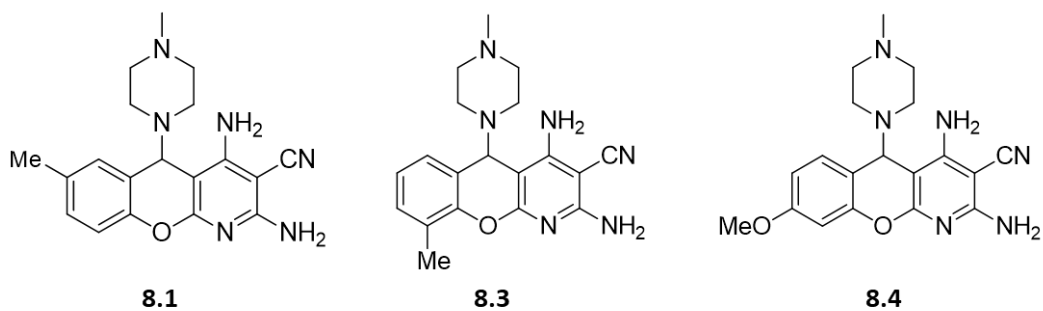
Figure 31 - Most promising compounds of DL-chromene-based family.

Structure-activity analysis revealed that methyl and methoxy groups linked to the chromene moiety potentialize the anticancer activity. Protein expression related assays indicated that these chromenes were able to induce regulated cell death through apoptosis and inhibit the expression of glycolytic key enzymes. A complete study on the anticancer activity of these chromenes was performed in our research group, that proved to exhibit a safe profile, inhibit cell proliferation, microtubule destabilization as well as to induce cell cycle arrest in G_2/M phase. The results were indeed very promising and supportive of the potential of these compounds as future anticancer drugs.

Chapter V – Future perspectives

DL-chromene-based compounds are still under study as part of Diogo Lopes' doctoral thesis, to improve their activity, delivery and safety profile.

In order to completely characterize the mode of action of the newly synthesized FD-chromene-based compounds, other specific assays need to be performed based on the highly promising results obtained in this work.

The combination of this chromenes with doxorubicin should be further studied since a synergistic profile was observed. To conclude about the potential of a less toxic therapeutic option, safety studies of this combination are important to address. It is essential to further investigate the metabolic pathways affected by the studied compounds, since they demonstrated to alter important oncogenic related pathways.

Currently, a full docking study is being performed to support this work, for the identification of the target(s) by which these compounds exert their activity, through a collaboration in the University of Santiago de Compostela. Once the study is completed, we expect to design and synthesize new derivatives, based on the most promising moieties, able to reduce the IC_{50} values and to enhance the anticancer potential, maintaining the good safety profile. After optimization of the compounds structure (IC_{50} in the nanomolar range), studies can pursue to more complex *in vivo* studies, as *in vivo* toxicity and efficacy in the mouse model.

Bibliography

1. Hanahan, D. and R.A. Weinberg, *The Hallmarks of Cancer.* Cell, 2000. **100**: p. 57–70.
2. Pordeli, M., et al., *Anticancer effects of synthetic hexahydrobenzo [g]chromen-4-one derivatives on human breast cancer cell lines.* Breast Cancer, 2017. **24**(2): p. 299-311.
3. Bray, F., et al., *Global cancer statistics 2018: GLOBOCAN estimates of incidence and mortality worldwide for 36 cancers in 185 countries.* CA: A Cancer Journal for Clinicians, 2018. **68**(6): p. 394-424.
4. Torre, L.A., et al., *Global cancer statistics, 2012.* CA: A Cancer Journal for Clinicians, 2015. **65**(2): p. 87-108.
5. Observatory, G.C. 2021 [cited 2021 16/02/2021]; Available from: https://gco.iarc.fr/today/online-analysis-pie?v=2020&mode=cancer&mode_population=continents&population=900&populations=900&key=total&sex=0&cancer=39&type=0&statistic=5&prevalence=0&population_group=0&ages_group%5B%5D=0&ages_group%5B%5D=17&nb_items=7&group_cancer=1&include_nmsc=1&include_nmsc_other=1&half_pie=0&donut=0.
6. Observatory, G.C. 2021 [cited 2021 18/02/2021]; Available from: https://gco.iarc.fr/tomorrow/en/dataviz/isotype?cancers=20&single_unit=100000.
7. Hanahan, D. and R.A. Weinberg, *Hallmarks of cancer: the next generation.* Cell, 2011. **144**(5): p. 646-74.
8. Moses, C., et al., *Hallmarks of cancer: The CRISPR generation.* European Journal of Cancer, 2018. **93**: p. 10-18.
9. Observatory, G.C. 2021 [cited 2021 20/02/2021]; Available from: https://gco.iarc.fr/today/online-analysis-pie?v=2020&mode=cancer&mode_population=continents&population=900&populations=620&key=total&sex=2&cancer=39&type=0&statistic=5&prevalence=0&population_group=0&ages_group%5B%5D=0&ages_group%5B%5D=17&nb_items=7&group_cancer=1&include_nmsc=1&include_nmsc_other=1&half_pie=0&donut=0#collapse-group-0-4.
10. Harbeck, N., et al., *Breast cancer.* NATURE REVIEWS, 2019. **5**(1): p. 66.
11. Forjaz de Lacerda, G., et al., *Breast cancer in Portugal: Temporal trends and age-specific incidence by geographic regions.* Cancer Epidemiology, 2018. **54**: p. 12-18.
12. Polyak, K., *Heterogeneity in breast cancer.* The Journal of Clinical Investigation, 2011. **121**(10): p. 3786-88.
13. Riedl, C.C., et al., *Triple-modality screening trial for familial breast cancer underlines the importance of magnetic resonance imaging and questions the role of mammography and ultrasound regardless of patient mutation status, age, and breast density.* JOURNAL OF CLINICAL ONCOLOGY, 2015. **33**(10): p. 1128-35.
14. Oeffinger, K.C., et al., *Breast Cancer Screening for Women at Average Risk: 2015 Guideline Update From the American Cancer Society.* JAMA, 2015. **314**(15): p. 1599-614.
15. Collina, F., et al., *Prognostic Value of Cancer Stem Cells Markers in Triple-Negative Breast Cancer.* BioMed Research International, 2015. **2015**: p. 158682.

16. Guiu, S., et al., *Molecular subclasses of breast cancer: how do we define them? The IMPAKT 2012 Working Group Statement.* Annals of Oncology 2012. **23**(12): p. 2997-3006.

17. Pandit, P., et al., *Prevalence of Molecular Subtypes of Breast Cancer: A Single Institutional Experience of 2062 Patients.* European Journal Of Breast Health, 2020. **16**(1): p. 39-43.

18. Rakha, E.A. and A.R. Green, *Molecular classification of breast cancer: what the pathologist needs to know.* Pathology, 2017. **49**(2): p. 111-119.

19. Makena, M.R. and R. Rao, *Subtype specific targeting of calcium signaling in breast cancer.* Cell Calcium, 2020. **85**: p. 102109.

20. Dai, X., et al., *Cancer Hallmarks, Biomarkers and Breast Cancer Molecular Subtypes.* Journal of Cancer Therapy, 2016. **7**(10): p. 1281-94.

21. Caiazzo, C., et al., *The role of MRI in predicting Ki-67 in breast cancer: preliminary results from a prospective study.* Tumori, 2018. **104**(6): p. 438-443.

22. Lehmann, B.D., et al., *Identification of human triple-negative breast cancer subtypes and preclinical models for selection of targeted therapies.* The Journal of Clinical Investigation, 2011. **121**(7): p. 2750-67.

23. Lehmann, B.D. and J.A. Pietenpol, *Clinical implications of molecular heterogeneity in triple negative breast cancer.* Breast, 2015. **24** (2): p. S36-40.

24. Prat, A., et al., *Phenotypic and molecular characterization of the claudin-low intrinsic subtype of breast cancer.* Breast Cancer Research and Treatment, 2010. **12**.

25. Zeichner, S.B., H. Terawaki, and K. Gogineni, *A Review of Systemic Treatment in Metastatic Triple-Negative Breast Cancer.* Breast Cancer, 2016. **10**: p. 25-36.

26. Perez-Herrero, E. and A. Fernandez-Medarde, *Advanced targeted therapies in cancer: Drug nanocarriers, the future of chemotherapy.* European Journal of Pharmaceutics and Biopharmaceutics, 2015. **93**: p. 52-79.

27. [cited 2020 30/01/2020]; Available from: https://www.cancer.org/cancer/breast-cancer/treatment/treatment-of-breast-cancer-by-stage.html.

28. Pontes, O., et al., *Exploitation of new chalcones and 4H-chromenes as agents for cancer treatment.* European Journal of Medicinal Chemistry, 2018. **157**: p. 101-114.

29. Rahnamay, M., et al., *Cytotoxic and apoptosis inducing effect of some pyrano [3, 2-c] pyridine derivatives against MCF-7 breast cancer cells.* Acta Biochimica Polonica, 2018. **65**(3): p. 397-402.

30. Cristofanilli, M., et al., *Fulvestrant plus palbociclib versus fulvestrant plus placebo for treatment of hormone-receptor-positive, HER2-negative metastatic breast cancer that progressed on previous endocrine therapy (PALOMA-3): final analysis of the multicentre, double-blind, phase 3 randomised controlled trial.* The Lancet Oncology, 2016. **17**(4): p. 425-439.

31. Homer, R.J., *Cancer treatment drugs*, in *Cancer Concepts: A Guidebook for the Non-Oncologist*, L.J. Pieters RS, Editor. 2011, Worcester, MA: University of Massachusetts Medical School.

32. Mehta, R.S., et al., *Overall Survival with Fulvestrant plus Anastrozole in Metastatic Breast Cancer.* The new england journal of medicine, 2019. **380**(13): p. 1226-1234.

33. Osborne, C.K., A. Wakeling, and R.I. Nicholson, *Fulvestrant: an oestrogen receptor antagonist with a novel mechanism of action.* British Journal of Cancer 2004. **90** (1): p. S2-6.

34. Finn, R.S., et al., *Palbociclib and Letrozole in Advanced Breast Cancer.* The new england journal of medicine, 2016. **375**(20): p. 1925-1936.

35. Ahmed, S., A. Sami, and J. Xiang, *HER2-directed therapy: current treatment options for HER2-positive breast cancer.* Breast Cancer, 2015. **22**(2): p. 101-16.

36. Lang, J.E., et al., *Molecular markers for breast cancer diagnosis, prognosis and targeted therapy.* Journal of Surgical Oncology 2015. **111**(1): p. 81-90.

37. Hao, Y., et al., *Cryo-EM structure of Her2 extracellular domain-Trastuzumab Fab-Pertuzumab Fab complex.* 2019, Protein Data Base.

38. Abramson, V.G., et al., *Subtyping of triple-negative breast cancer: implications for therapy.* Cancer, 2015. **121**(1): p. 8-16.

39. Chen, S., et al., *Pharmacogenetics of irinotecan, doxorubicin and docetaxel transporters in Asian and Caucasian cancer patients: a comparative review.* Drug Metabolism Reviews, 2016. **48**(4): p. 502-540.

40. Morris, P.G. and M.N. Fornier, *Microtubule active agents: beyond the taxane frontier.* Clinical Cancer Research, 2008. **14**(22): p. 7167-72.

41. Sherry, A.D., et al., *Combining Adjuvant Radiotherapy With Capecitabine in Chemotherapy-resistant Breast Cancer: Feasibility, Safety, and Toxicity.* Clinical Breast Cancer 2020. **20**(4): p. 344-352 e1.

42. Schmid, P., et al., *Atezolizumab plus nab-paclitaxel as first-line treatment for unresectable, locally advanced or metastatic triple-negative breast cancer (IMpassion130): updated efficacy results from a randomised, double-blind, placebo-controlled, phase 3 trial.* The Lancet Oncology, 2020. **21**(1): p. 44-59.

43. Zhang, F., Qi, X., Wang, X., Wei, D., Wu, J., Feng, L., Cai, H., Wang, Y., Zeng, N., Xu, T., Zhou, A., Zheng, Y. *Crystal structure of PD-L1 complexed with atezolizumab fab at 2.9A.* [cited 2020 11/2020]; Available from: https://www.rcsb.org/structure/5XXY.

44. Alblewi, F.F., et al., *Antiproliferative effect, cell cycle arrest and apoptosis generation of novel synthesized anticancer heterocyclic derivatives based 4H-benzo[h]chromene.* Bioorganic Chemistry, 2019. **87**: p. 560-571.

45. Chirumbolo, S., *Quercetin in cancer prevention and therapy.* Integrative Cancer Therapies, 2013. **12**(2): p. 97-102.

46. Badal, S., et al., *Cytochrome P450 1 enzyme inhibition and anticancer potential of chromene amides from Amyris plumieri.* Fitoterapia, 2011. **82**(2): p. 230-36.

47. Dias, T.A., et al., *Superior anticancer activity of halogenated chalcones and flavonols over the natural flavonol quercetin.* European Journal of Medicinal Chemistry, 2013. **65**: p. 500-10.

48. Pratap, R. and V.J. Ram, *Natural and synthetic chromenes, fused chromenes, and versatility of dihydrobenzo[h]chromenes in organic synthesis.* Chemical Reviews, 2014. **114**(20): p. 10476-526.

49.   Costa, M., et al., *Biological importance of structurally diversified chromenes.* European Journal of Medicinal Chemistry, 2016. **123**: p. 487-507.

50.   *A Phase I/II Trial of Crolibulin (EPC2407) Plus Cisplatin in Adults With Solid Tumors With a Focus on Anaplastic Thyroid Cancer (ATC).* [cited 2020 26/09/2020]; Available from: https://clinicaltrials.gov/ct2/show/NCT01240590.

51.   Patil, S.A., et al., *Chromenes: potential new chemotherapeutic agents for cancer.* Future Medicinal Chemistry, 2013. **5**(14): p. 1647–1660.

52.   Schwartsmann, G., *Breast cancer in South America: challenges to improve early detection and medical management of a public health problem.* Journal of Clinical Oncology, 2001. **19**: p. 118S—124S.

53.   Chen, Y., et al., *Cytotoxicity and Anti-inflammatory Properties of Apigenin-Derived Isolaxifolin.* Journal of Natural Products, 2019. **82**(9): p. 2451-2459.

54.   Abbaszadeh, H., B. Keikhaei, and S. Mottaghi, *A review of molecular mechanisms involved in anticancer and antiangiogenic effects of natural polyphenolic compounds.* Phytotherapy Research, 2019. **33**(8): p. 2002-2014.

55.   Massi, A., et al., *Research Progress in the Modification of Quercetin Leading to Anticancer Agents.* Molecules, 2017. **22**(8).

56.   Salehi, B., et al., *Therapeutic Potential of Quercetin: New Insights and Perspectives for Human Health.* ACS Omega, 2020. **5**(20): p. 11849-11872.

57.   Vafadar, A., et al., *Quercetin and cancer: new insights into its therapeutic effects on ovarian cancer cells.* Cell & Bioscience, 2020. **10**: p. 32.

58.   Jia, L., et al., *Quercetin suppresses the mobility of breast cancer by suppressing glycolysis through Akt-mTOR pathway mediated autophagy induction.* Life Sciences 2018. **208**: p. 123-130.

59.   Aghapour, F., et al., *Quercetin conjugated with silica nanoparticles inhibits tumor growth in MCF-7 breast cancer cell lines.* Biochemical and Biophysical Research Communications 2018. **500**(4): p. 860-865.

60.   Li, S., et al., *Kaempferol inhibits the activity of pancreatic lipase and its synergistic effect with orlistat.* Journal of Functional Foods, 2020. **72**.

61.   Wang, X., et al., *The mechanism of anticancer action and potential clinical use of kaempferol in the treatment of breast cancer.* Biomedicine & Pharmacotherapy 2019. **117**: p. 109086.

62.   Zhu, L. and L. Xue, *Kaempferol Suppresses Proliferation and Induces Cell Cycle Arrest, Apoptosis, and DNA Damage in Breast Cancer Cells.* Oncology Research, 2019. **27**(6): p. 629-634.

63.   Wang, X., et al., *Estrogen receptor-a36 is involved in icaritin induced growth inhibition of triple-negative breast cancer cells.* Journal of Steroid Biochemistry and Molecular Biology, 2017. **171**: p. 318-327.

64.   Zhao, H., et al., *A novel anti-cancer agent Icaritin suppresses hepatocellular carcinoma initiation and malignant growth through the IL-6/ Jak2/Stat3 pathway.* Oncotarget, 2015. **6**(31): p. 31927-43.

65. Zhang, Q., J. Bao, and J. Yang, *Genistein-triggered anticancer activity against liver cancer cell line HepG2 involves ROS generation, mitochondrial apoptosis, G2/M cell cycle arrest and inhibition of cell migration.* Archives of Medical Science, 2019. **15**(4): p. 1001-1009.

66. Sun, X., et al., *Oroxylin A Suppresses the Cell Proliferation, Migration, and EMT via NF-kB Signaling Pathway in Human Breast Cancer Cells.* BioMed Research International, 2019. **2019**: p. 9241769.

67. Iida, K., et al., *Luteolin suppresses bladder cancer growth via regulation of mechanistic target of rapamycin pathway.* Cancer Science, 2020. **111**(4): p. 1165-1179.

68. Chen, L., et al., *Deguelin induces apoptosis in colorectal cancer cells by activating the p38 MaPK pathway.* Cancer Management and Research, 2019. **11**: p. 95-105.

69. Kang, W., et al., *Deguelin exerts anticancer activity of human gastric cancer MGC-803 and MKN-45 cells in vitro.* INTERNATIONAL JOURNAL OF MOLECULAR MEDICINE 2018. **41**(6): p. 3157-3166.

70. Ahagh, M.H., et al., *Synthesis, characterization, anti-proliferative properties and DNA binding of benzochromene derivatives: Increased Bax/Bcl-2 ratio and caspase-dependent apoptosis in colorectal cancer cell line.* Bioorganic Chemistry, 2019. **93**: p. 103329.

71. Luque-Agudo, V., et al., *Synthesis and antiproliferative activity of new 2-glyco-3-nitro-2H-chromenes.* Bioorganic Chemistry, 2019. **87**: p. 112-116.

72. Wang, Y., et al., *Design, synthesis and bioactivity evaluation of coumarin-chalcone hybrids as potential anticancer agents.* Bioorganic Chemistry, 2020. **95**: p. 103530.

73. Sashidhara, K.V., et al., *Neo-tanshinlactone inspired synthesis, in vitro evaluation of novel substituted benzocoumarin derivatives as potent anti-breast cancer agents.* Bioorganic & Medicinal Chemistry Letters, 2010. **20**(23): p. 7127-31.

74. Azizmohammadi, M., et al., *2H-chromene derivatives bearing thiazolidine-2,4-dione, rhodanine or hydantoin moieties as potential anticancer agents.* European Journal of Medicinal Chemistry 2013. **59**: p. 15-22.

75. Ahmed, H.E.A., et al., *Introducing novel potent anticancer agents of 1H-benzo[f]chromene scaffolds, targeting c-Src kinase enzyme with MDA-MB-231 cell line anti-invasion effect.* Journal of Enzyme Inhibition and Medicinal Chemistry, 2018. **33**(1): p. 1074-1088.

76. Chen, R., et al., *Synthesis and Evaluation of Anticancer Activity of New 4-Acyloxy Derivatives of Robustic Acid.* International Journal of Molecular Sciences, 2019. **20**(21).

77. Qiu, J., et al., *Hyperoside Induces Breast Cancer Cells Apoptosis via ROS-Mediated NF-kB Signaling Pathway.* International Journal of Molecular Sciences, 2019. **21**(1).

78. Hussain, M.K., et al., *A Novel Benzocoumarin-Stilbene Hybrid as a DNA ligase I inhibitor with in vitro and in vivo anti-tumor activity in breast cancer models.* Scientific Reports, 2017. **7**(1): p. 10715.

79. Bhosle, M.R., et al., *An efficient multicomponent synthesis and in vitro anticancer activity of dihydropyranochromene and chromenopyrimidine-2,5-diones.* Synthetic Communications, 2018. **48**(16): p. 2046-2060.

80. El-Agrody, A.M., et al., *In vitro anticancer activity of pyrano[3, 2-c]chromene derivatives with both cell cycle arrest and apoptosis induction.* Medicinal Chemistry Research, 2020. **29**(4): p. 617-629.

81. Oliveira-Pinto, S., et al., *Unravelling the anticancer potential of functionalized chromeno[2,3-b]pyridines for breast cancer treatment.* Bioorganic Chemistry, 2020. **100**: p. 103942.

82. Oliveira-Pinto, S., et al., *Unravelling the anticancer potential of functionalized chromeno[2,3-b]pyridines for breast cancer treatment.* Bioorg Chem, 2020. **100**: p. 103942.

83. Pontes, O., et al., *Exploitation of new chalcones and 4H-chromenes as agents for cancer treatment.* Eur J Med Chem, 2018. **157**: p. 101-114.

84. Aslam, M.S., et al., *Side Effects of Chemotherapy in Cancer Patients and Evaluation of Patients Opinion about Starvation Based Differential Chemotherapy.* Journal of Cancer Therapy, 2014. **05**(08): p. 817-822.

85. Azim, H.A., Jr., et al., *Long-term toxic effects of adjuvant chemotherapy in breast cancer.* Ann Oncol, 2011. **22**(9): p. 1939-1947.

86. Meredith, A.M. and C.R. Dass, *Increasing role of the cancer chemotherapeutic doxorubicin in cellular metabolism.* J Pharm Pharmacol, 2016. **68**(6): p. 729-41.

87. Partridge, A.H., H.J. Burstein, and E.P. Winer, *Side Effects of Chemotherapy and Combined Chemohormonal Therapy in Women With Early-Stage Breast Cancer.* Journal of the National Cancer Institute Monographs 2001. **30**.

88. Waks, A.G. and E.P. Winer, *Breast Cancer Treatment: A Review.* JAMA, 2019. **321**(3): p. 288-300.

89. Wefel, J.S., et al., *Acute and late onset cognitive dysfunction associated with chemotherapy in women with breast cancer.* Cancer, 2010. **116**(14): p. 3348-56.

90. Scambia, G., et al., *Antiproliferative Effect of Silybin on Gynaecological Malignancies: Synergism with Cisplatin and Doxorubicin.* E,,ropean&,mal of Cancer, 1996. **32**(5): p. 877-882.

91. Borges, G.S.M., et al., *Sclareol is a potent enhancer of doxorubicin: Evaluation of the free combination and co-loaded nanostructured lipid carriers against breast cancer.* Life Sci, 2019. **232**: p. 116678.

92. El-Awady, R.A., et al., *Modulation of DNA damage response and induction of apoptosis mediates synergism between doxorubicin and a new imidazopyridine derivative in breast and lung cancer cells.* DNA Repair (Amst), 2016. **37**: p. 1-11.

93. Khaki-Khatibi, F., et al., *Adjuvant therapy with stattic enriches the anti-proliferative effect of doxorubicin in human ZR-75-1 breast cancer cells via arresting cell cycle and inducing apoptosis.* Biomed Pharmacother, 2019. **109**: p. 1240-1248.

94. Mielczarek, L., et al., *In the triple-negative breast cancer MDA-MB-231 cell line, sulforaphane enhances the intracellular accumulation and anticancer action of doxorubicin encapsulated in liposomes.* Int J Pharm, 2019. **558**: p. 311-318.

95. Shi, J., et al., *Synergistic breast cancer suppression efficacy of doxorubicin by combination with glycyrrhetinic acid as an angiogenesis inhibitor.* Phytomedicine, 2021. **81**: p. 153408.

96. Vittorio, O., et al., *Doxorubicin synergism and resistance reversal in human neuroblastoma BE(2)C cell lines: An in vitro study with dextran-catechin nanohybrids.* Eur J Pharm Biopharm, 2018. **122**: p. 176-185.

97. Edwardson, D.W., et al., *Role of Drug Metabolism in the Cytotoxicity and Clinical Efficacy of Anthracyclines.* Current Drug Metabolism, 2015. **16**: p. 412-426.

98. Lin, S.R., et al., *Doxorubicin metabolism moderately attributes to putative toxicity in prodigiosin/doxorubicin synergism in vitro cells.* Mol Cell Biochem, 2020. **475**(1-2): p. 119-126.

99. Staedle, D., et al., *Drug combinations with quercetin: doxorubicin plus quercetin in human breast cancer cells.* Cancer Chemother Pharmacol, 2011(68): p. 1161-1172.

100. Vaclavikova, R., et al., *The effect of flavonoid derivatives on doxorubicin transport and metabolism.* Bioorg Med Chem, 2008. **16**(4): p. 2034-42.

101. Wang, G., et al., *Quercetin potentiates doxorubicin mediated antitumor effects against liver cancer through p53/Bcl-xl.* PLoS One, 2012. **7**(12): p. e51764.

102. Hanahan, D. and R.A. Weinberg, *The Hallmarks of Cancer.* Cell, 2000. **100**(1): p. 57-70.

103. Meirson, T., H. Gil-Henn, and A.O. Samson, *Invasion and metastasis: the elusive hallmark of cancer.* Oncogene, 2020. **39**(9): p. 2024-2026.

104. Duan, Y.D., et al., *The antitumor activity of naturally occurring chromones: A review.* Fitoterapia, 2019. **135**: p. 114-129.

105. Choi, E.J., S.M. Bae, and W.S. Ahn, *Antiproliferative effects of quercetin through cell cycle arrest and apoptosis in human breast cancer MDA-MB-453 cells.* Archives of Pharmacal Research, 2008. **31**(10): p. 1281-5.

106. Ezzati, M., et al., *A review on anti-cancer properties of Quercetin in breast cancer.* Life Sciences, 2020. **248**: p. 117463.

107. Xu, X., Y. Lai, and Z.C. Hua, *Apoptosis and apoptotic body: disease message and therapeutic target potentials.* Bioscience Reports, 2019. **39**(1).

108. Abotaleb, M., et al., *Flavonoids in Cancer and Apoptosis.* Cancers 2018. **11**(1).

109. Bock, F.J. and S.W.G. Tait, *Mitochondria as multifaceted regulators of cell death.* Nature Reviews Molecular Cell Biology, 2020. **21**(2): p. 85-100.

110. Wong, R., S., Y., *Apoptosis in cancer: from pathogenesis to treatment.* Journal of Experimental & Clinical Cancer Research, 2011. **30**(87).

111. Lopez, J. and S.W.G. Tait, *Mitochondrial apoptosis: killing cancer using the enemy within.* British Journal of Cancer, 2015. **112**(6): p. 957-62.

112. Bratton, S.B. and G.S. Salvesen, *Regulation of the Apaf-1-caspase-9 apoptosome.* Journal of Cell Science, 2010. **123**(19): p. 3209-14.

113. Li, X.X., et al., *The role of c-Myc-RBM38 loop in the growth suppression in breast cancer.* Journal of Experimental & Clinical Cancer Research, 2017. **36**(1): p. 49.

114. McIlwain, D.R., T. Berger, and T.W. Mak, *Caspase functions in cell death and disease.* Cold Spring Harb Perspect Biol, 2013. **5**(4): p. a008656.

115. Fouda, A.M., et al., *A proficient microwave synthesis with structure elucidation and the exploitation of the biological behavior of the newly halogenated 3-amino-1H-benzo[f]chromene molecules, targeting dual inhibition of topoisomerase II and microtubules.* Bioorganic Chemistry, 2020. **95**: p. 103549.

116.   Mondal, A. and L.L. Bennett, *Resveratrol enhances the efficacy of sorafenib mediated apoptosis in human breast cancer MCF7 cells through ROS, cell cycle inhibition, caspase 3 and PARP cleavage.* Biomedicine & Pharmacotherapy 2016. **84**: p. 1906-1914.

117.   Yusoh, N.A., et al., *Metallointercalator [Ru(dppz)2(PIP)](2+) Renders BRCA Wild-Type Triple-Negative Breast Cancer Cells Hypersensitive to PARP Inhibition.* ACS Chem Biol, 2020. **15**(2): p. 378-387.

118.   Wu, H., L.J. Medeiros, and K.H. Young, *Apoptosis signaling and BCL-2 pathways provide opportunities for novel targeted therapeutic strategies in hematologic malignances.* Blood Rev, 2018. **32**(1): p. 8-28.

119.   Shimamura, H., et al., *The PI3-kinase-Akt pathway promotes mesangial cell survival and inhibits apoptosis in vitro via NF-kB and Bad.* Journal of the American Society of Nephrology, 2003. **14**(6): p. 1427-34.

120.   Schug, Z.T., et al., *BID is cleaved by caspase-8 within a native complex on the mitochondrial membrane.* Cell Death and Differentiation, 2011. **18**(3): p. 538-48.

121.   Vermes, I., C. Haanen, and C. Reutelingsperger, *Flow cytometry of apoptotic cell death.* Journal of Immunological Methods 2000. **243**(1-2): p. 167-190.

122.   Vermes, I., et al., *A novel assay for apoptosis*

Flow cytometric detection of phosphatidylserine expression on early apoptotic cells using fluorescein labelled Annexin V. Journal of Immunological Methods 1995. **184**(1): p. 39-51.

123.   Lizarbe, M.A., et al., *Annexin-phospholipid interactions. Functional implications.* International Journal of Molecular Sciences, 2013. **14**(2): p. 2652-83.

124.   Darzynkiewicz, Z., et al., *Features of Apoptotic Cells Measured by Flow Cytometry.* Cytometry, 1992. **13**(8): p. 795-808.

125.   Heo, S.J., et al., *Chromene induces apoptosis via caspase-3 activation in human leukemia HL-60 cells.* Food and Chemical Toxicology, 2011. **49**(9): p. 1998-2004.

126.   Kumar, M.S.L., et al., *Diversity oriented synthesis of chromene-xanthene hybrids as anti-breast cancer agents.* Bioorganic & Medicinal Chemistry Letters, 2018. **28**(4): p. 778-782.

127.   Qin, J., et al., *Rational design and synthesis of 6-aryl-6H-benzo[c]chromenes as non-steroidal progesterone receptor antagonists for use against cancers.* Bioorganic & Medicinal Chemistry, 2021. **32**: p. 116003.

128.   Rahmani-Nezhad, S., et al., *Synthesis, in vitro cytotoxicity and apoptosis inducing study of 2-aryl-3-nitro-2H-chromene derivatives as potent anti-breast cancer agents.* European Journal of Medicinal Chemistry, 2014. **86**: p. 562-69.

129.   Lima, C.F., et al., *Novel structurally similar chromene derivatives with opposing effects on p53 and apoptosis mechanisms in colorectal HCT116 cancer cells.* European Journal of Pharmaceutical Sciences, 2015. **72**: p. 34-45.

130.   Otto, T. and P. Sicinski, *Cell cycle proteins as promising targets in cancer therapy.* Nature Reviwes Cancer, 2017. **17**(2): p. 93-115.

131.   Leal-Esteban, L.C. and L. Fajas, *Cell cycle regulators in cancer cell metabolism.* BBA - Molecular Basis of Disease, 2020. **1866**(5): p. 165715.

132.   Fouda, A.M., et al., *Microwave synthesis of novel halogenated beta-enaminonitriles linked 9-bromo-1H-benzo[f]chromene moieties: Induces cell cycle arrest and apoptosis in human cancer cells via dual inhibition of topoisomerase I and II.* Bioorganic Chemistry, 2019. **93**: p. 103289.

133.   Uthamacumaran, A., *Cancer: A turbulence problem.* Neoplasia, 2020. **22**(12): p. 759-769.

134.   Baltazar, F., et al., *Lactate Beyond a Waste Metabolite: Metabolic Affairs and Signaling in Malignancy.* Frontiers in Oncology, 2020. **10**(231).

135.   DeBerardinis, R.J. and N.S. Chandel, *Fundamentals of cancer metabolism.* Science Advances, 2016. **2**: p. e1600200.

136.   Movahed, Z.G., et al., *Cancer cells change their glucose metabolism to overcome increased ROS: One step from cancer cell to cancer stem cell?* Biomedicine & Pharmacotherapy, 2019. **112**: p. 108690.

137.   Smith, R.L., et al., *Metabolic Flexibility as an Adaptation to Energy Resources and Requirements in Health and Disease.* Endocrine Reviews, 2018. **39**(4): p. 489-517.

138.   Lanning, N.J., et al., *Metabolic profiling of triple-negative breast cancer cells reveals metabolic vulnerabilities.* Cancer & Metabolism, 2017. **5**: p. 6.

139.   Dang, C.V., A. Le, and P. Gao, *MYC-induced cancer cell energy metabolism and therapeutic opportunities.* Clin Cancer Res, 2009. **15**(21): p. 6479-83.

140.   Lee, J., et al., *Hypoxia-inducible factor (HIF-1)α: its protein stability and biological functions.* EXPERIMENTAL and MOLECULAR MEDICINE, 2004. **36**(1): p. 1-12.

141.   Osthus, R.C., et al., *Deregulation of glucose transporter 1 and glycolytic gene expression by c-Myc.* J Biol Chem, 2000. **275**(29): p. 21797-800.

142.   Hoefflin, R., et al., *HIF-1a and HIF-2a differently regulate tumour development and inflammation of clear cell renal cell carcinoma in mice.* Nature Communications, 2020. **11**(1): p. 4111.

143.   Bartoszewski, R., et al., *Primary endothelial cell-specific regulation of hypoxia-inducible factor (HIF)-1 and HIF-2 and their target gene expression profiles during hypoxia.* The FASEB Journal, 2019. **33**(7): p. 7929-7941.

144.   Sato-Tadano, A., et al., *Hexokinase II in breast carcinoma: a potent prognostic factor associated with hypoxia-inducible factor-1a and Ki-67.* Cancer Science 2013. **104**(10): p. 1380-88.

145.   Luo, P., et al., *Transcriptional positive cofactor 4 promotes breast cancer proliferation and metastasis through c-Myc mediated Warburg effect.* Cell Communication and Signaling, 2019. **17**(1): p. 36.

146.   Amiri, A., et al., *Inhibition of carbonic anhydrase IX in glioblastoma multiforme.* European Journal of Pharmaceutics and Biopharmaceutics, 2016. **109**: p. 81-92.

147.   Benej, M., S. Pastorekova, and J. Pastorek, *Carbonic Anhydrase IX: Regulation and Role in Cancer*, in *Subcellular Biochemistry*, M.R. Frost S., Editor. 2014, Springer, Dordrecht. p. 199-219.

148.   Robertson, N., C. Potter, and A.L. Harris, *Role of Carbonic Anhydrase IX in Human Tumor Cell Growth, Survival, and Invasion.* CANCER RESEARCH, 2004. **64**: p. 6160–6165.

149.   Liu, Y., et al., *The Warburg effect: A new insight into atrial fibrillation.* Clinica Chimica Acta, 2019. **499**: p. 4-12.

150.   Mirzaei, H. and M.R. Hamblin, *Regulation of Glycolysis by Non-coding RNAs in Cancer: Switching on the Warburg Effect.* Molecular Therapy: Oncolytics, 2020. **19**: p. 218-239.

151.   Spencer, N.Y. and R.C. Stanton, *The Warburg Effect, Lactate, and Nearly a Century of Trying to Cure Cancer.* Seminars in Nephrology, 2019. **39**(4): p. 380-393.

152.   Oh, S., et al., *Glut1 promotes cell proliferation, migration and invasion by regulating epidermal growth factor receptor and integrin signaling in triple-negative breast cancer cells.* BMB Rep, 2017. **50**(3): p. 132-137.

153.   Zhang, J.Y., et al., *Critical protein GAPDH and its regulatory mechanisms in cancer cells.* Cancer Biol Med, 2015. **12**(1): p. 10-22.

154.   Rodrigues-Ferreira, S., A. Molina, and C. Nahmias, *Microtubule-associated tumor suppressors as prognostic biomarkers in breast cancer.* Breast Cancer Research and Treatment, 2020. **179**(2): p. 267-273.

155.   Cao, Y.N., et al., *Recent advances in microtubule-stabilizing agents.* European Journal of Medicinal Chemistry, 2018. **143**: p. 806-828.

156.   Ziegler, U. and P. Groscurth, *Morphological Features of Cell Death.* News in Physiological Sciences, 2004. **19**: p. 124-128.

157.   Coleman, M.L., et al., *Membrane blebbing during apoptosis results from caspase-mediated activation of ROCK I.* NATURE CELL BIOLOGY, 2001. **3**(4): p. 339-45.

158.   Hunt, P.R., *The C. elegans model in toxicity testing.* Journal of Applied Toxicology, 2017. **37**(1): p. 50-59.

159.   Boyd, W.A., et al., *A high-throughput method for assessing chemical toxicity using a Caenorhabditis elegans reproduction assay.* Toxicology and Applied Pharmacology, 2010. **245**(2): p. 153-59.

160.   Tejeda-Benitez, L. and J. Olivero-Verbel, *Caenorhabditis elegans, a Biological Model for Research in Toxicology.* Reviews of Environmental Contamination and Toxicology, 2016. **237**: p. 1-35.

161.   Kaletta, T. and M.O. Hengartner, *Finding function in novel targets: C. elegans as a model organism.* Nature Reviews Drug Discovery, 2006. **5**(5): p. 387-98.

162.   Dunker, N. and V. Jendrossek, *Implementation of the Chick Chorioallantoic Membrane (CAM) Model in Radiation Biology and Experimental Radiation Oncology Research.* Cancers 2019. **11**(10).

163.   Pawlikowska, P., et al., *Exploitation of the chick embryo chorioallantoic membrane (CAM) as a platform for anti-metastatic drug testing.* Scientific Reports, 2020. **10**(1): p. 16876.

164.   Ribatti, D., *The chick embryo chorioallantoic membrane as a model for tumor biology.* Exp Cell Res, 2014. **328**(2): p. 314-24.

165.   Liu, M., et al., *The Histone Methyltransferase EZH2 Mediates Tumor Progression on the Chick Chorioallantoic Membrane Assay, a Novel Model of Head and Neck Squamous Cell Carcinoma.* Translational Oncology, 2013. **6**(3): p. 273-81.

166.   Ribatti, D., *The chick embryo chorioallantoic membrane (CAM). A multifaceted experimental model.* Mechanisms of Development, 2016. **141**: p. 70-77.

167.   Schmitt, F., et al., *New naphthopyran analogues of LY290181 as potential tumor vascular-disrupting agents.* European Journal of Medicinal Chemistry, 2019. **163**: p. 160-168.

168.   Lopes, D., et al., *A Convenient One-pot Synthesis of Chromenyl Acrylates and Acrylonitriles.* Synlett, 2020. **31**(13): p. 1298-1302.

169.   Fernald, K. and M. Kurokawa, *Evading apoptosis in cancer.* Trends in Cell Biology, 2013. **23**(12): p. 620-33.

170.   Wegiel, B., et al., *Metabolic Switch in the Tumor Microenvironment Determines Immune Responses to Anti-cancer Therapy.* Frontiers in Oncology, 2018. **8**: p. 284.